

Two-stage Catalytic Reduction of NO_x with Hydrocarbons

Final Report

Reporting Period Start Date: October 1st, 2002

Reporting Period End Date: September 30th, 2005

P.I.: Professor Umit S. Ozkan

Team members:

Erik M. Holmgren

Matthew M. Yung

Jonathan Halter

Joel Hiltner

December 21th, 2005

DE-FC26-02NT41610

The Ohio State University

Department of Chemical and Biomolecular Engineering

140 W. 19th Ave.

Columbus, OH 43210

Disclaimer

The report was prepared as an account of work sponsored by an agency of the United States Government. Neither the United States Government nor any agency thereof, nor any of their employees, makes any warranty, express or implied, or assumes any legal liability or responsibility for the accuracy, completeness, or usefulness of any information, apparatus, product, or process disclosed, or represents that its use would not infringe privately owned rights. Reference herein to any specific commercial product, process, or service by trade name, trademark, manufacturer, or otherwise does not necessarily constitute or imply its endorsement, recommendation, or favoring by the United States Government or any agency thereof. The views and opinions of authors expressed herein do not necessarily state or reflect those of the United States Government or any agency thereof.

Abstract

A two-stage system for the catalytic reduction of NO from lean-burn natural gas reciprocating engine exhaust is investigated. Each of the two stages uses a distinct catalyst. The first stage is oxidation of NO to NO₂ and the second stage is reduction of NO₂ to N₂ with a hydrocarbon. The central idea is that since NO₂ is a more easily reduced species than NO, it should be better able to compete with oxygen for the combustion reaction of hydrocarbon, which is a challenge in lean conditions. Early work focused on demonstrating that the N₂ yield obtained when NO₂ was reduced was greater than when NO was reduced. NO₂ reduction catalysts were designed and silver supported on alumina (Ag/Al₂O₃) was found to be quite active, able to achieve 95% N₂ yield in 10% O₂ using propane as the reducing agent. The design of a catalyst for NO oxidation was also investigated, and a Co/TiO₂ catalyst prepared by sol-gel was shown to have high activity for the reaction, able to reach equilibrium conversion of 80% at 300°C at GHSV of 50,000h⁻¹.

After it was shown that NO₂ could be more easily reduced to N₂ than NO, the focus shifted on developing a catalyst that could use methane as the reducing agent. The Ag/Al₂O₃ catalyst was tested and found to be inactive for NO_x reduction with methane. Through iterative catalyst design, a palladium-based catalyst on a sulfated-zirconia support (Pd/SZ) was synthesized and shown to be able to selectively reduce NO₂ in lean conditions using methane. Development of catalysts for the oxidation reaction also continued and higher activity, as well as stability in 10% water, was observed on a Co/ZrO₂ catalyst, which reached equilibrium conversion of 94% at 250°C at the same GHSV. The Co/ZrO₂ catalyst was also found to be extremely active for oxidation of CO, ethane, and propane, which could potential eliminate the need for any separate oxidation catalyst. At every stage, catalyst synthesis was guided by the insights gained through detailed characterization of the catalysts using many surface and bulk analysis techniques such as X-ray diffraction, X-ray photoelectron spectroscopy, Temperature-programmed Reduction, Temperature programmed Desorption, and Diffuse Reflectance InfraRed Fourier Transform Spectroscopy as well as steady state reaction experiments.

Once active catalysts for each stage had been developed, a physical mixture of the two catalysts was tested for the reduction of NO with methane in lean conditions. These experiments using a mixture of the catalysts produced N₂ yields as high as 90%. In the presence of 10% water, the catalyst mixture produced 75% N₂ yield, without any optimization. The dual catalyst system developed has the potential to be implemented in lean-burn natural gas engines for reducing NO_x in lean exhaust as well as eliminating CO and unburned hydrocarbons without any fuel penalty or any system modifications. If funding continues, future work will focus on improving the hydrothermal stability of the system to bring the technology closer to application.

Table of Contents

Abstract.....	3
Table of Contents.....	4
List of Graphical Materials.....	5
Introduction/Executive Summary.....	8
Experimental.....	12
<i>Catalyst Preparation</i>	12
<i>Physisorption for BET Surface Area Analysis</i>	12
<i>Steady-State Reaction System</i>	13
<i>Temperature Programmed Desorption (TPD)</i>	14
<i>X-ray Photoelectron Spectroscopy (XPS)</i>	15
<i>X-ray Diffraction (XRD)</i>	16
<i>Thermogravimetric Analysis (TGA)</i>	16
<i>Temperature Programmed Reaction (TPRxn)</i>	16
<i>Diffuse Reflectance Infrared Fourier Transform Spectroscopy (DRIFTS)</i>	17
<i>Temperature Programmed Reduction (TPR)</i>	17
Results and Discussion.....	18
<i>Co-Based Catalysts for the Oxidation of NO to NO₂</i>	18
<i>Ag-Based Catalysts for the Reduction of NO₂ with Hydrocarbons...</i>	33
<i>NO₂ Reduction with CH₄ over Pd-Based Sulfated Zirconia</i>	40
<i>NO Reduction with CH₄ over Mixed Oxidation and Reduction Catalyst Beds</i>	63
<i>Two-Stage Reduction of NO Under Simulated Lean Exhaust</i>	68
<i>Effect of Water Vapor</i>	71
Outreach and Information Dissemination.....	79
Conclusions.....	82
References.....	83
List of Acronyms and Abbreviations.....	84

List of Graphical Materials

Table 1: Catalyst preparation precursor list.....	12
Figure 1: Schematic diagram of the steady-state reaction system.....	13
Figure 2: Schematic of the temperature programmed desorption system.....	15
Figure 3: Equilibrium NO ₂ yields for 1000ppm in various O ₂ concentrations	18
Figure 4: NO oxidation over 10% Co/TiO ₂ Sol-Gel catalysts calcined at different temperatures. 1000ppm NO, 10% O ₂	20
Figure 5: NO oxidation over 10% Co/TiO ₂ Incipient Wetness catalysts calcined at different temperatures. 1000ppm NO, 10% O ₂	20
Figure 6: Effect of calcination temperature on BET surface areas of 10% Co/TiO ₂ catalysts prepared through incipient wetness and sol-gel methods...	21
Figure 7: TPR profiles of 10% Co/TiO ₂ prepared through sol-gel and incipient wetness methods and calcined at different temperatures.....	22
Figure 8: Co 2p _{3/2} XPS spectra of 10% Co/TiO ₂ SG300 and IW300.....	23
Figure 9: Co 2p _{3/2} XPS spectra of 10% Co/TiO ₂ IW calcined at different temperatures	24
Figure 10: Calcination by TGA of 10% Co/TiO ₂ prepared by incipient wetness impregnation. Both percent weight loss (left) and the differential weight signal (right) is shown.....	25
Figure 11: <i>In-situ</i> XRD during the calcination of 10% Co/TiO ₂ prepared by sol-gel...	26
Figure 12: <i>In-situ</i> XRD during the calcination of 10% Co/TiO ₂ prepared by incipient wetness.....	27
Table 2: BET surface area on incipient wetness 10% Co/ZrO ₂ calcined at different temperatures.....	28
Figure 13: Oxidation of NO to NO ₂ over 10% Co/ZrO ₂ catalysts prepared by incipient wetness and calcined at different temperatures.....	28
Figure 14: TPR profiles of 10% Co/ZrO ₂ catalysts prepared through incipient wetness and calcined at different temperatures.....	29
Figure 15: Co 2p _{3/2} XPS spectra of 10% Co/ZrO ₂ IW calcined at different temperatures.....	30
Figure 16: <i>In-situ</i> XRD during the calcination of 10% Co/ZrO ₂ prepared by incipient wetness.....	31
Figure 17: Effect of metal loading on Co/ZrO ₂ IWI 350.....	32
Table 3: BET surface areas of Ag-based catalysts.....	33
Figure 18: NO ₂ reduction with C ₃ H ₆ over Ag-based catalysts. NO ₂ conversion and N ₂ yield.....	34
Figure 19: NO ₂ reduction with C ₃ H ₈ over Ag/Al ₂ O ₃ and Pd/Al ₂ O ₃ catalysts. NO ₂ conversion and N ₂ yield.....	35
Figure 20: NO ₂ reduction using C ₃ H ₆ and C ₃ H ₈ over 1% Ag/Al ₂ O ₃ . NO ₂ conversion and N ₂ yield.....	36
Figure 21: NO ₂ reduction using C ₃ H ₆ and C ₃ H ₈ over 3% Ag/Al ₂ O ₃ . NO ₂ conversion and N ₂ yield.....	37
Figure 22: NO ₂ reduction under 5% and 10% O ₂ using C ₃ H ₈ over 3% Ag/Al ₂ O ₃ . NO ₂ conversion and N ₂ yield.....	38
Figure 23: XRD pattern of Ag/Al ₂ O ₃ catalysts.....	39
Figure 24: XPS spectra is the Ag 3d region of Ag/Al ₂ O ₃ catalysts.....	39

Figure 25: Comparison of reaction results of the NO ₂ +CH ₄ and the NO+CH ₄ reduction reactions over 0.5%Pd/5%SZ.....	41
Figure 26: Temperature programmed reaction, NO+CH ₄	42
Figure 27: Temperature programmed reaction, NO ₂ +CH ₄	43
Figure 28: Reaction results showing N ₂ yield and CH ₄ conversion over 0.5%Pd/5%SZ and 0.5%Pd/ZrO ₂	44
Figure 29: XPS spectra of the S 2p and Zr 5d regions after each step in the synthesis of 0.5%Pd/5%SZ.....	46
Figure 30: XPS spectra of the O 1s region after each step in the synthesis of 0.5%Pd/5%SZ.....	46
Figure 31: Effect metal loading on activity of Pd/SZ catalysts for the NO ₂ +CH ₄ reduction reaction.....	47
Figure 32: Adsorption of NO and NO ₂ on a 0.5%Pd/5%SZ and KBr mixture.....	49
Figure 33: NO temperature programmed desorption by DRIFTS.....	50
Figure 34: NO temperature programmed desorption by DRIFTS. High wavenumber region.....	51
Figure 35: NO ₂ temperature programmed desorption by DRIFTS.....	52
Figure 36: NO ₂ temperature programmed desorption by DRIFTS. High wavenumber region.....	53
Figure 37: NO temperature programmed desorption by DRIFTS. TPD performed under CH ₄ flow.....	54
Figure 38: NO temperature programmed desorption by DRIFTS. TPD performed under CH ₄ flow. High wavenumber region.....	55
Figure 39: NO ₂ temperature programmed desorption by DRIFTS. TPD performed under CH ₄ flow.....	57
Figure 40: NO ₂ temperature programmed desorption by DRIFTS. TPD performed under CH ₄ flow. High wavenumber region.....	58
Figure 41: NO temperature programmed desorption by DRIFTS. TPD performed under CH ₄ and O ₂ flow.....	59
Figure 42: NO temperature programmed desorption by DRIFTS. TPD performed under CH ₄ and O ₂ flow. High wavenumber region.....	60
Figure 43: NO ₂ temperature programmed desorption by DRIFTS. TPD performed under CH ₄ and O ₂	61
Figure 44: NO ₂ temperature programmed desorption by DRIFTS. TPD performed under CH ₄ and O ₂ . High wavenumber region.....	62
Figure 45: N ₂ yield from the NO reduction over mixed bed of 0.5%Pd/5%SZ and 10%Co/TiO ₂	64
Figure 46: CH ₄ conversion from the NO reduction over mixed bed of 0.5%Pd/5%SZ and 10%Co/TiO ₂	64
Figure 47: Effect of residence time on NO reduction over a mixture of 10%Co/TiO ₂ IW1400 and 0.5%Pd/5%SZ.....	65
Figure 48: N ₂ yield from the NO reduction over mixed bed of 0.3%Pd/5%SZ and 10%Co/ZrO ₂	66
Figure 49: CH ₄ conversion from the NO reduction over mixed bed of 0.3%Pd/5%SZ and 10%Co/ZrO ₂	67

Figure 50: Steady-state CO oxidation on 10%Co/ZrO ₂ . CO and CO ₂ concentrations are presented as % of inlet concentration at various temperatures....	68
Figure 51: N ₂ yield from the NO reduction over mixed beds containing 0.3%Pd/5%SZ and 10%Co/ZrO ₂	69
Figure 52: Hydrocarbon conversions from the NO reduction over mixed beds containing 0.3%Pd/5%SZ and 10%Co/ZrO ₂	70
Figure 53: TPrxn for CO oxidation on 10%Co/ZrO ₂	71
Figure 54: N ₂ yields from NO reduction under dry and 3% H ₂ O streams, over mixed beds containing 0.3%Pd/5%SZ and 10%Co/ZrO ₂	72
Figure 55: CH ₄ conversion from NO reduction under dry and 3% H ₂ O streams, over mixed beds containing 0.3%Pd/5%SZ and 10%Co/ZrO ₂	73
Figure 56: Maximum N ₂ yield in NO reduction with CH ₄ over the mixed bed as a function of H ₂ O concentration.....	73
Figure 57: NO oxidation under dry and 10% H ₂ O streams over 10%Co/TiO ₂ IW.	74
Figure 58: CO ₂ and SO ₂ mass spectra during the temperature programmed reaction of NO+CH ₄ , with and without 1% H ₂ O in the feed.....	75
Figure 59: DRIFTS spectra of H ₂ O TPD from 0.3%Pd/5%SZ. Low wavenumber region.....	76
Figure 60: DRIFTS spectra of H ₂ O TPD from 0.3%Pd/5%SZ. High wavenumber region.....	77
Figure 61: Effect of water vapor on N ₂ yield over mixed beds containing 0.3%Pd/5%SZ and 0.3%Pd/15%SZ.....	78

Introduction/Executive Summary

Natural gas fired reciprocating engines represent an important and growing share of the distributed energy marketplace. Reciprocating engines are a well-understood technology from both a use and business model standpoint. As such they represent both the best-selling and lowest-cost distributed energy technology in the world. With slight modifications reciprocating engines can run using light hydrocarbons such as landfill gas as well as across a wide range of natural gas compositions. Lean-burn natural gas fired engines have several advantages as next generation power sources, and commonly see use in a stationary capacity as back-up generators, in industrial service, as pipeline pump drivers, and at local heat and power cogeneration sites. Using natural gas as a fuel contributes to lower engine out emissions due the lack of organically bound nitrogen and sulfur. Operation under lean conditions results in higher engine efficiency, as well as further reducing engine out emissions. Although emission profiles are greatly improved, engine out emissions are not low enough to meet upcoming environmental regulation. The control of nitrogen oxides is of particular concern and has prompted the Department of Energy's Advanced Reciprocating Engine Systems Project to target a 90% reduction from current levels.

Emission of nitrogen oxides (NO, NO₂, and N₂O) into the atmosphere is associated with many environmental hazards. These include global warming, ground level ozone formation, smog, and acid rain production. NO formation at the high temperatures found in combustion processes is responsible for the majority of NO_x emissions. Some reduction of NO_x emissions is possible through the modification of fuels or by altering combustion parameters, but in order to reach acceptable emission levels, an effective aftertreatment technology must be used. Current catalytic NO_x reduction control technologies include three-way catalysts and ammonia or urea-based selective catalytic reduction (SCR). While these methods are highly effective for current combustion technologies, they are unsuitable for the next generation of high efficiency lean-burn natural gas engines. Three-way catalysts quickly deactivate under oxygen rich environments, while the large size, cost and storage/handling issues involved in ammonia and urea SCR installations make them an impractical solution in a distributed energy context.

The use of hydrocarbons as reducing agents in NO_x removal has attracted significant research attention. The low cost and wide availability of natural gas make it a good option as a NO_x reducing agent in addition to it being an attractive fuel. This is especially true for natural gas fueled power generation where the gas is already present, and is in fact typically found to some extent in the exhaust. Ideally these unburned hydrocarbons would be used as the reducing agent, as this scheme would eliminate both fuel penalty costs and injection control issues. Despite significant research towards these ends inherent problems in performing lean hydrocarbon SCR have prevented the commercialization of such a system. The principle barrier to the use of hydrocarbons, particularly in oxygen rich environments, is competition between the reduction mechanism and hydrocarbon combustion.

In response to this challenge, the present work is devoted to the development of a novel two-stage NO_x reduction system. The proposed system will first oxidize NO to NO₂, and in a second stage perform the hydrocarbon reduction of NO₂. NO₂ is a more easily reduced species than NO, and thus should be better able to compete with oxygen for reaction with the hydrocarbon. Furthermore, as NO oxidation is a thermodynamically limited reaction at high temperatures, high excess oxygen will be a benefit to the performance of the system.

During the first year of the project experimental work was focused on synthesis and screening of catalysts active for both the NO oxidation and NO₂ reduction stages. At every stage, catalyst synthesis was guided by the insights gained through detailed characterization of the catalysts using many surface and bulk analysis techniques such as X-ray diffraction, X-ray photoelectron spectroscopy, Temperature-programmed Reduction, Temperature programmed Desorption, and Diffuse Reflectance Infrared Fourier Transform Spectroscopy as well as steady state reaction experiments. Active catalysts were identified for both stages. Because the oxidation is thermodynamically limited high activity at low reaction temperatures is necessary. 10%Co/TiO₂ prepared through both sol-gel and incipient wetness techniques was shown to be capable of reaching equilibrium conversion at 300°C and a gas hour space velocity of 50,000 hr⁻¹. This corresponds to an NO conversion to NO₂ of above 85%. The choice of synthesis method and calcination temperature in catalyst preparation was observed to play a key role in activity of these catalysts. In both sol-gel and incipient wetness samples increased calcination temperature resulted in a less active catalyst. This effect was stronger with the sol-gel preparation method. Characterization of these catalysts was performed to explain the activity loss. Results from temperature programmed reduction, X-ray photoelectron spectroscopy, thermogravimetric analysis, and X-ray diffraction demonstrated that increased calcination temperature resulted in an increased metal-support interaction. This increased interaction eventually led to the formation of an inactive cobalt titanate phase, explaining the thermal instability. For the reduction of NO₂ under lean conditions, Ag-based catalysts were active for the reaction with propene and propane. 1 and 3% Ag/Al₂O₃ catalysts were the most promising, reaching above 90% N₂ yield by 400°C. This high reduction activity was observed in lean feed streams, under both 5 and 10% oxygen. Physical characterization by XRD and XPS showed that the active Ag metal is present on the catalyst in a well-dispersed oxide phase. Although the Ag/Al₂O₃ catalysts were shown to be inactive for the reduction of NO₂ with methane, they may find application in areas where propane may be readily available such as well-head gas compression systems.

Further catalyst development in the projects second year sought to design a more thermally stable NO oxidation catalyst, as well as a NO₂ reduction catalyst capable of using methane. 10%Co/ZrO₂ catalysts were prepared and shown to be more active for the oxidation reaction than those supported on titania. The most active of the new series of catalysts was capable of reaching equilibrium conversion at 265°C, above 90% NO₂ yield under the same conditions as the titania catalysts. A small decrease in activity with increased calcination temperature was observed, but this was much less severe than in previous formulations. Characterization of 10%Co/ZrO₂ indicated that cobalt is present on the catalyst surface as clusters of Co₃O₄, and that even at 600°C did not form a bulk

phase with the support analogous to the titanate previously observed. The change in support material thus represented a significant improvement in oxidation catalyst activity and stability.

Since the primary goal was to develop a system that would work with methane as a reducing agent, the effort was focused on formulating catalysts for the NO₂ reduction with methane. The catalysts developed are Pd-based and supported on sulfated zirconia. Initial testing of these catalysts showed that they were active for the reduction using methane, and that much higher nitrogen yields were reached in the reaction with NO₂ as compared to the reduction of NO. A maximum yield of 62% was observed at 375°C over 0.3%Pd/5%SZ in the reduction of NO₂. Palladium supported on zirconia which did not receive sulfate treatment resulted in a completely inactive catalyst. This result highlighted the importance of catalytic solid acid sites in the reduction reaction. These species are observed to be stable at typical reaction temperatures. Mechanistic studies performed using diffuse reflectance infrared Fourier transform revealed several differences in the reduction of NO and NO₂ with methane. Most importantly NO₂ appears to interact more strongly with surface sulfate groups and reacts with methane at lower temperatures. Initial experiments examining the effectiveness of the combined system showed that NO reduction with methane over a mixed catalyst bed attained nitrogen yields comparable to the direct reduction of NO₂. These first combined system tests proved the merit of the two-stage approach.

During the third and final year of the project further catalyst development was performed, and the best formulations of oxidation and reduction catalysts were combined to examine overall system performance under model conditions and simulated exhaust streams. The reduction of NO with methane was performed over mixed beds containing 10%Co/ZrO₂ IW300 and 0.3%Pd/5%SZ. Under a feed of 1000 ppm NO, 3000 ppm CH₄ and 10% oxygen the combined two-stage system achieved N₂ yields of approximately 80% within the temperature range of 350-400°C. The effect of other exhaust components on the activity of the systems were also examined though testing under simulated lean natural gas engine exhaust. Additional species included a simulated natural gas containing methane, ethane, and propane, carbon monoxide, carbon dioxide, and water vapor. Mixed bed testing in fact revealed that the two-stage system is also highly effective for oxidizing both carbon monoxide and excess hydrocarbons in the feed stream. Analysis of this activity has shown that carbon monoxide oxidation occurs over the Co-based oxidation catalyst even at very low temperatures. The oxidation of excess hydrocarbons appears to be a function of the combined catalyst system. At temperatures corresponding to maximum nitrogen yield oxidation of ethane and propane was complete, and oxidation of methane was between 60-80%. The addition of water vapor caused a loss in NO reduction activity. Testing with the individual oxidation and reduction catalysts revealed that this deactivation was due to a competitive adsorption effect on the sulfated zirconia NO₂ reduction catalyst. The presence of water does not appear to cause a permanent deactivation through a structural or surface change of the catalyst. The formulation of reduction catalysts with increased surface acidity has begun to combat this activity loss. Nitrogen yields of 75% have been achieved in activity tests containing 10% water streams. Characterization results have also provided important leads for “fine-tuning” the catalysts for long-term hydrothermal stability.

The project has successfully demonstrated a highly effective dual catalyst system for exhaust cleanup from lean-burn natural gas reciprocating engines. This dual-catalyst system holds significant promise for the clean up nitrogen oxides, unburned hydrocarbons, and carbon monoxide from engine exhaust with zero fuel penalty, easy retrofitting and simple operation.

Experimental

Catalyst Preparation

Catalysts prepared for this work were synthesized by both incipient wetness impregnation and sol-gel techniques. All catalyst loadings are calculated and designated as weight percent. A complete list of catalyst precursors is presented in Table 1. The impregnation to incipient wetness technique consists of the physical mixing of unloaded support and a solution containing the dissolved metal salt. Water was used as the solvent for all catalysts presented here. The appropriate amount of metal salt is first dissolved in a volume of water equal to the pore volume of the support material and the solution is then added to the support powder and thoroughly mixed. The impregnated support is dried overnight at 100°C, and then calcined in air for four hours. The sol-gel method allows for greater control of support characteristics and is generally seen to improve surface area and metal dispersion. The catalyst structure is built by the controlled hydrolysis of metal alkoxide precursors with a water solution containing the active metal. All sol-gel preparations were based on the synthesis of 5 grams of catalyst. The alkoxide precursor was added to 50mL of isopropyl alcohol, which acted as a solvent. This solution was constantly stirred with a magnetic stir bar. The appropriate amount of active metal salt was dissolved in water. To speed hydrolysis the amount of water used in all preparations was above the stoichiometric amount necessary. (Water to metal alkoxide ratio 7:1.) The metal solution was added to the alkoxide mixture at 0.2mL/min by syringe pump, under constant stirring. Upon complete addition of water, the gel was allowed to dry in air overnight, then the resulting powder was calcined in air for 4 hours.

Material	Supplier
Cobalt nitrate hexahydrate	Aldrich
Palladium chloride	Aldrich
Titanium dioxide	Harshaw
Titanium isopropoxide	Aldrich
Zirconia Oxide	Harshaw
Zirconium propoxide	Aldrich
Isopropyl alcohol	Fisher
Titanium dioxide	Saint Gobain
Zirconium dioxide	Saint Gobain
Ammonium sulfate	Aldrich

Table 1: Catalyst preparation precursor list.

Physisorption for BET Surface Area Analysis

Physisorption and chemisorption experiments were performed on a Micromeritics ASAP 2010 accelerated surface area and porosimetry system. Surface area measurements were performed by N₂ physisorption using the BET method. Sample tubes were sealed, evacuated and weighed before 200 mg of catalyst was added. The sample is degassed overnight at 130°C, and the tube containing sample is weighed again. Sample weight is then calculated from the difference of these two measurements. The sample tube is

immersed in liquid N₂ and exposed to N₂ gas. Pressure measurements are logged by the ASAP 2010 software to calculate pore volume and surface area of the samples.

Steady-State Reaction System

A schematic of the reaction system is given in Figure 1. The system is constructed of stainless steel tubing connected by Swagelok fittings. Up to six feed gases can be introduced to the reactor through Brooks 5850 and Tylan FC-280 mass flow controllers. In addition, water can be added to the feed by directing the feed gas through a bubbler. Feed gases are mixed and then sent through a four-port valve. This valve allows gas to bypass the reactor for feed analysis measurements. The reactor is a 0.635-cm (1/4-inch) outer diameter stainless steel tube placed in a resistively heated furnace capable of temperatures up to 700°C. Catalyst samples are packed in the reactor between plugs of quartz wool, and the sample is centered in the furnace. Temperature monitoring and control is done using an Omega CN4400 temperature controller, and an Omega 0.159-cm (1/16-inch) K-type thermocouple. The thermocouple is inserted into the reactor tubing and is in contact with the quartz wool upstream of the catalyst sample. Downstream of the reactor the product gases pass through a packed tube of Drierite desiccant to remove water before the analysis portion of the system.

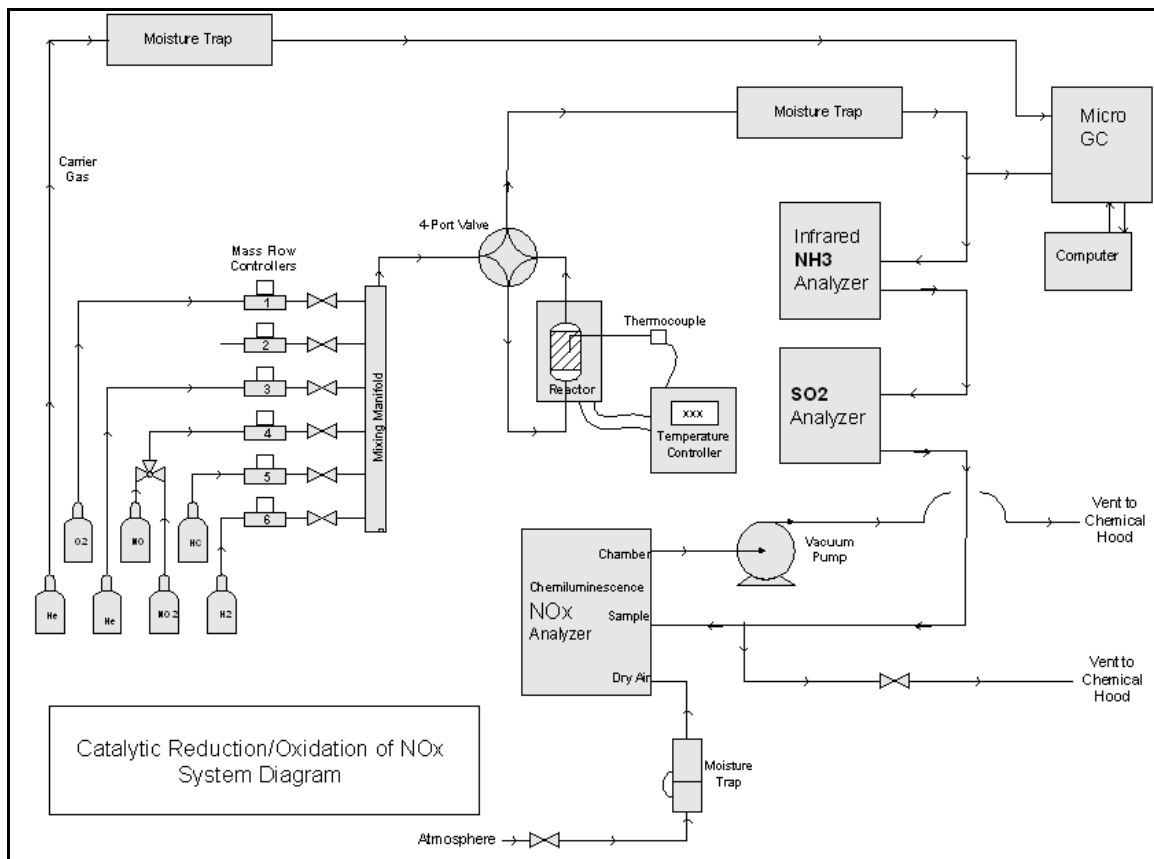


Figure 1: Schematic diagram of the steady-state reaction system.

Analysis of O₂, N₂, CH₄, CO₂, CO, and N₂O concentrations is performed by a Varian CP-4900 micro gas chromatograph. The micro-GC draws sample for 30 seconds to ensure flushing of the injection ports. The gas sample is then injected a Molecular Sieve 5A and a Porapak Q GC column. The two columns are arranged in parallel to reduce analysis time to less than 70 seconds. Gas concentrations are calculated from response factors determined using gases of known concentration.

NO and NO₂ concentrations are measured by a Thermo Environmental Model 42H Chemiluminescence NO_x analyzer. Sample is drawn into the instrument by an external pump. As sample enters the detection chamber it is mixed with O₃ generated by the instrument. The reaction of NO and O₃ results in an excited NO₂ molecule which decays to a lower energy state by light emission. A photomultiplier tube measures this emission. For the measurement of NO₂, the sample is passed through a molybdenum converter before entering the detection chamber. The converter reduces NO₂ to NO for detection. When the samples is passed through the converter a total NO_x measurement is taken, and NO₂ concentration is calculated as the difference of NO_x and NO.

Although it has not been used in the experiments conducted so far, a Thermo Environmental Model 43C Pulsed Fluorescence SO₂ Analyzer can also be incorporated into the analytical system. The analyzer operates by UV absorption by SO₂ molecules. The molecules reemit UV light at a different wavelength from what they absorb. This emitted light is measured by a photomultiplier tube and correlated to SO₂ concentration.

For both oxidation and reduction reaction experiments a steady gas flow of 45 cm³/min was maintained, corresponding to a gas hourly space velocity of around 50,000 hr⁻¹. The GHSV varies to some extent based on the porosity and density of the different catalysts formulations. Reaction temperatures were varied between 200°C and 500°C. Temperature steps were 100°C for course screening experiments, and ranged between 10°C and 50°C for more detailed analysis. At each temperature product monitoring was used to determine when steady state was reached (usually about 1 hour) before data were collected. In the experiments in which water was introduced, a heated bubbler was used in order to achieve the necessary H₂O vapor pressure. All lines downstream of the water bubbler were heated in order to prevent condensation. Reactant concentrations in NO₂ reduction experiments were set at: 1000ppm NO₂, 3000ppm methane, 10% oxygen, and balance helium. NO oxidation reactions were performed with 1000ppm NO and 10% O₂ in balance helium. Concentrations are based on volumetric measurements. All catalysts were pretreated by in-reactor calcination at 400°C in 10% O₂ for thirty minutes.

Temperature Programmed Desorption (TPD)

Temperature programmed desorption techniques were used in the characterization of catalyst surfaces, specifically in quantifying relative abundance of and strength of adsorption of reactant species to different types of catalyst sites. A catalyst sample was packed between quartz wool plugs in a quartz U-tube reactor. The reactor was placed in an electrically heated furnace controlled by an Omega CN4400 temperature controller and an Omega K-type thermocouple. Tylan FC-280 mass flow controllers controlled gas concentrations. Before TPD experiments catalysts were calcined in 5% O₂ at 400°C for 1

hour. Samples were then cooled under helium flow and flushed for 30 minutes. Analysis gas was then adsorbed at room temperature for 30 minutes, and the sample was again flushed with helium for 30 minutes to remove physisorbed species. After flushing the sample temperature was ramped at 10°C/min up to 600°C under helium. Analysis of desorbing species was performed by a HP-5989 mass spectrometer. A schematic of the temperature programmed desorption system is given in Figure 2.

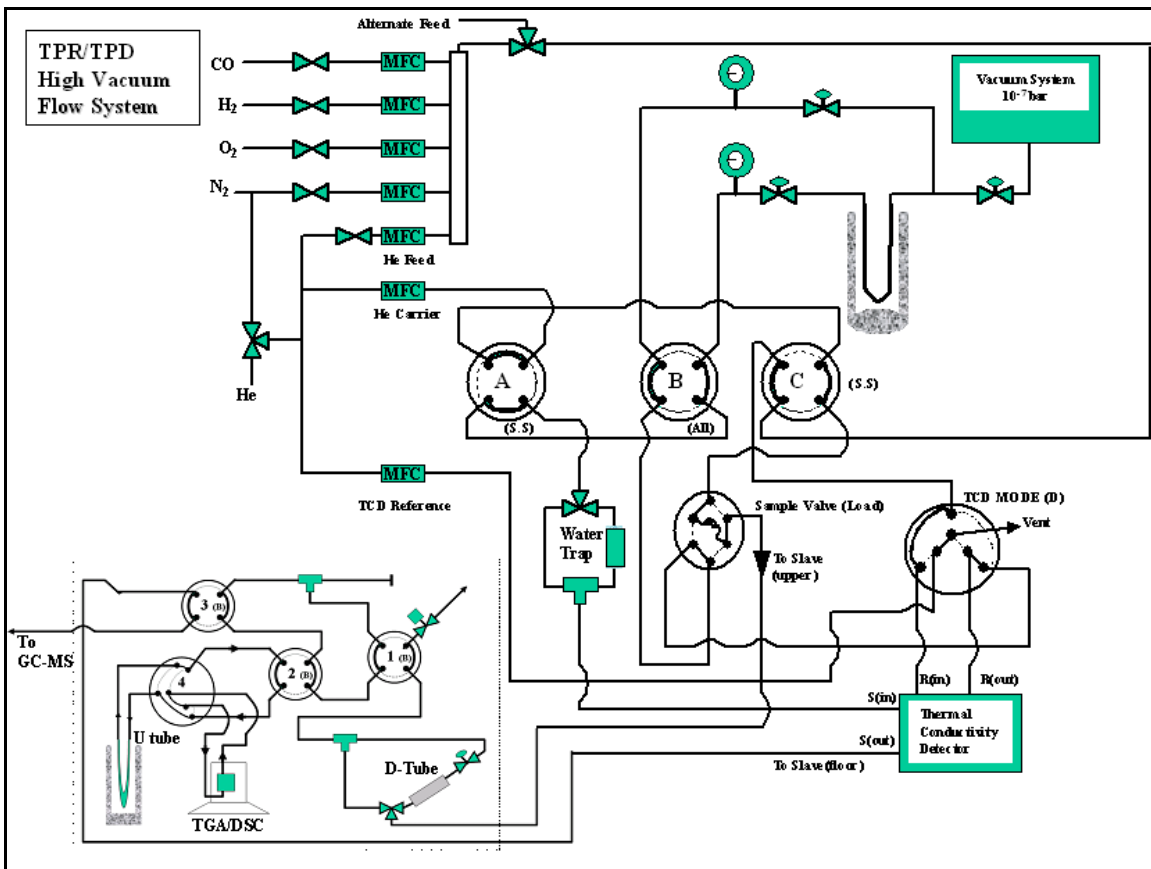


Figure 2: Schematic of the temperature programmed desorption system.

X-ray Photoelectron Spectroscopy (XPS)

XPS is a highly surface sensitive technique capable of elemental analysis as well as determination of oxidation state and chemical environment of surface atoms. An X-ray source is used to bombard the sample resulting in electrons being removed from surface atoms. The “binding” energy of these electrons is measured, and is characteristic of the element and its chemical environment. XPS experiments were performed on an AXIS Ultra instrument using a magnesium anode. Before analysis, samples are loaded in a high-vacuum preparation chamber where they are degassed overnight to a pressure of 10^{-6} torr. Samples are then transferred to the analysis chamber, which operates at an ultra-high vacuum of 10^{-9} torr. A survey of the complete binding energy range is performed to confirm expected peaks, then a more detailed scan of the binding energy range characteristic of each species of interest is performed. Charge shift correction was

performed based on the location of the carbon 1s peak. Peak deconvolution is done using the GRAMS software package.

X-ray Diffraction (XRD)

XRD is a technique for determining crystal structure of materials. A flat sample is exposed to X-rays, which diffract off the atomic planes of the crystal structure. Constructive interference occurs when the atomic spacing is an integer multiple of the X-ray wavelength, resulting in a characteristic diffraction peak. By moving source and detector through a range of angles relative to the sample a diffraction pattern is obtained. This pattern is characteristic of the material and crystalline phase being observed. XRD experiments were performed for phase identification and observations of supported metal crystal size. Diffraction patterns were taken using a Bruker D8 Advance X-ray diffractometer equipped with a Cu K α source with wavelength 1.54 Å. The unit is equipped with a controlled atmosphere/controlled temperature chamber, and a position sensitive detector capable of simultaneously scanning across an 8° angle. The temperature can be varied from cryogenic temperatures to 1200°C. Samples are placed in shallow sample holders and pressed flat with a glass microscope slide. Diffraction patterns were taken across a range of 20-90° 2 θ .

Thermogravimetric Analysis (TGA)

TGA experiments were performed to examine the weight changes associated with catalyst preparation procedures. Both precursor removal and bulk crystalline structure changes during calcination were observed. Experiments were run on a Perkin-Elmer TGA7 thermogravimetric analyzer. After taring, approximately 40 mg of catalyst was loaded into the sample pan. Under a flow of 40 cm³/min of air the catalyst was calcined up to 800°C while monitoring weight.

Temperature-Programmed Reaction (TPR_{xn})

Temperature programmed reaction experiments were conducted in order to observe the reactor effluent composition at any given temperature throughout the range of interest. These experiments also allow for the observation of the light-off temperature, at which point selective catalytic reduction producing N₂ occurs, and also the temperature range in which hydrocarbon combustion begins to dominate the selective reduction.

Catalyst samples of 130mg were loaded between two quartz wool plugs in a quartz U-tube reactor. The reactor is placed in an electrically heated furnace controlled by an Omega CSC32 temperature controller and an Omega K-type thermocouple. The sample was then calcined in 5% O₂ at 300°C for 1 hour and then cooled to room temperature under helium flow. Gas flow rates were controlled by Brooks 5850E mass flow controllers and total gas flow rates were 30 mL/min. The feed gas containing 1000ppm NO_x, 3000ppm CH₄, and 5% O₂ was then introduced to the sample and allowed to equilibrate. The temperature was then ramped at 10°C/min from room temperature to 600°C. To prevent condensation of any H₂O formed during the reaction, the stainless steel lines downstream of the reactor were heated using heating tape controlled by a

Variac voltage controller. The analysis of gas phase products and reactants was conducted by monitoring the effluent with a Shimadzu QP5050 GC/MS mass spectrometer. In order to attribute various mass to charge (m/z) signals to a particular molecular species, corrections were made to eliminate interference caused from molecular fragmentation due to the electron impact ionization process.

Diffuse Reflectance Infrared Fourier Transform Spectroscopy (DRIFTS)

DRIFT spectroscopy is an IR absorption technique particularly suited to analysis of powdered samples. Signal is based on the diffuse reflectance portion of the light coming off of the sample. Specular reflectance, which has not interacted with the sample, is blocked. The diffuse reflectance signal has penetrated particles and interacted with adsorbed species. Control of sample temperature and surrounding atmosphere allow for the monitoring of surface species under temperature ramps and feed concentration changes. A Bruker IFS66 instrument equipped with both a liquid N₂ cooled MCT detector and a DTGS detector and a KBr beamsplitter was used for DRIFTS experiments. Catalyst samples were placed in a sample cup inside a Spectratech diffuse reflectance cell equipped with KBr windows and a thermocouple mount that allowed direct measurement of the surface temperature. Spectra were averaged over 1000 scans in the mid-IR range (400-4000cm⁻¹) to a nominal 2 cm⁻¹ resolution. Catalyst samples were placed in the spectrometer and calcined at 400°C for 1 hour. The sample was then flushed with helium for 30 minutes, and the reactant feed adsorbed for 30 minutes at room temperature. Spectra were then taken at increasing temperature to monitor the evolution of surface species.

Temperature-Programmed Reduction (TPR)

Temperature-programmed reduction experiments were carried out on the oxidation catalysts on a versatile system that was designed and built by the P.I.'s research group. TPR is a bulk technique and allows for the determination of the strength of the metal-support interaction, the average metal oxidation state, quantification of metal sites in various oxidation states, and the number of different types of metal sites.

The hydrogen that is consumed in reducing the metal species was measured using a thermal conductivity detector (TCD). The TCD was interfaced to a computer, allowing for data acquisition and control, and operates by comparing the thermal conductivity of the gas stream entering the reactor (reference) to the stream leaving the reactor (sample) and sending a voltage signal proportional to the difference to the computer. A water trap located after the reactor but before the TCD is used to remove gas phase water that is created during the reduction so that there is no interference from additional species between the reference and sample gas streams.

In these TPR experiments, 100mg of catalyst was positioned between two quartz wool plugs and loaded into a quartz, U-tube reactor. The sample surface was pretreated by exposure to 10% O₂ at 300°C for one hour. The sample was then cooled to room temperature under nitrogen flow and allowed for flush for 30 minutes. The catalyst was then exposed to 10% H₂ and the temperature was ramped at 10°C/min from room

temperature to 800°C. The temperature was controlled with an Omega CN4400 temperature controller and measured using an Omega K-type thermocouple. All gas flow rates were 30 mL/min.

Results and Discussion

Co-Based Catalysts for the Oxidation of NO to NO₂

The oxidation of NO to NO₂ is an exothermic reaction and is thus thermodynamically limited at higher temperatures. In the upper end of the temperature range of interest thermodynamics rather than kinetics will limit the oxidation of NO to NO₂. Figure 3 shows the achievable equilibrium NO₂ yields for 1000ppm NO in various O₂ concentrations. Higher O₂ concentrations push the equilibrium to the right and allow for greater NO₂ yields due to Le Chatelier's Principle. Since the reaction is exothermic however, increasing the temperature results in a decrease in the equilibrium constant, pushing the equilibrium to the left and decreasing the equilibrium NO₂ yield.



Due to the temperature sensitivity of the reaction, catalysts active at low temperatures must be developed in order to achieve high NO₂ yields.

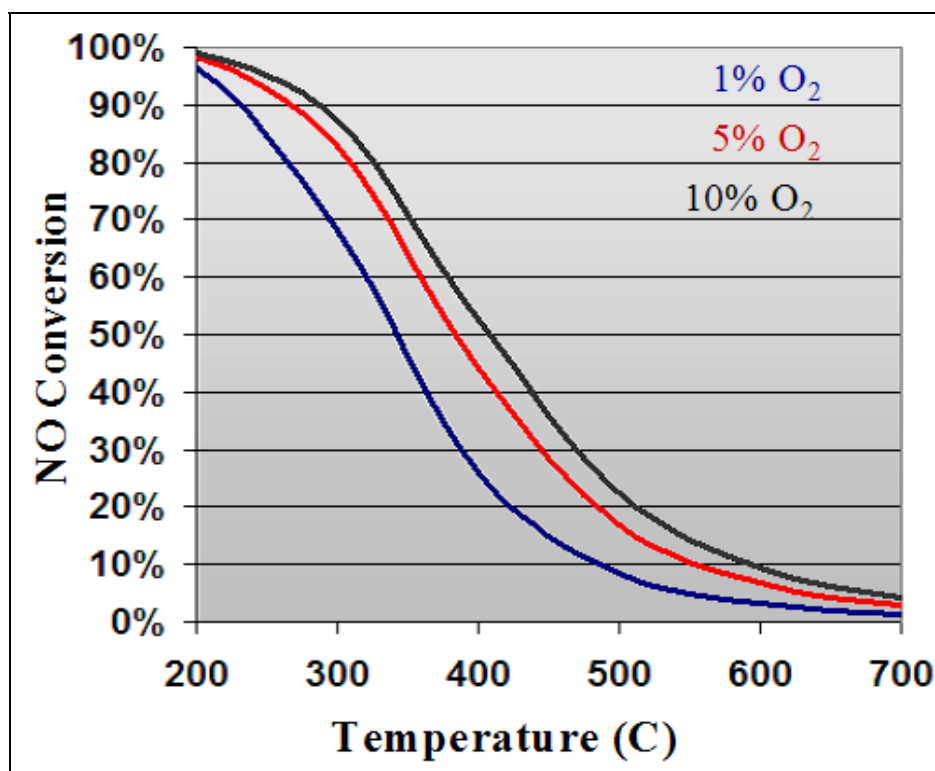


Figure 3: Equilibrium NO₂ yields for 1000ppm NO in various O₂ concentrations.

Literature references have shown that high loadings of cobalt can be active for the oxidation of NO to NO₂^{1,2,3,4,5}. Several series of Co-based catalysts were synthesized and tested for the NO to NO₂ oxidation reaction. Oxidation catalysts were prepared through both incipient wetness impregnation and sol-gel methods, on both titania and zirconia supports. The effect of Co loading on activity was also examined over zirconia supports. Support choice, preparation procedure, and metal loading have all been shown to be important in determining NO oxidation activity.

NO oxidation results over 10%Co/TiO₂ prepared through sol-gel synthesis are shown in Figure 4. These catalysts were prepared through the same method, but calcined at different temperatures in the range of 300-600°C. Reaction conditions were 1000ppm NO, and 10% O₂ in balance He. Reactions were performed based on equal catalyst weight. For 10%Co/TiO₂ SG catalysts an activity maximum is observed with increasing calcination temperature. The sample calcined at 400°C shows that highest activity, reaching the equilibrium conversion above 85% at around 300°C at a GHSV of 50,000 hr⁻¹. The catalysts calcined at 300, 500, and 600°C all performed significantly worse and did not reach equilibrium conversion until approximately 400°C using the same GHSV. For all of the reactions, once equilibrium conversion was reached, activity followed the expected equilibrium curve.

10%Co/TiO₂ catalysts prepared through incipient wetness impregnation were also calcined at various temperatures, and the effect of this preparation step on activity was examined. NO oxidation results over incipient wetness prepared catalysts are presented in Figure 5. Reactions were again performed under 1000 ppm NO, and 10% O₂ in balance He, with catalyst weight held constant in all reactions. As with the sol-gel samples the calcination temperature strongly affects NO oxidation activity. This trend however is not the same as in the sol-gel prepared catalysts. Instead, over the incipient wetness catalysts maximum activity decreases with increasing calcination temperature. The catalysts calcined at 300°C reaches equilibrium conversion above 85% near 300°C, similar to the best performing sol-gel catalyst. The loss of activity observed with increasing calcination temperature is less significant than in the sol-gel formulations, with even the least active 10%Co/TiO₂ IW600 reaching equilibrium conversion below 350°C. The GHSV for these runs are about 50,000 hr⁻¹.

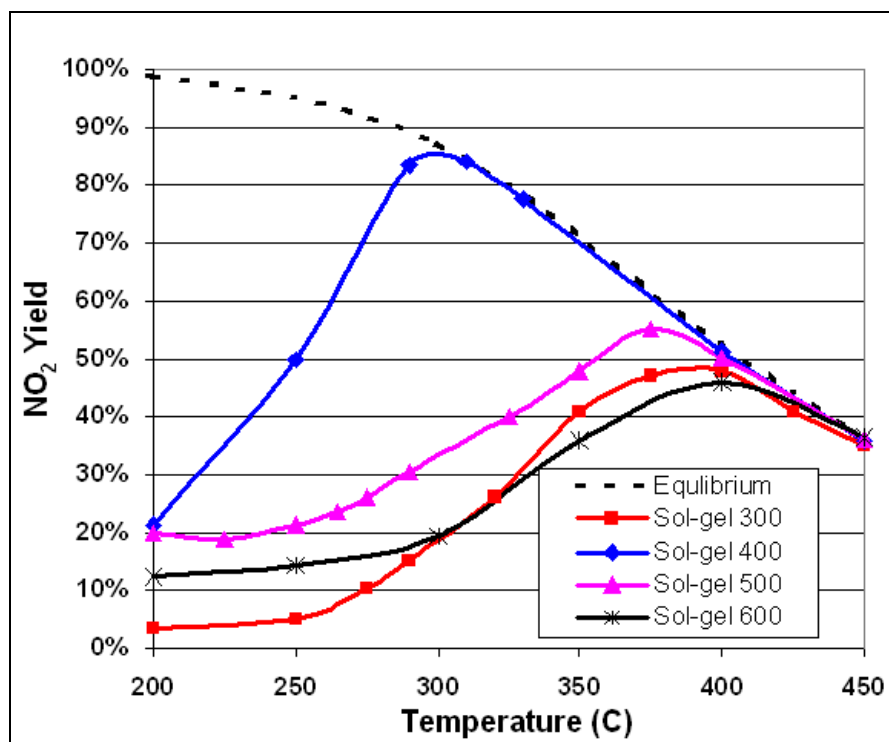


Figure 4: NO oxidation over 10%Co/TiO₂ Sol-Gel catalysts calcined at different temperatures. 1000ppm NO, 10% O₂.

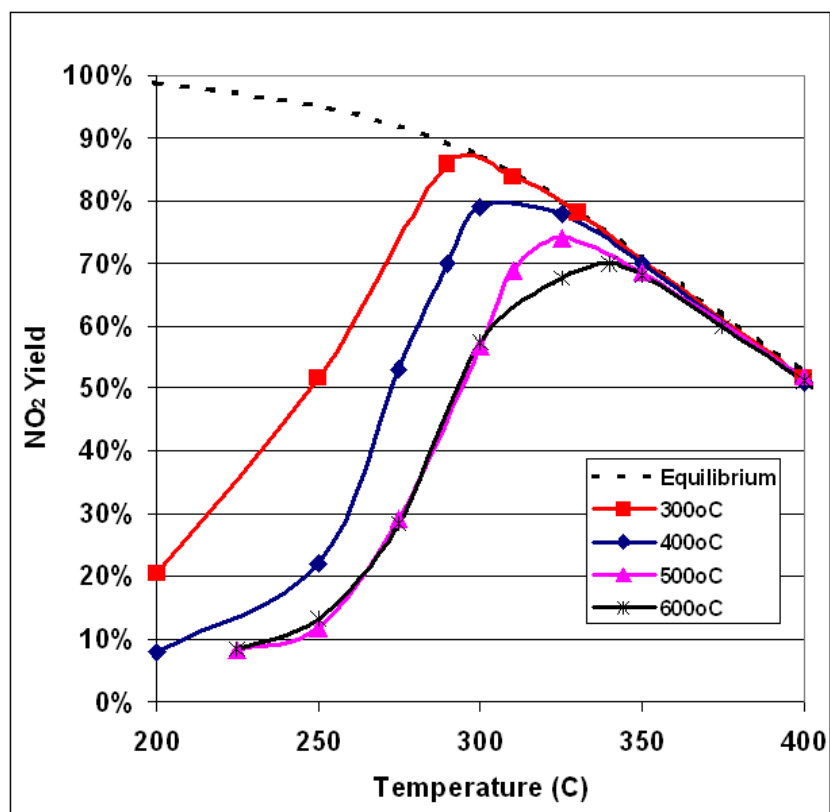


Figure 5: NO oxidation over 10%Co/TiO₂ Incipient Wetness catalysts calcined at different temperatures. 1000ppm NO, 10% O₂.

To investigate the thermal stability of these 10%Co/TiO₂ catalysts, several characterization methods were employed to explain the activity differences observed with changing preparation methods. BET surface area analysis shows that calcination temperature affects catalyst surface area. This effect is particularly strong for the sol-gel prepared samples. BET surface area results are shown in Figure 6. The 10%Co/TiO₂ SG catalysts suffered an enormous surface area loss with increased calcination temperature. When the sol-gel catalyst is calcined at 300°C the surface area was 274m²/g. Increased calcination temperature decreases this value to 5m²/g for 10%Co/TiO₂ SG600. The surface area change is less severe in the incipient wetness samples with a reduction from 64 to 32 m²/g over this calcination temperature range. Comparison to steady-state activity measurements indicates that the loss of surface area does not fully explain the activity loss with increasing calcination temperature. This is most evident when comparing the sol-gel 300°C and 400°C samples. The sample calcined at lower temperature has a much higher surface area, but a lower oxidation activity.

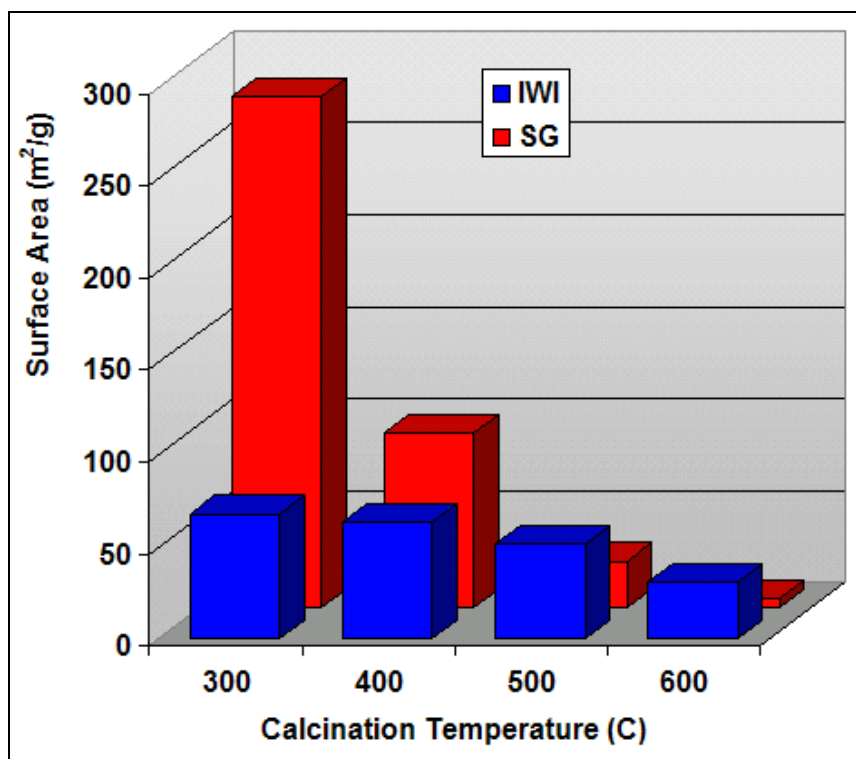


Figure 6: Effect of calcination temperature on BET surface areas of 10%Co/TiO₂ catalysts prepared through incipient wetness and sol-gel methods.

TPR was used to examine the supported Co species and their interaction with the support. After calcination in the reactor under 10%O₂/He to ensure complete oxidation of the metal, the samples were reduced under a flow of 5%H₂/He at a ramp rate of 10°C/min. Figure 7 shows the complete results for both preparation methods. The main reduction features are observed to occur at lower temperatures over the incipient wetness prepared catalysts at all calcination temperatures. With both preparations the main reduction feature shifts to higher temperatures with increasing calcination temperature. Such a shift

is indicative of a stronger interaction between Co and the TiO₂ support. Over the incipient wetness samples a second, smaller reduction peak is observed 50-100°C lower than the principle peak. This smaller feature is most visible in the sample calcined at 300°C, and it seems to blend into a shoulder of the main peak at higher calcination temperatures. Such a feature is not observed on the sol-gel samples. In the literature the low temperature peak is assigned to the reduction of Co³⁺ to Co²⁺, while the high temperature feature is due to the reduction of Co²⁺ to metallic Co. These TPR results then indicate that Co is present in the sol-gel catalysts mainly in the 2+ (CoO or Co(OH)₂) oxidation state, while the incipient wetness catalysts contain a mixture of oxidation states. Additionally the higher temperature of reduction in the sol-gel samples reveals a much stronger interaction between metal and support than in the incipient wetness samples.

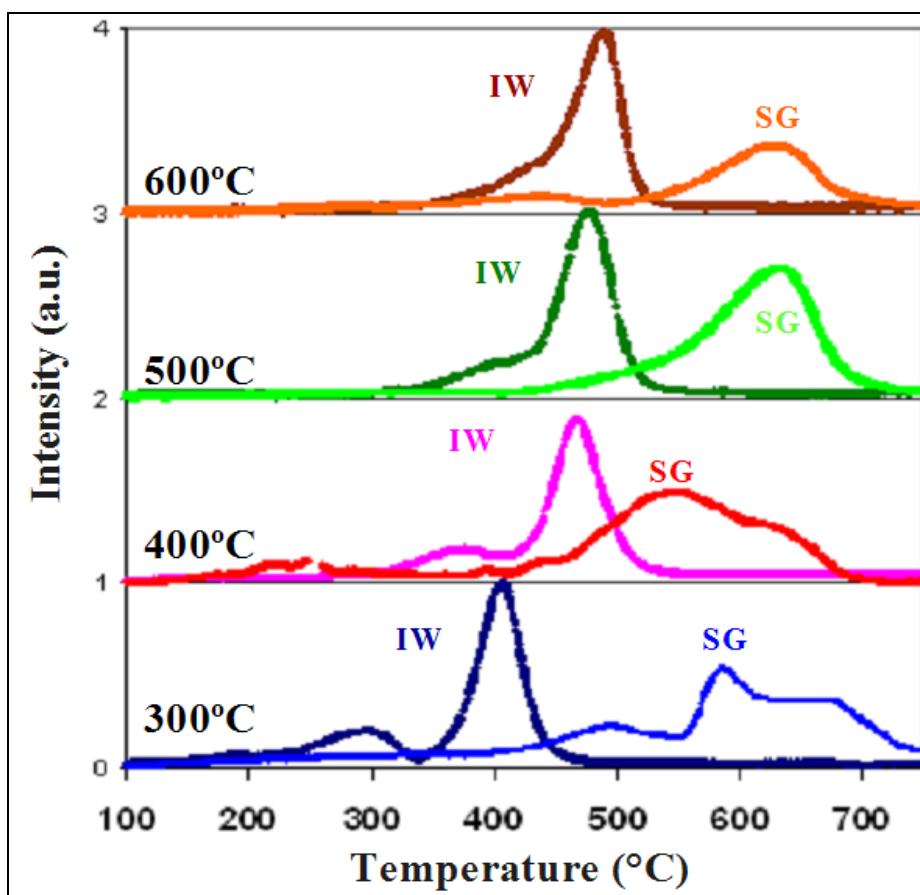


Figure 7: TPR profiles of 10%Co/TiO₂ prepared through sol-gel and incipient wetness methods and calcined at different temperatures.

Confirmation of different Co oxidation states on the catalyst surface was obtained through XPS. Figure 8 shows the Co $2p_{3/2}$ XPS region of both the 10%Co/TiO₂ SG300 and the 10%Co/TiO₂ IW300 catalysts. In the incipient wetness sample the peak is centered on 778.5 eV, in the range of the binding energy of the Co³⁺ oxidation state, characteristic of Co₃O₄. In the sol-gel sample the peak is located at 781.0 eV in the characteristic range of Co²⁺. Since this is a higher binding energy than what is expected for a CoO species, it seems more likely that this feature is due to a Co(OH)₂ species left over from the preparation. The shake-up peak at 786.7 eV only occurs for the 2+ oxidation state and is consistent with this the assignment.

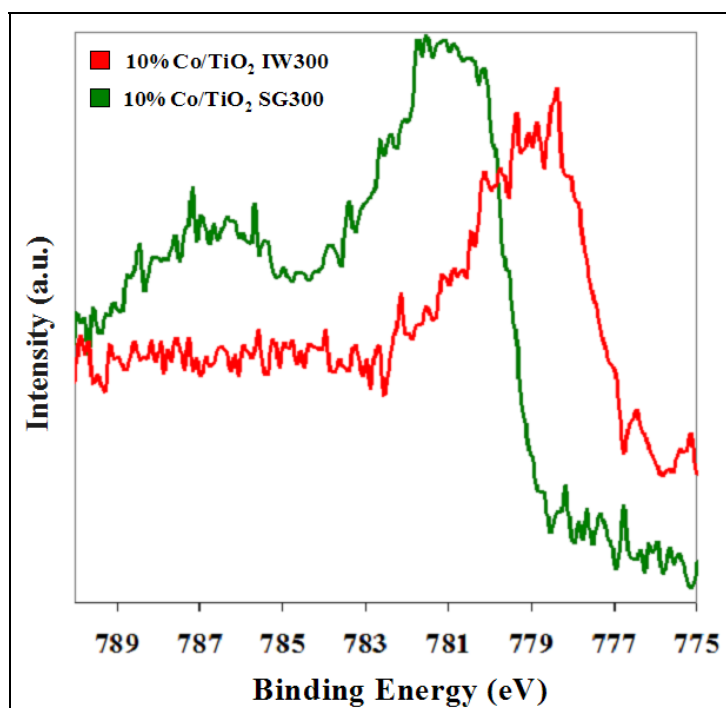


Figure 8: Co $2p_{3/2}$ XPS spectra of 10%Co/TiO₂ SG300 and IW300.

XPS was also used to confirm the stronger metal-support interaction with increasing calcination temperature. Figure 9 shows a shift in the Co $2p_{3/2}$ binding energy in 10%Co/TiO₂ incipient wetness samples with increasing calcination temperature. As interaction with the support increases, the electron environment of surface Co changes leading to a shift in binding energy. The shift is observed to occur toward higher binding energy, closer to the characteristic range of the Co²⁺ oxidation state. The appearance of a shake-up peak also supports this assignment. Although XPS alone does not allow a definite assignment, it is possible that this feature is due to a titanate phase. In-situ XRD results presented in the following sections confirm this hypothesis.

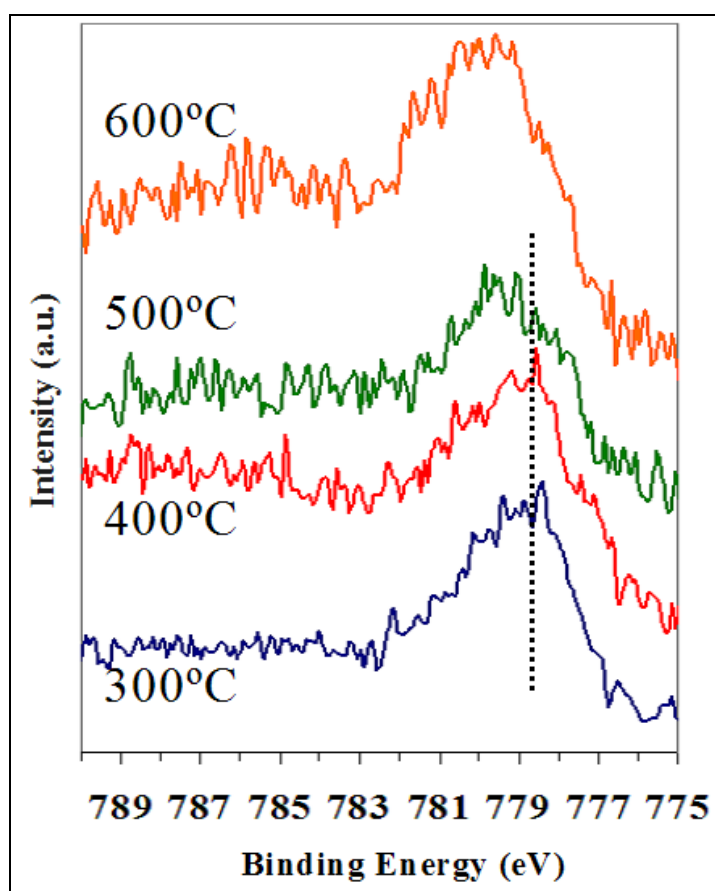


Figure 9: Co $2p_{3/2}$ XPS spectra of 10%Co/TiO₂ IW calcined at different temperatures.

Changes in oxidation state can be indicative of a transformation to a different metal oxide. Such bulk changes would be accompanied by a sample weight change. TGA analysis of the calcination of 10%Co/TiO₂ prepared by incipient wetness was performed up to 800°C. Figure 10 shows both the percent weight loss and the differential signal from this experiment. Significant weight loss is observed at temperatures below 300°C. Such a loss is expected due to the evaporation of water from the catalyst pores, and from the decomposition of remaining nitrate precursors. A gradual weight loss occurs with increasing temperature until just above 660°C when a sudden drop occurs. Adsorbed water and precursor remnants would no longer be present at this high of a temperature. This mass loss is thus due to a bulk transformation in the catalyst.

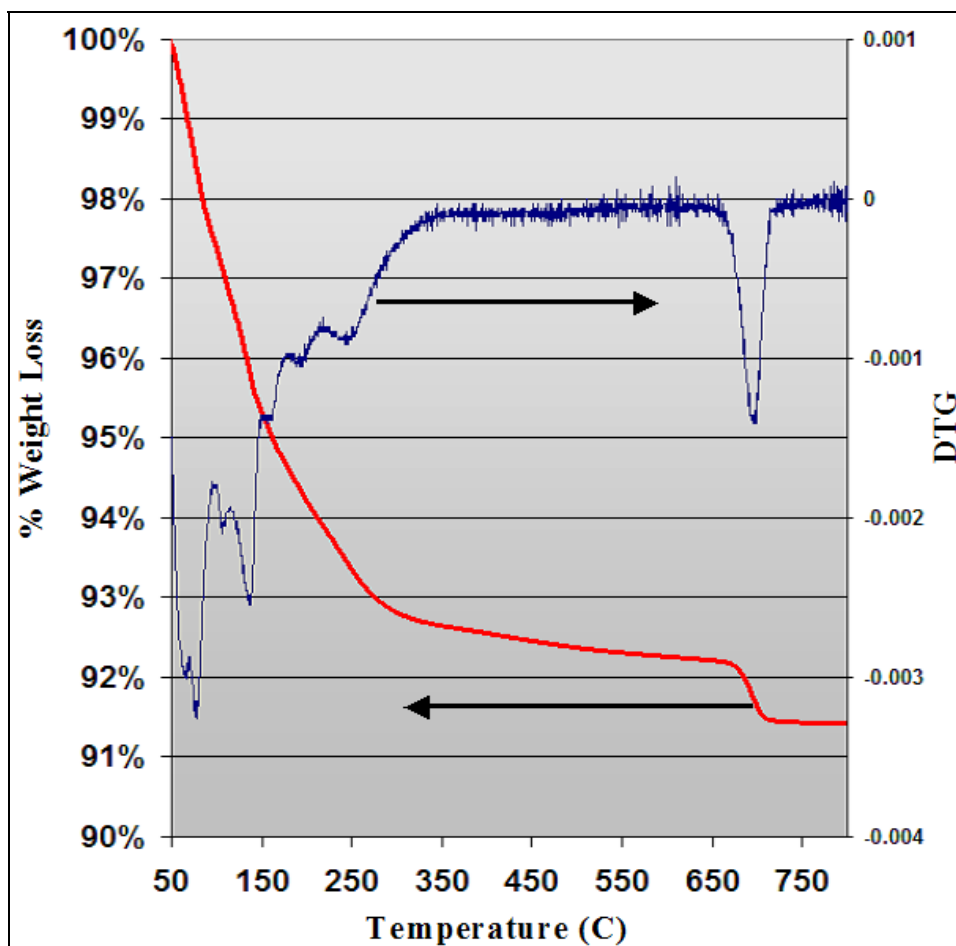


Figure 10: Calcination by TGA of 10%Co/TiO₂ prepared by incipient wetness impregnation. Both percent weight loss (left) and the differential weight signal (right) is shown.

TGA calcination of 10%Co/TiO₂ prepared by sol-gel has a much larger weight loss at low temperatures, associated with the burning off of the organic precursor material. A gradual weight loss continues with increasing temperature, but no sudden change is observed.

To observe this bulk change in the catalyst, the crystalline phases were examined by performing the calcination using *in-situ* XRD measurements. Under a constant flow of 10% O₂/He the sample temperature was raised in 50°C increments, and a XRD scan was taken at each step. Figures 11 and 12 show XRD patterns taken between 350 and 750°C over the 10%Co/TiO₂ catalysts prepared by sol-gel and incipient wetness, respectively.

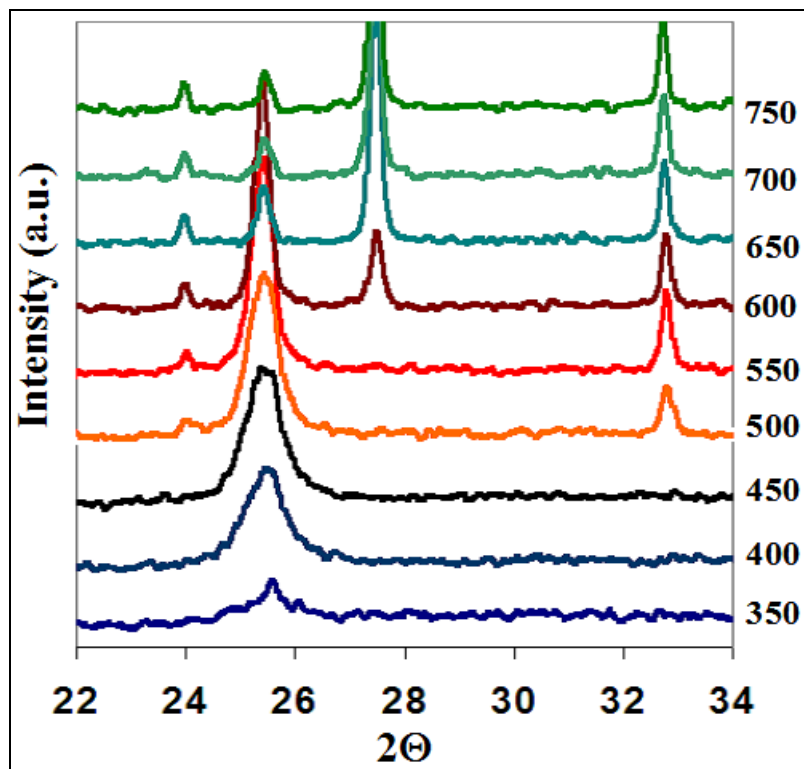


Figure 11: *In-situ* XRD during the calcination of 10%Co/TiO₂ prepared by sol-gel.

For both catalysts a large, sharp peak was observed at around 25.5° 2θ across the temperature range. This peak is characteristic of the anatase TiO₂ phase. At low temperatures in the sol-gel sample very little crystallinity was observed, however this increases with increasing temperature. This observation likely explains the low reaction activity of the 10%Co/TiO₂ SG300. In the calcination of the sol-gel prepared catalyst the anatase TiO₂ peak decreases in intensity corresponding to the growth of a peak at 27.5° 2θ, starting at 600°C. This new peak is characteristic of the rutile TiO₂ phase and demonstrates that the support undergoes a bulk phase transition at high temperatures. The 27.5° 2θ peak is also observed during the calcination of the incipient wetness catalyst, not however until 750°C. Crystalline Co phases are not observed over either catalyst. The lack of observed Co crystals indicates a high dispersion of the metal. With increasing calcination temperature in both preparations the formation of an additional cobalt titanate phase was observed. This phase was identified through the development of peaks near 24 and 33° 2θ. In the sol-gel sample the titanate phase appears at 500°C, while over the incipient wetness sample it is not observed until 650°C is reached. The formation of the titanate at lower temperatures in the sol-gel sample may be due to

atomic scale mixing of Co and Ti during the preparation. Incipient wetness impregnation on the other hand would result in metal clusters across the surface only. The more intimate contact may allow the earlier formation of the mixed material. Such an analysis is supported by the differences in reduction temperature observed through TPR. Additionally, the high temperature weight loss seen in TGA of the incipient wetness calcination corresponds closely to the appearance of the titanate as observed by XRD.

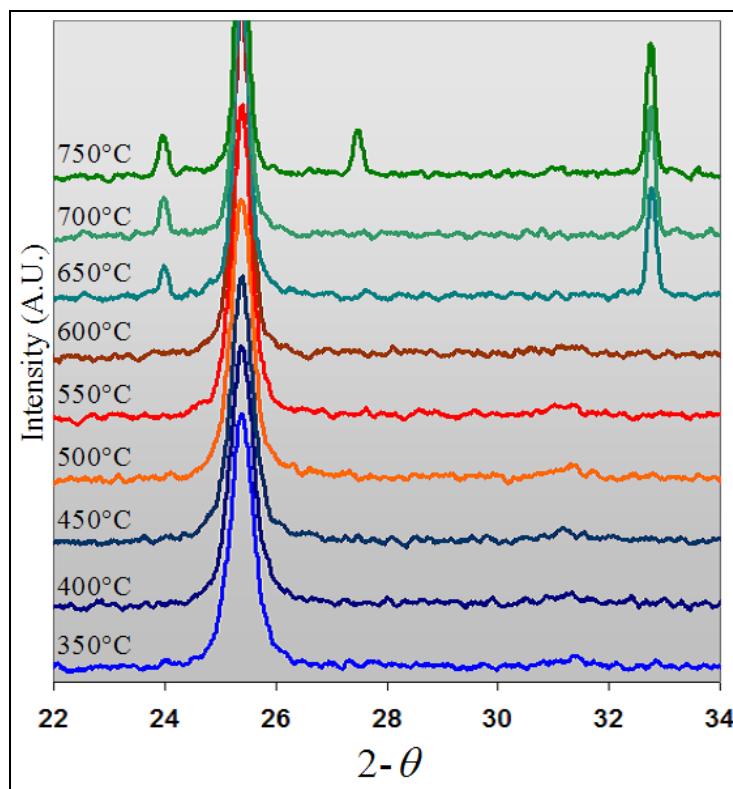


Figure 12: *In-situ* XRD during the calcination of 10%Co/TiO₂ prepared by incipient wetness.

Characterization of 10%Co/TiO₂ catalysts prepared through both sol-gel and incipient wetness methods, when correlated to activity studies, yields important information on the synthesis of an effective NO oxidation catalyst. Improved activity correlates with relatively low metal-support interactions, as well as with the presence of some Co in the 3+ oxidation state. Co supported on TiO₂ can be an active catalyst with proper preparation, however such systems appear to be highly thermally sensitive as they form an inactive cobalt titanate phase at high temperature.

To improve the thermal stability of the NO oxidation catalysts a series of Co-based catalysts supported on ZrO₂ was prepared. ZrO₂ is not known to form a mixed phase analogous to the cobalt titanate. Table 2 contains BET surface area measurements for 10%Co/ZrO₂ catalysts prepared through incipient wetness impregnation. Surface areas decrease slightly with increasing calcination temperature; although the decrease is much less than on the TiO₂ supported samples.

Calcination Temperature (°C)	BET Surface Area (m ² /g)
300	43
400	42
500	41
600	37

Table 2: BET surface area on incipient wetness 10%Co/ZrO₂ calcined at different temperatures.

Figure 13 shows steady-state reaction results obtained over 10%Co/ZrO₂ catalysts. Reaction conditions were 1000ppm NO, 10% O₂ in balance He, with catalyst weight is kept constant. Oxidation activity decreases slightly with increasing calcination temperature, however this effect is much less significant than over the TiO₂ supported catalysts. 10%Co/ZrO₂ IW300 reaches the equilibrium conversion above 90% at around 250°C. The 10%Co/ZrO₂ IW600, while slightly less active, still outperforms the best TiO₂ supported catalysts, reaching equilibrium conversion near 275°C at a GHSV of 50,000 hr⁻¹.

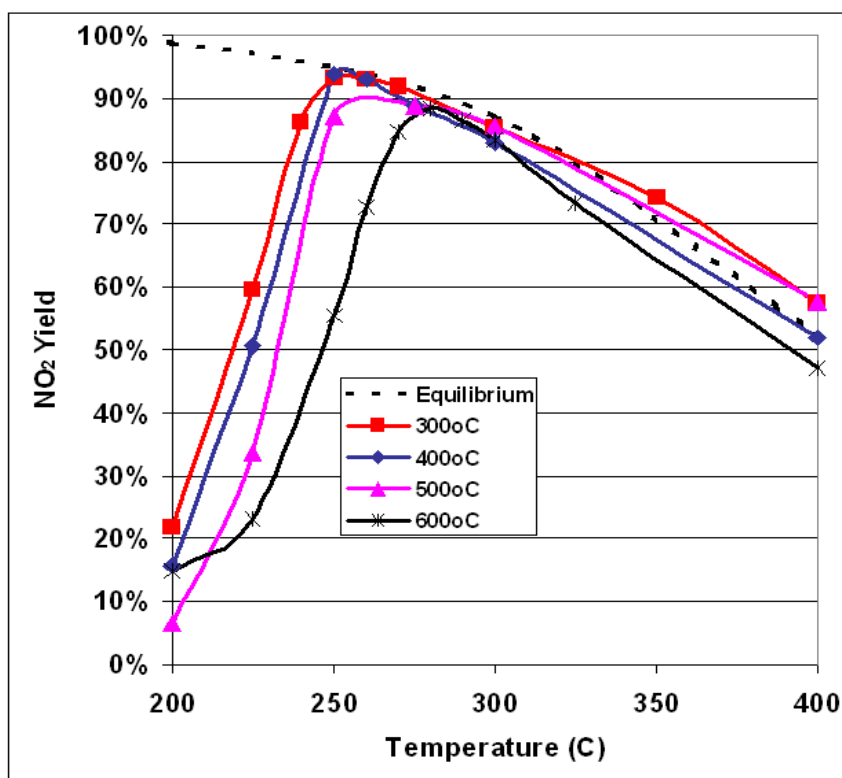


Figure 13: Oxidation of NO to NO₂ over 10%Co/ZrO₂ catalysts prepared by incipient wetness and calcined at different temperatures.

TPR results from the ZrO_2 supported oxidation catalysts are presented in Figure 14. Two distinct reduction features are observed. The low temperature feature between 250-300°C is due to the reduction of Co^{3+} to Co^{2+} while the high temperature feature between 450-500°C is due to the reduction of Co^{2+} to metallic Co. These feature assignments are similar to those made over Co/TiO_2 IW catalysts, however the relative intensities of these features is significantly different. The low temperature peak is much more intense, and does not disappear with increasing calcination temperature. This therefore indicates the presence of significant amounts of Co_3O_4 on the catalyst. The peak locations do shift to higher temperature with increasing calcination temperature again indicating increased metal-support interaction. In the ZrO_2 supported samples this does not seem to change the Co oxidation state.

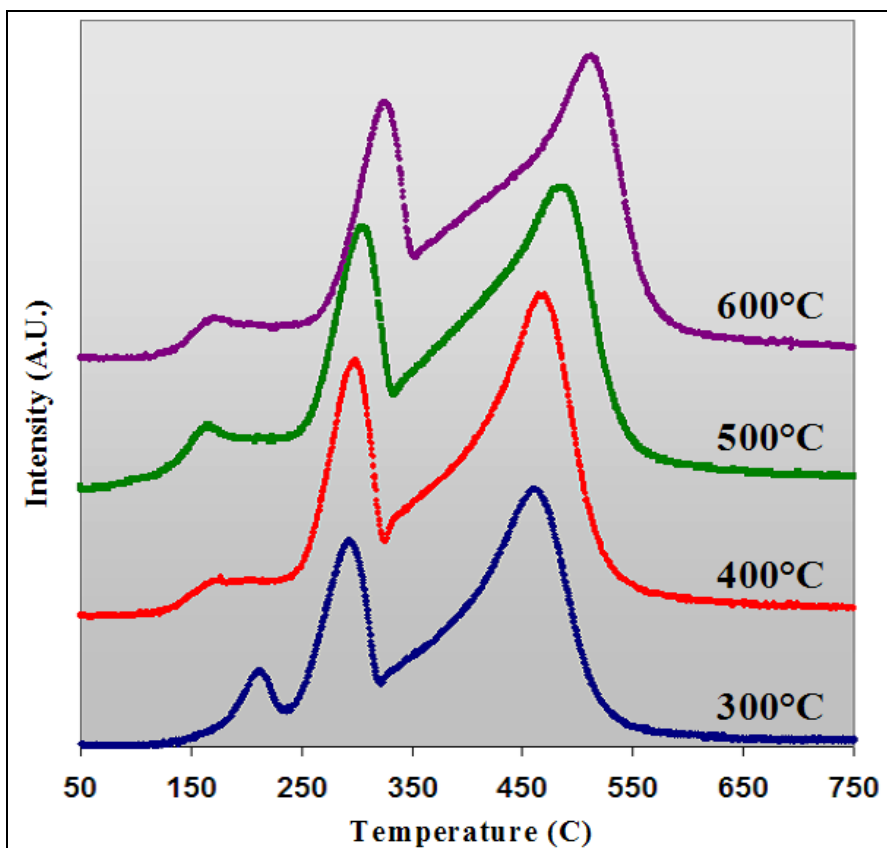


Figure 14: TPR profiles of 10%Co/ ZrO_2 catalysts prepared through incipient wetness and calcined at different temperatures.

XPS was used to characterize the 10%Co/ ZrO_2 IWI samples calcined at 300°C, 400°C, 500°C, and 600°C. Figure 15 shows the XPS spectra of the Co 2p region that were obtained. The observed binding energies of the Co $2p_{1/2}$ and $2p_{3/2}$ at 795.8 eV and 780.3 eV correspond to the cobalt oxide as Co_3O_4 . There is no significant change in the electron binding energies as the calcination temperature is increased. The stability of the Co 2p region indicates that the electronic environment around the cobalt atoms is virtually unchanged as the catalyst is calcined from 300°C to 600°C, suggesting that

cobalt is present in the highly oxidized form of Co_3O_4 even at a relatively low calcination temperature of 300°C .

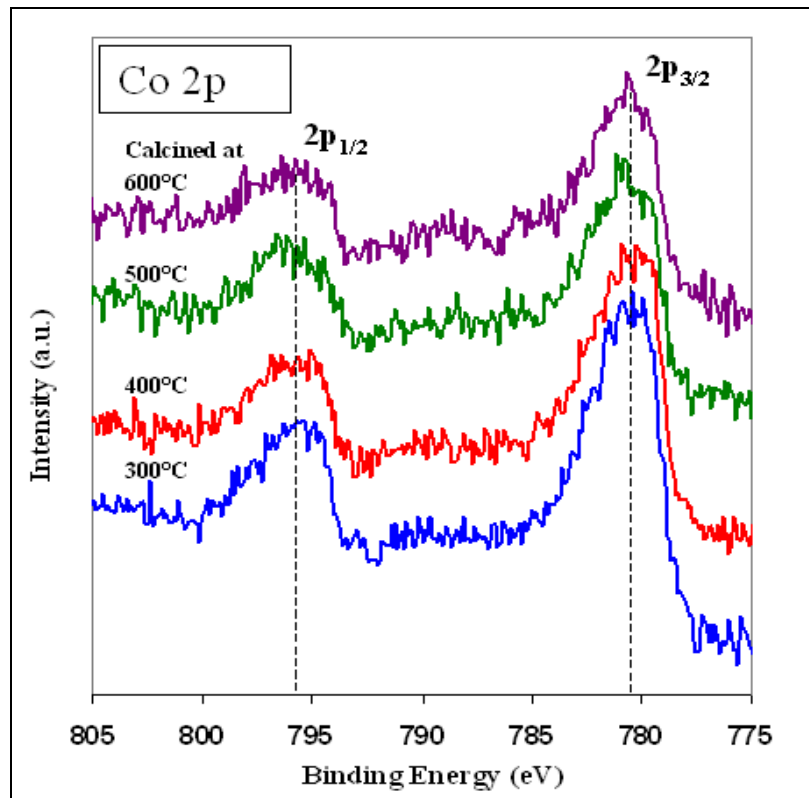


Figure 15: Co $2p_{3/2}$ XPS spectra of 10%Co/ZrO₂ IW calcined at different temperatures.

Results from *in-situ* XRD measurements during the calcination of 10%Co/ZrO₂ prepared by incipient wetness are shown in Figure 16. Under a constant flow of 10% O₂ the sample temperature was raised in 50°C increments and a XRD scan was taken at each step. The principle peaks observed at 28 and 31.5° 2θ are characteristic of the monoclinic ZrO₂ support. These characteristic peaks narrow with increasing temperature indicating increased crystallinity. Throughout the temperature range there was no development of additional peaks that would indicate a bulk phase change or the formation of a Zr-Co mixed phase. On the ZrO₂ supported oxidation catalyst bulk Co₃O₄ is observed by a characteristic peak near 36.5° 2θ.

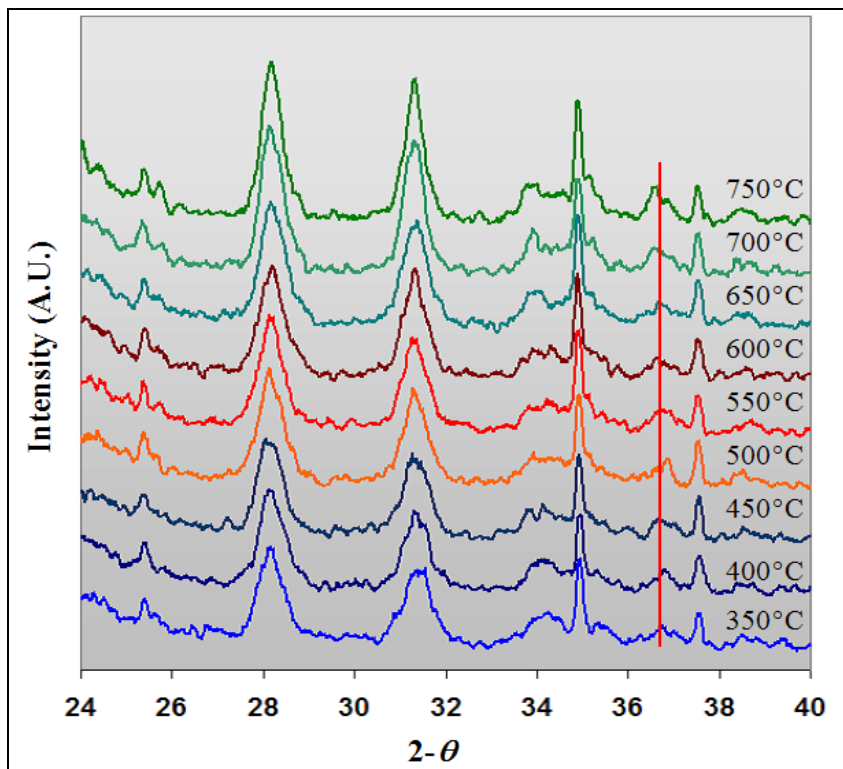


Figure 16: *In-situ* XRD during the calcination of 10%Co/ZrO₂ prepared by incipient wetness.

A crystalline Co phase was not observed over the TiO₂ supported catalysts. The overall characterization of the 10%Co/ZrO₂ IW catalysts indicate that using the ZrO₂ support results in a significant amount of Co³⁺ in Co₃O₄ present on the surface. Furthermore XRD indicates that this species is present in larger crystallite clusters than over TiO₂. The presence of Co in this phase correlates with higher activity for the NO oxidation reaction and with higher thermal stability.

Reduction of Co loading while maintaining oxidation activity would lead to a reduction in eventual catalyst cost. The effect of Co loading on the NO oxidation activity of Co/ZrO₂ catalysts prepared through incipient wetness was thus examined. Catalysts were prepared with Co loadings of 15%, 10%, 5%, and 1% and calcined at 350°C. Reaction test conditions were 1000 ppm NO, and 10% O₂ in balance helium. Catalyst weight was kept constant in these reactions. High NO oxidation activity was observed over all Co loadings, with no appreciable difference between the 15%, 10%, and 5% Co catalysts. Each attained equilibrium conversion above 90% near 250°C. When the loading is reduced to 1% decreased activity is observed, although equilibrium conversion is still reached by 300°C.

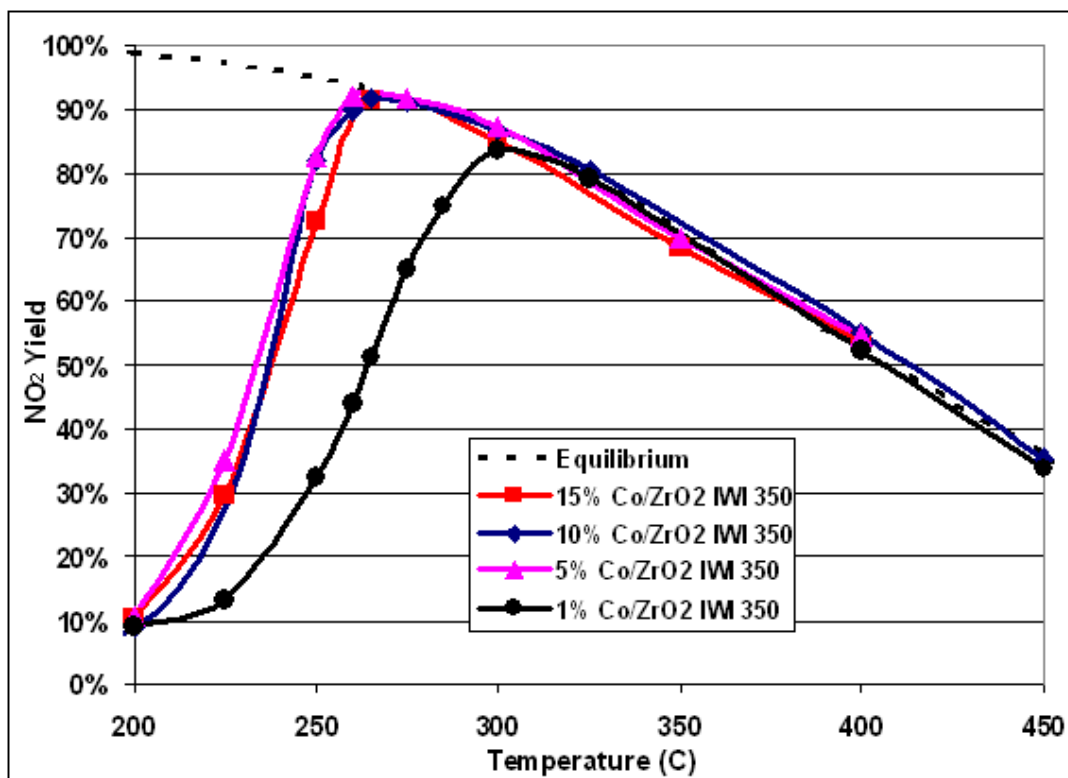


Figure 17: Effect of metal loading on Co/ZrO₂ IWI 350.

The selection of ZrO₂ as support material for Co-based NO oxidation catalysts results in highly active and thermally stable materials. Correlation of steady-state activity measurements with detailed characterization has allowed for the designed synthesis of these catalysts.

Ag-Based Catalysts for the Reduction of NO₂ with Hydrocarbons

Low loadings of transition metals, particularly silver, have been examined in the literature for the hydrocarbon reduction of NO.^{6,7} Mechanistic studies of the propane reduction of NO over Ag/Al₂O₃ have been performed by Meunier and Ross indicating that adsorbed NO_x species are key intermediates in the reduction to N₂.⁵ Improved activity for the reduction of NO₂ has also been noted.⁸ Several Ag-based catalysts were synthesized and tested for the reduction of NO₂ with propene, propane, and methane. Catalysts were prepared by both sol-gel and wet impregnation methods. Table 3 presents synthesis parameters and BET surface area measurements for these catalysts. Ag/TiO₂-ZrO₂ catalysts were prepared through sol-gel techniques, while Ag/Al₂O₃ catalysts were prepared by incipient wetness impregnation of a commercial Al₂O₃ support.

Catalyst	Calcination	SA m ² /g
1%Ag/TiO ₂ -ZrO ₂	500C 4hr Air	104
3%Ag/TiO ₂ -ZrO ₂	500C 4hr Air	65
1%Ag/Al ₂ O ₃	500C 4hr Air	161
3%Ag/Al ₂ O ₃	500C 4hr Air	171

Table 3: BET surface areas of Ag-based catalysts.

Figure 18 presents the NO₂ reduction data for several Ag-based catalysts using propene as a reducing agent. Reactant concentrations were 5% O₂, 1000 ppm NO₂, and 5000 ppm C₃H₆. NO₂ conversions are quite high even at 300C. The 1% and 3%Ag/TiO₂-ZrO₂ catalysts reached slightly above 80%, while the 1%Ag and 3%Ag/Al₂O₃ were above 90%. All four catalysts showed a slight decrease in conversion at higher temperatures. This behavior was most pronounced over the 3%Ag/Al₂O₃. N₂ yields were seen to differ significantly over the four catalysts. The 3%Ag/TiO₂-ZrO₂ showed the highest low temperature yield, nearly 70% at 300°C. The 1%Ag/TiO₂-ZrO₂ reaches a maximum conversion at 400°C. These two catalysts both suffer a drop in yield at 500°C. The 3%Ag/Al₂O₃ had a higher N₂ yield than the 1%Ag/Al₂O₃ at 300°C, but both then achieved above 90% yield at 400°C and 500°C. The loss of conversion in all catalysts, and loss of yield in the TiO₂-ZrO₂ catalysts at higher temperatures is a function of competition for the hydrocarbon as combustion takes off. These catalysts are highly active and selective for reduction of NO₂ using propene as a reducing agent.

NO₂ reduction with propane is presented in Figure 19 over 1%Ag and 3%Ag/Al₂O₃, the bare Al₂O₃ support, and 2%Pd/Al₂O₃. The Pd-based catalyst was synthesized based on the known ability of precious metals to activate hydrocarbons. Reactant concentrations were 5% O₂, 1000 ppm NO₂, and 5000 ppm C₃H₈. Ag supported on the TiO₂-ZrO₂ mixed oxide was not active for the reduction with C₃H₈. The 3%Ag/Al₂O₃ and 2%Pd/Al₂O₃ achieve above 80% conversion by 300°C, and all four samples are at this level by 350°C. 2%Pd/Al₂O₃ loses conversion at higher temperatures, dropping to 65% conversion by 500°C. Nitrogen yields over the Ag/Al₂O₃ catalysts increases with reaction temperature, with the other product being NO. Superior yield is seen with 3%Ag over 1%Ag loading at low temperatures, 300°C and 350°C. At 400°C the yields over the two catalysts equalize at just above 90%. 2%Pd/Al₂O₃ gives the best low temperature

yields reaching 47% and 67% at 300°C and 350°C respectively. After 350°C nitrogen yield on Pd decreases, dropping to 42% by 500°C. Nitrogen yield over the alumina support reaches a maximum of 47% at 400°C. The low yield demonstrates that the supported Ag is playing an important role in nitrogen selectivity, especially at high temperatures. The high conversion and low yield may also indicate that the support is largely responsible for the partial reduction to NO.

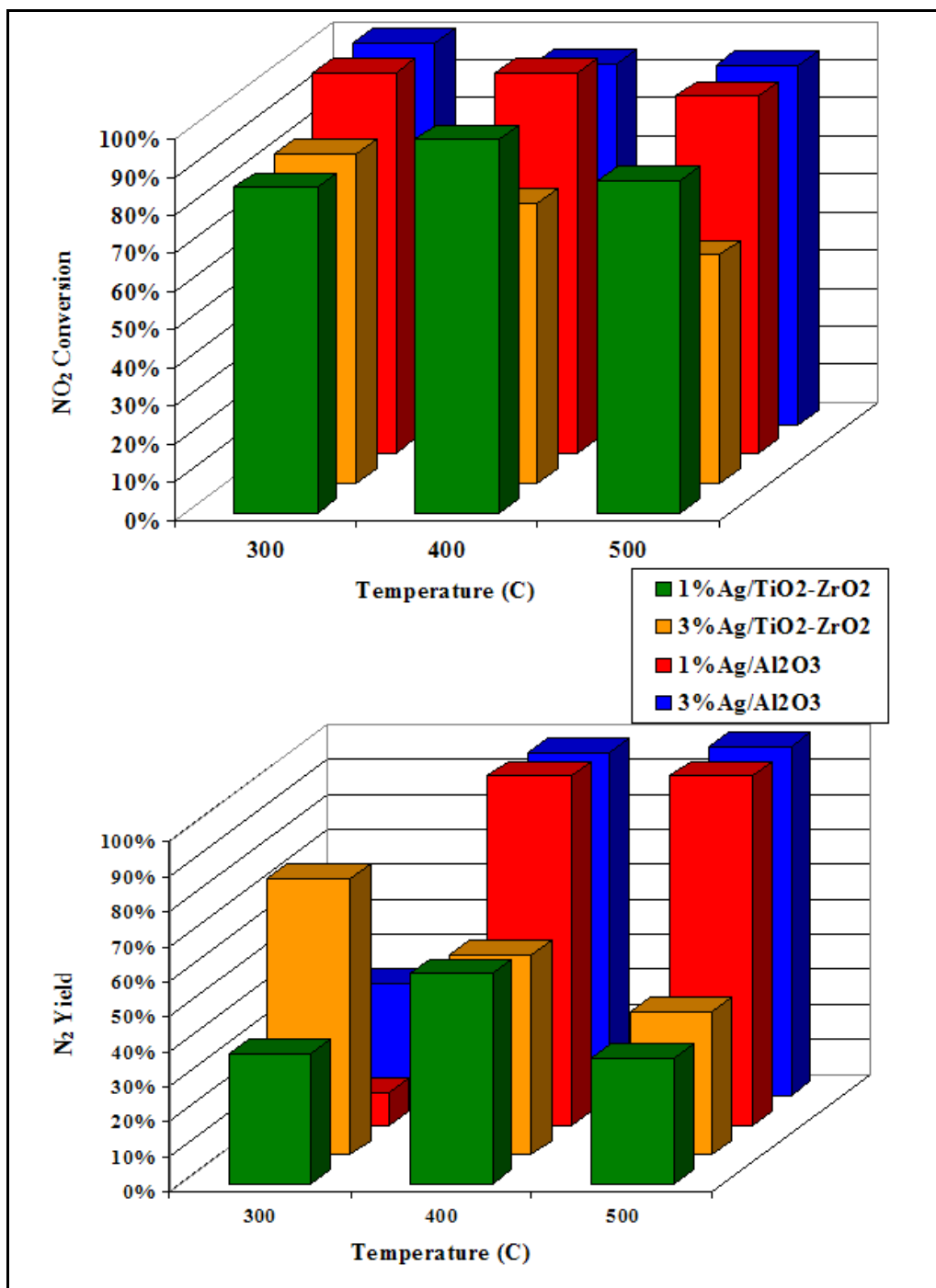


Figure 18: NO₂ reduction with C₃H₆ over Ag-based catalysts. NO₂ conversion and N₂ yield.

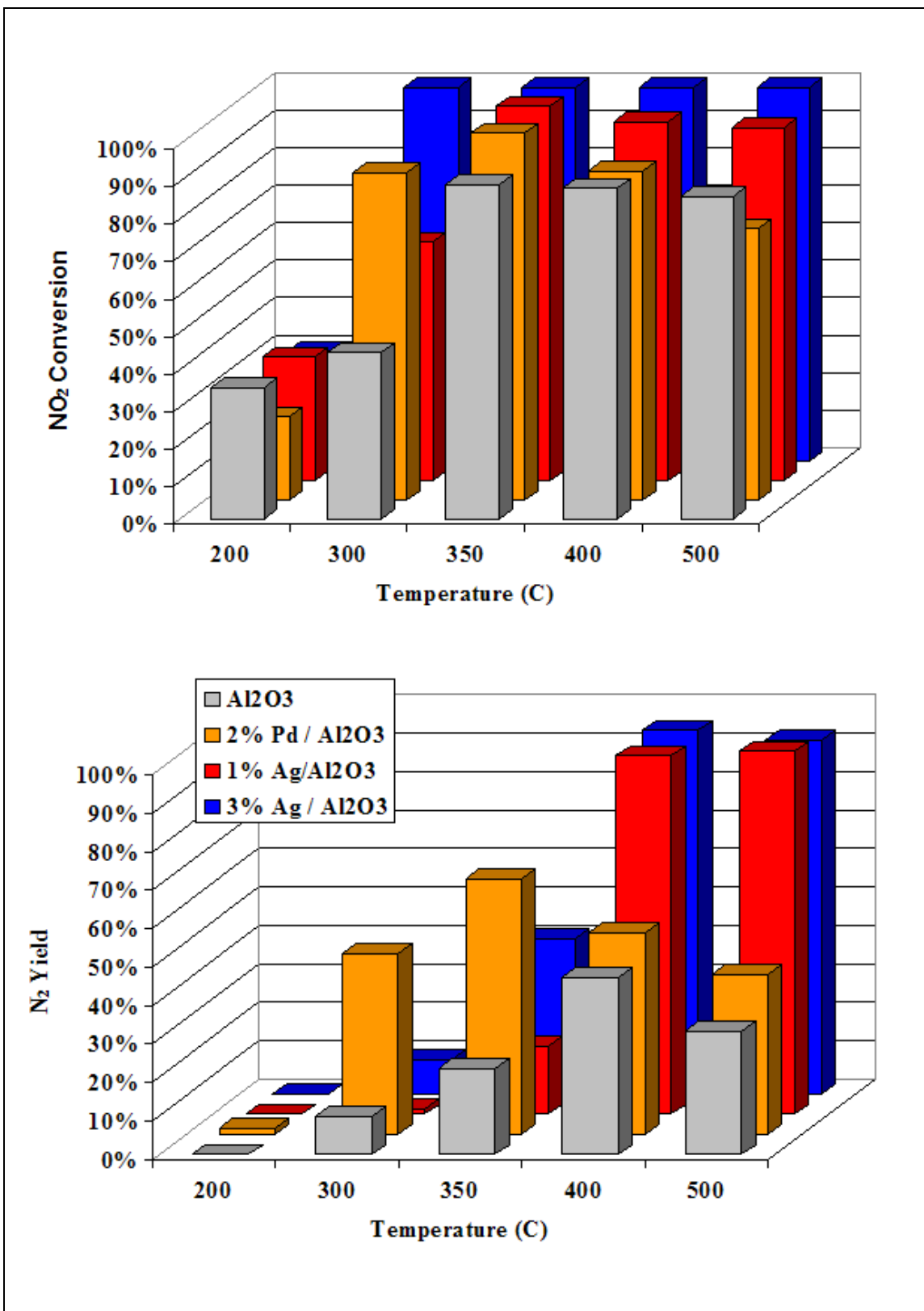


Figure 19: NO₂ reduction with C₃H₈ over Ag/Al₂O₃ and Pd/Al₂O₃ catalysts. NO₂ conversion and N₂ yield.

The catalyst testing discussed above demonstrates that the 1% and 3%Ag/Al₂O₃ catalysts are the most active in this series for the reduction reaction and the most selective to nitrogen, particularly at 400°C and above. With these catalysts being identified as the most promising, further testing was performed. Figures 20-22 present comparisons of different reduction conditions over the two Ag/Al₂O₃ catalysts. Comparisons of catalyst activity for 1% and 3% Ag/Al₂O₃ using propane and propene as reducing agents are shown in Figures 20 and 21.

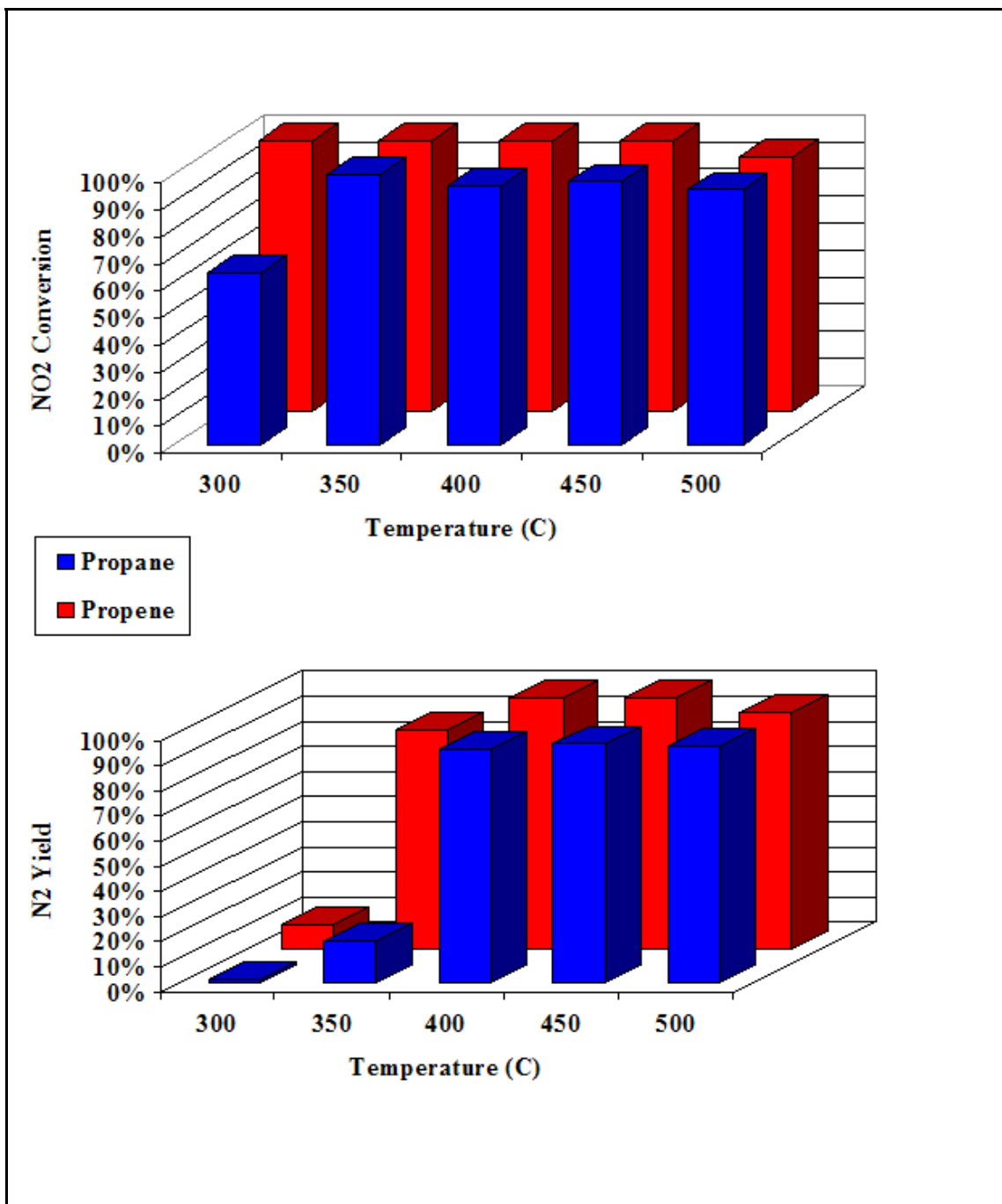


Figure 20: NO₂ reduction using C₃H₆ and C₃H₈ over 1%Ag/Al₂O₃. NO₂ conversion and N₂ yield.

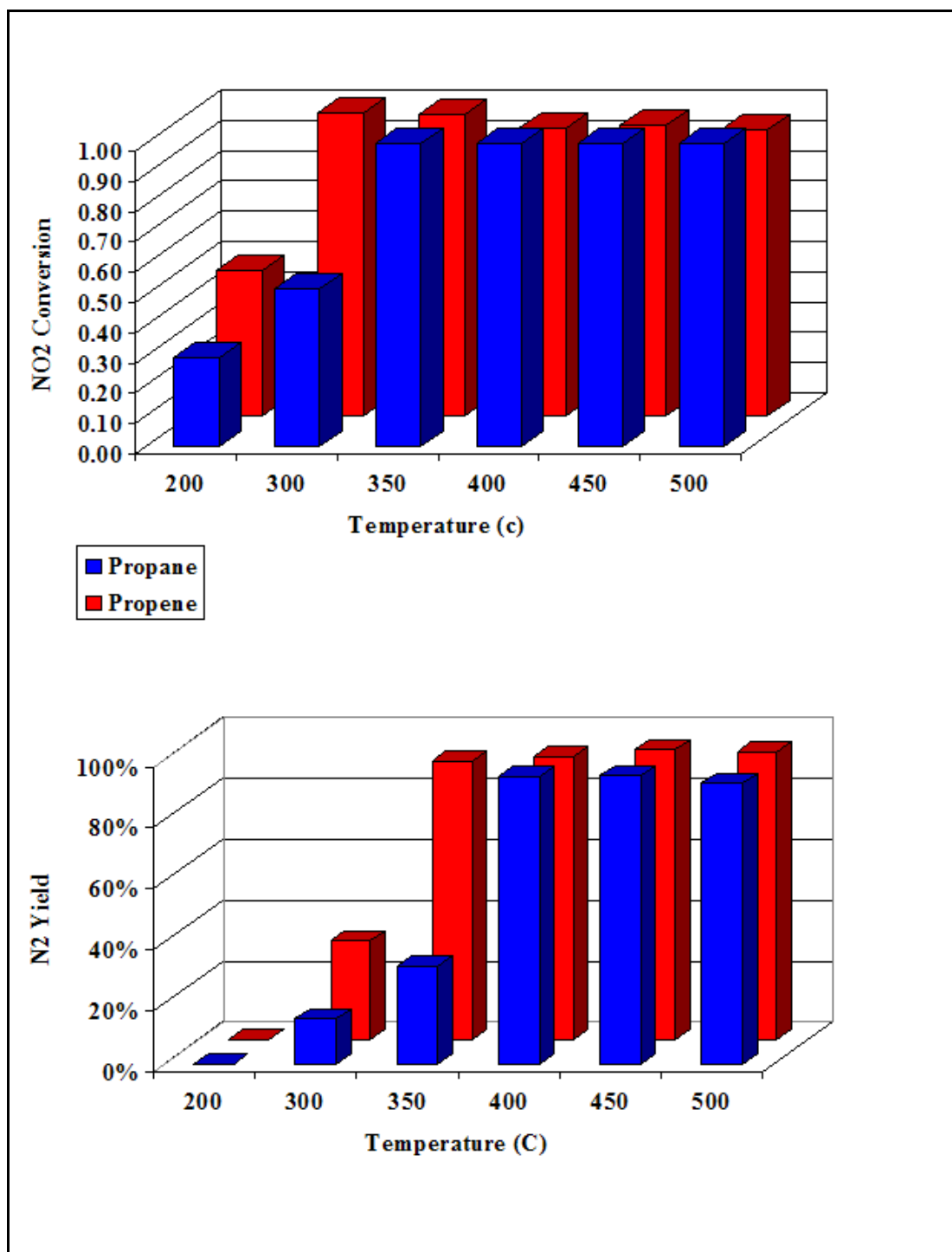


Figure 21: NO₂ reduction using C₃H₆ and C₃H₈ over 3%Ag/Al₂O₃. NO₂ conversion and N₂ yield.

Reactant concentrations were 5% O₂, 1000 ppm NO₂, and 5000 ppm of the hydrocarbon. At 350°C, over both catalysts and with both hydrocarbons, above 95% NO₂ conversions are attained. Over both the 1% and 3% Ag, NO₂ conversion at 300°C is higher with propene. This matches expectations, as the double-bond containing alkene should be easier to activate than the alkane. Nitrogen yields all reach above 90% by 400°C. At

both 300°C and 350°C the yields with propene are greater than with propane. Over 1%Ag at 350°C nitrogen yield with propene is 87% and with propane only 17%. Over 3%Ag the difference is 91% to 32%. Nitrogen yields below 400°C are higher for both hydrocarbons over the 3%Ag/Al₂O₃.

To examine catalyst activity changes with increased O₂ concentration, further tests were performed on the 1%Ag/Al₂O₃ catalyst in 10% O₂, 1000 ppm NO₂, and 5000 ppm C₃H₈. Comparisons with the 5% O₂ tests using propane are presented in Figure 4.5. In 10% O₂, 82% N₂ yield is attained at 350°C. N₂ yield is improved at this temperature in by the increase in oxygen concentration. At 400°C and above N₂ yield is above 90% under both O₂ concentrations.

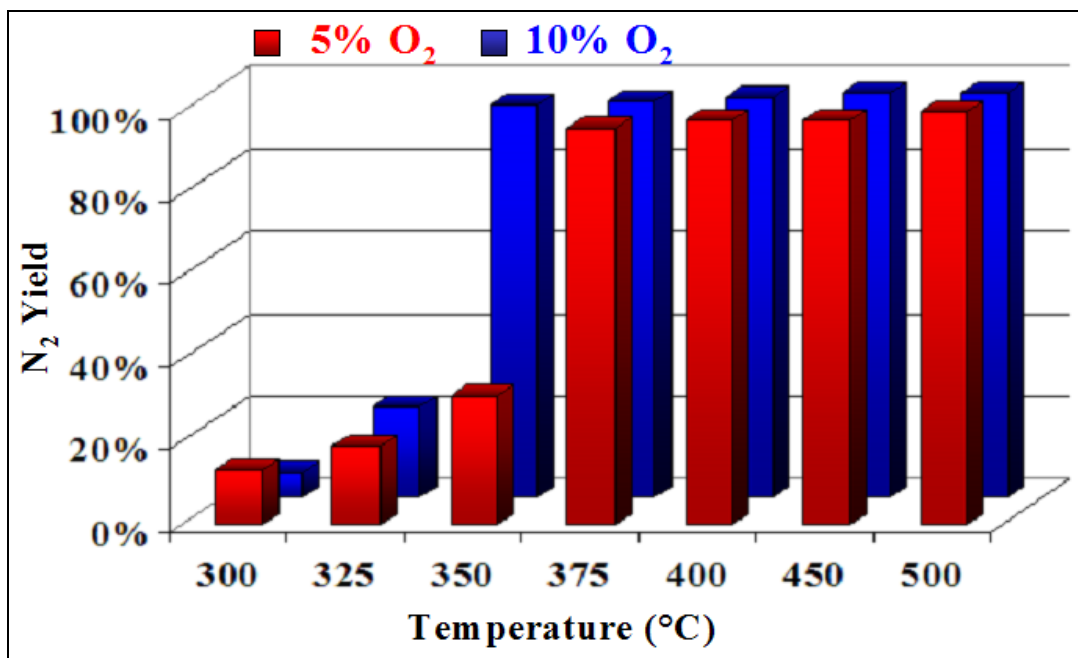


Figure 22: NO₂ reduction under 5% and 10% O₂ using C₃H₈ over 3%Ag/Al₂O₃. NO₂ conversion and N₂ yield.

Analysis of the catalyst structure and supported Ag phase were performed using XRD and XPS. The x-ray diffraction patterns of the 1% and 3%Ag/Al₂O₃ in Figure 23 demonstrate that the incipient wetness preparation results in well-dispersed surface silver species, as no diffraction peaks characteristic of silver species are observed. The observed diffraction peaks are characteristic of the alumina support. The XPS spectra of the 1% and 3%Ag/Al₂O₃ catalysts contain peaks at identical binding energies of 374.0 and 368.1 eV, characteristic of a silver oxide phase. The larger intensity of the Ag peaks on the 3%Ag/Al₂O₃ sample is expected with the higher metal loading.

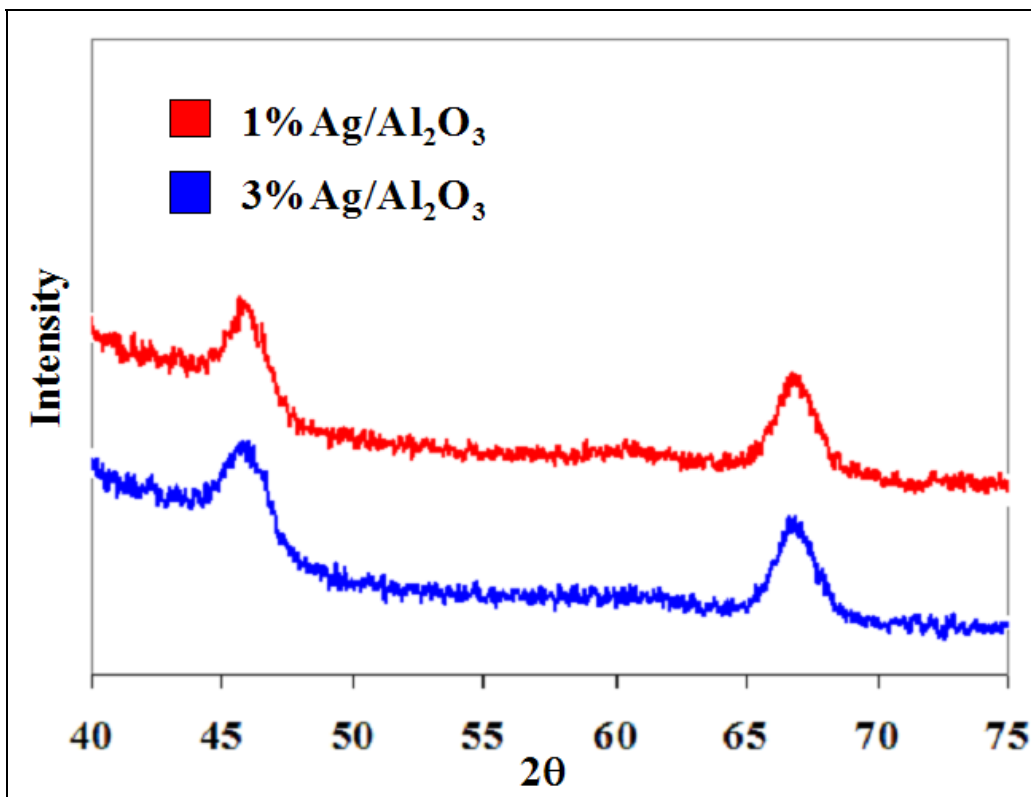


Figure 23: XRD pattern of Ag/Al₂O₃ catalysts.

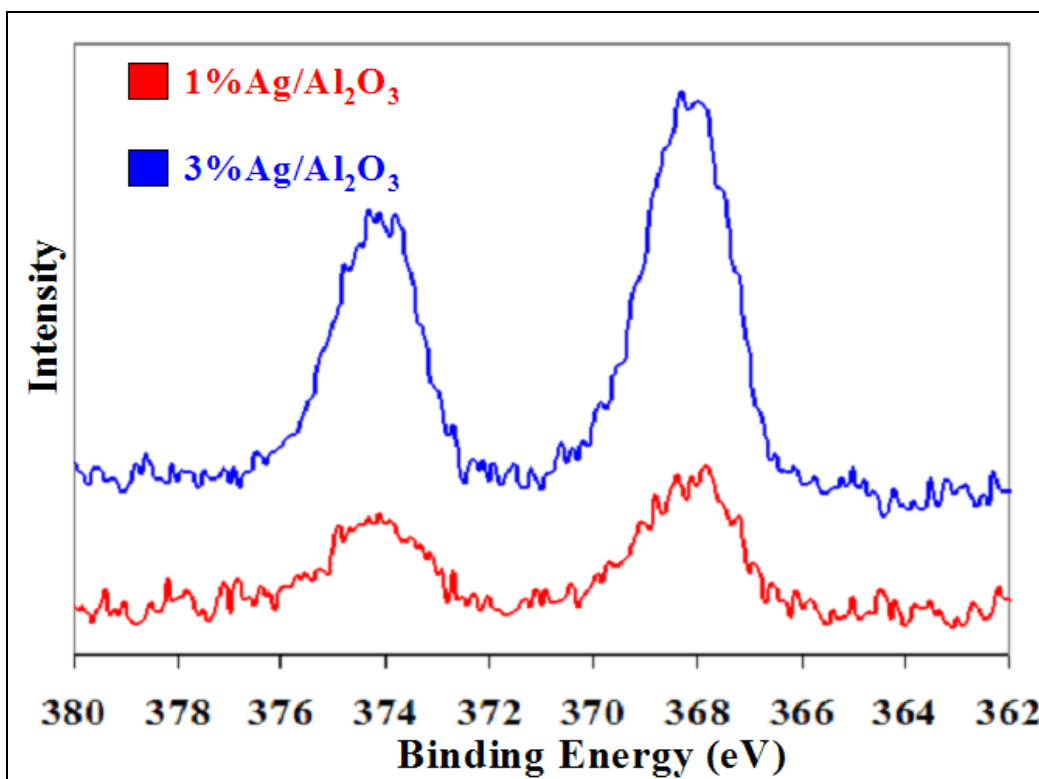


Figure 24: XPS spectra is the Ag 3d region of Ag/Al₂O₃ catalysts.

The high activity of these Ag-based catalysts for the reduction of NO₂ to N₂ under excess oxygen conditions was a promising result in the development of the two-stage system. When using methane as a reducing agent with 1% and 3% Ag/TiO₂-ZrO₂, and the 1% and 3% Ag/Al₂O₃ for the reduction of NO₂ under a feed of 1000 ppm CH₄, 5000 ppm CH₄, and 5% O₂, they showed very little activity. Although they are not active when used with methane as a reducing agent, and it will not be feasible to use them in natural gas engines, these reduction catalysts could find application at specific engine sites with high propane or propene gas concentrations, for example well head sites where propane and propylene would be more readily available.

NO₂ Reduction with CH₄ Over Pd-Based Sulfated Zirconia

Pd-based catalysts supported on solid acid supports have previously been shown to be active in the reduction of NO with CH₄. Acidic zeolites such as Pd/H-ZSM-5 are effective for the reduction^{9,10,11} but are structurally unstable in the presence of water vapor. Non-zeolitic acid supports are also known to have reduction activity. Sulfated zirconia in particular has been proposed.^{12,13} Metal oxide supports such as ZrO₂ are known to be hydrothermally stable.

Pd/SZ catalysts were prepared using a two-step incipient wetness impregnation method. A commercial monoclinic zirconia support was first sulfated using a water solution of ammonium sulfate. After drying and calcination Pd was added using a PdCl₂ in water solution. The catalyst was dried and calcined a second time. Steady-state reaction experiments were performed for the series of palladium supported on sulfated zirconia catalysts. Model reaction conditions used were 1000ppm NO_x, 3000ppm CH₄, and 10% O₂ in balance He, at a GHSV of 50,000 hr⁻¹.

As a proof of concept experiment for the two-stage approach the reduction of both NO and NO₂ with CH₄ was performed. Figure 25 shows the reaction results comparing the NO₂+CH₄ reaction and the NO+CH₄ reaction over 0.5%Pd/5%SZ. The NO₂+CH₄ reaction over 0.5%Pd/5%SZ has a maximum N₂ yield above 50% in the temperature range examined. A maximum yield occurs as CH₄ combustion begins to dominate and less hydrocarbon is available for the NO₂ reduction reaction. This maximum occurs across the temperature range of 350-375°C. CH₄ conversion increases with temperature reaching a maximum near 75% at 450°C. Significantly lower N₂ yields were observed in the NO+CH₄ reduction reaction over 0.5%Pd/5%SZ. A maximum N₂ yield of 23% was reached at 425°C. Across the temperature range, CH₄ conversions were very similar to the NO₂ reduction, with a maximum conversion around 75% observed at 450°C. Higher NO₂ reduction activity at the same level of CH₄ conversion demonstrates that NO₂ is more easily reduced and is able to react more selectively with the CH₄.

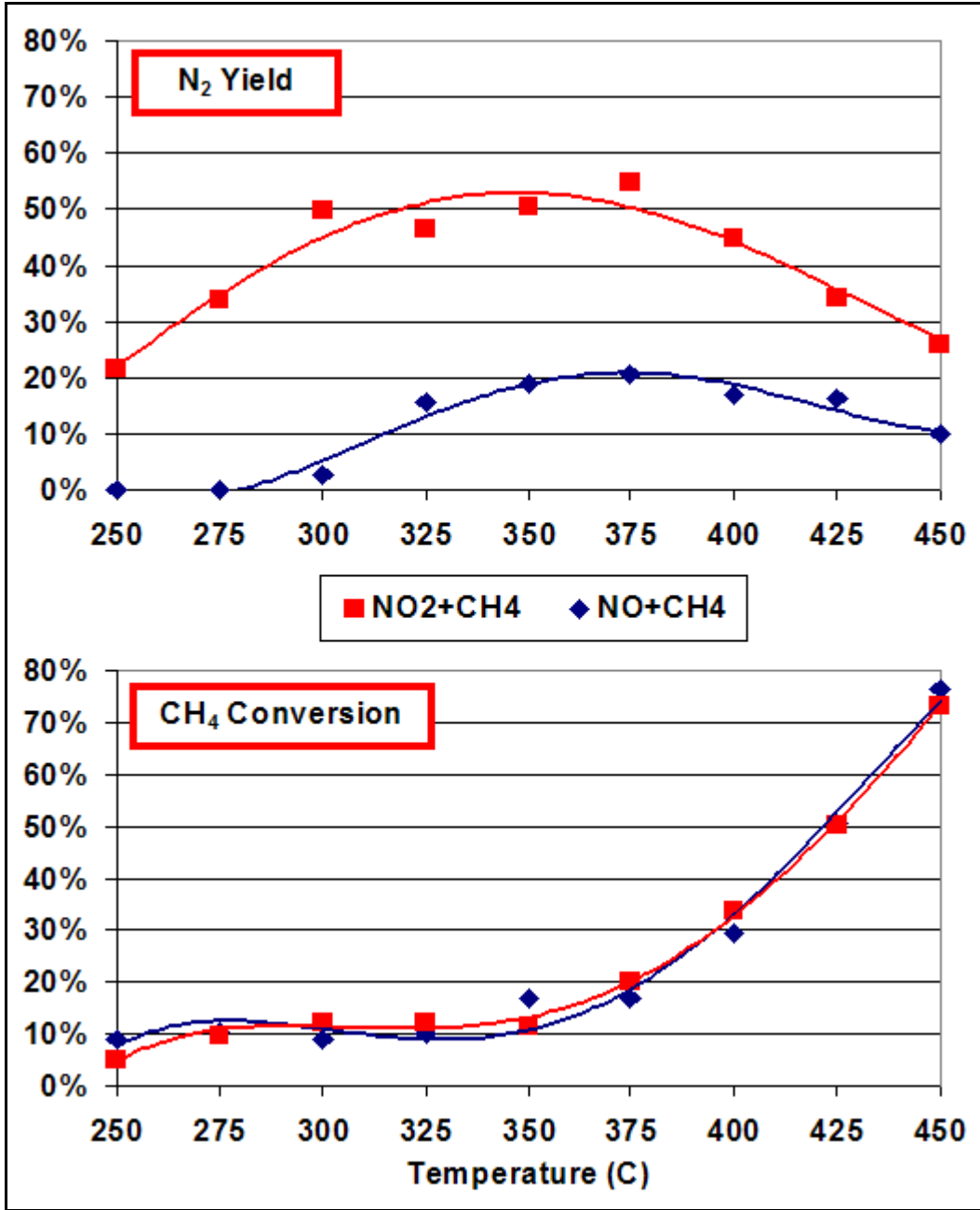


Figure 25: Comparison of reaction results of the NO₂+CH₄ and the NO+CH₄ reduction reactions over 0.5%Pd/5%SZ.

TPRxn experiments were performed over 0.5%Pd/5%SZ to investigate the light-off temperatures in the NO and NO₂ reduction reactions. Reaction conditions were 1000ppm NO_x, 3000ppm CH₄, and 5% O₂ at 20,000 hr⁻¹ GHSV. The temperature ramp was performed at 10°C/min.

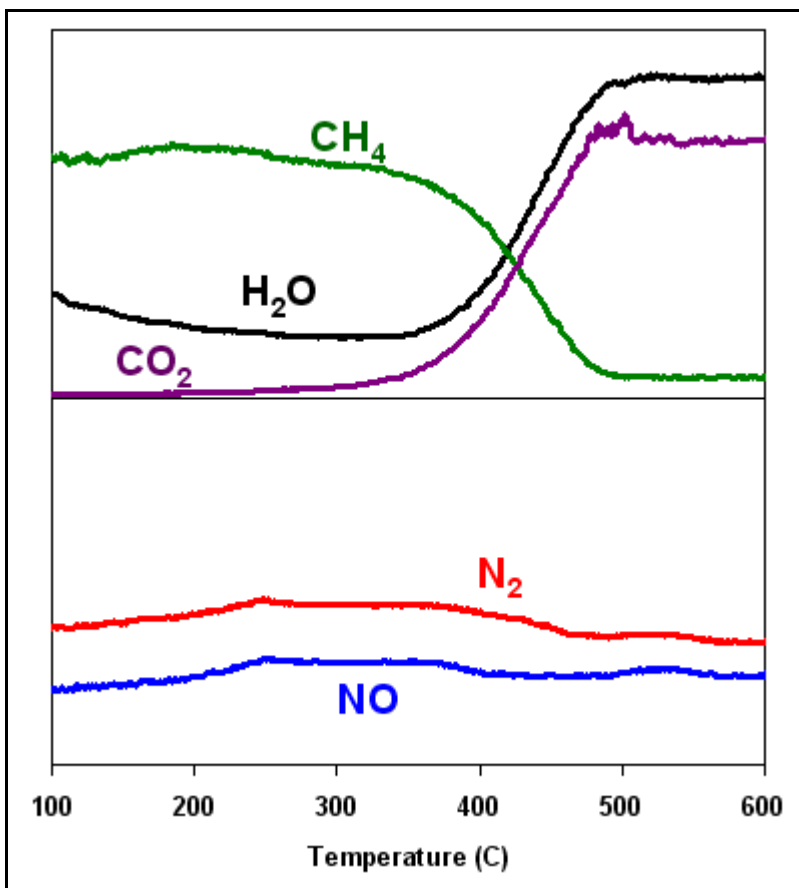


Figure 26: Temperature programmed reaction, NO+CH₄.

Figure 26 shows the TPRxn results for the NO+CH₄ reaction. Across the temperature range essentially no change was observed for either the N₂ or NO signals. A decrease in CH₄ was observed beginning around 400°C. This feature coincides with a simultaneous production of H₂O and CO₂. These results agree well with the steady-state reaction observations where low N₂ yields were observed and CH₄ combustion was seen to dominate at higher temperatures.

TPRxn results for the NO₂+CH₄ reaction are presented in Figure 27. Differences corresponding to the improved reduction performance were observed. A light off in N₂ production was observed around 250°C that corresponded to a sudden reduction in the NO₂ signal. The N₂ signal was seen to present a broad maximum with increasing temperature. These features correspond with light off of the reduction reaction and agree with observations from the steady-state reaction experiments. At 250°C a small decrease

in CH₄ concentration occurred corresponding to the start of NO₂ reduction. Around 400°C, a large decrease in CH₄ and an increase in both H₂O and CO₂ production were seen. This is in agreement with steady-state experiments that showed the light off of CH₄ combustion around 400°C with coinciding reduction in N₂ yield. Comparison of the TPR_{rxn} results for the NO+CH₄ and the NO₂+CH₄ reduction reactions again demonstrates that NO₂ reduction is an easier reaction, resulting in higher N₂ yields and activity at lower temperature.

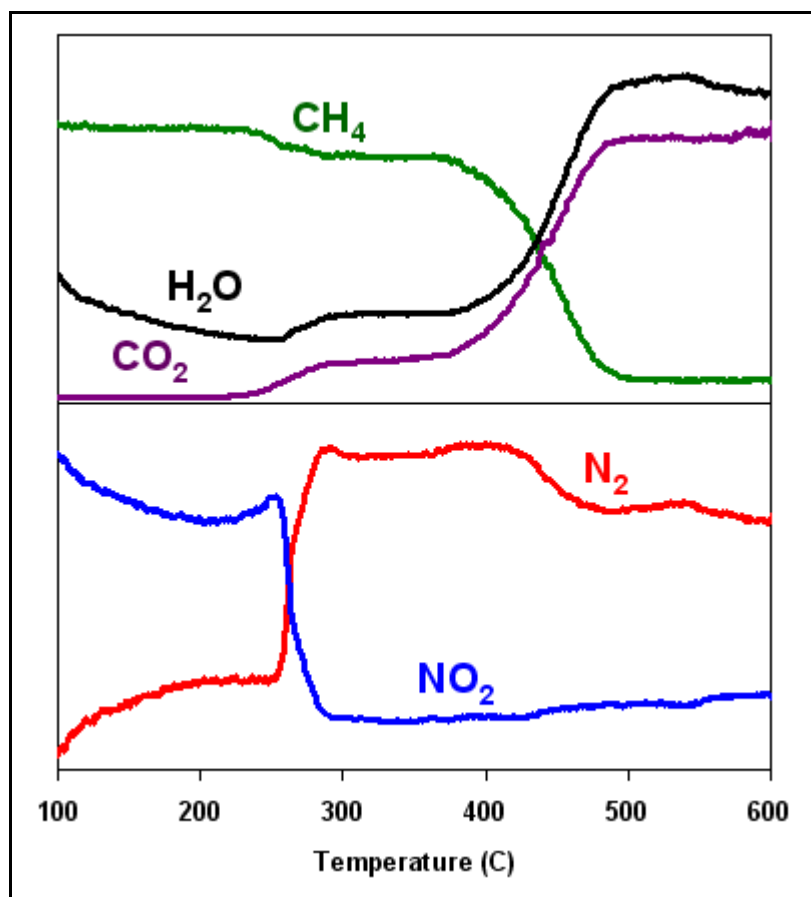


Figure 27: Temperature programmed reaction, NO₂+CH₄.

Literature studies of solid acid supports used for NO_x reduction have indicated that the acidic property is important in determining activity. Acidity in sulfated zirconia is imparted by electron accepting sulfate groups added to the surface. The role of these groups was examined by comparison of 0.5%Pd/5%SZ to a 0.5%Pd/ZrO₂ prepared through the same incipient wetness methods, but without sulfate treatment. Figure 28 compares the activities of 0.5%Pd/5%SZ and 0.5%Pd/ZrO₂. It was observed that the sulfidation of the zirconia support has a drastic effect on both the N₂ yield from the reduction reaction, and on CH₄ conversion over the catalyst. In the NO₂+CH₄ reduction reaction over the 0.5%Pd/ZrO₂ catalyst N₂ yields are very low across the temperature investigated. A maximum N₂ yield of 10% was observed at 450°C. CH₄ conversion was also low, reaching a maximum of 19% at 450°C. As discussed above reaction results

were significantly different over the 0.5%Pd/5%SZ sample. N₂ yields reached a maximum above 50%, and CH₄ conversions near 75% were observed.

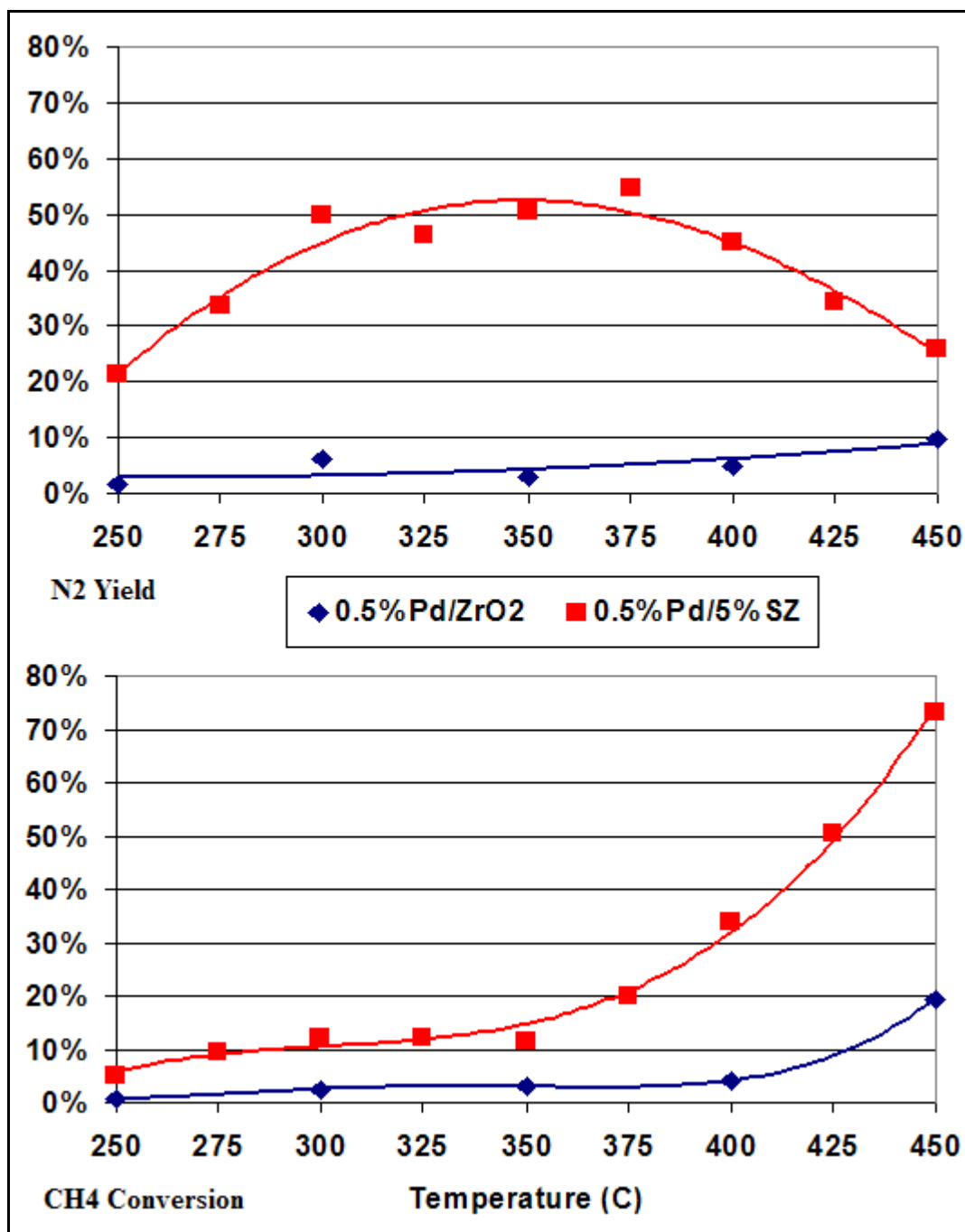


Figure 28: Reaction results showing N₂ yield and CH₄ conversion over 0.5%Pd/5%SZ and 0.5%Pd/ZrO₂.

Based upon these reaction results it is apparent that surface acidity due to surface sulfate species is key to NO_2 reduction activity. The stability of these species is thus of particular interest in the characterization of these catalysts. The effect of individual preparation steps and the stability of surface sulfate species were examined through XPS. The five samples examined were the commercial zirconia support, an uncalcined sample of ZrO_2 treated with ammonium sulfate, calcined ammonium sulfate treated ZrO_2 (sulfated zirconia), uncalcined sulfated zirconia after impregnation with PdCl_2 solution, and the final calcined sample (0.5%Pd/5%SZ). Figure 29 shows the characteristic binding energy regions of the sulfur 2p and zirconium 3d spectra of the five samples. In the sulfur 2p region a peak develops after treatment of the zirconia support with ammonium sulfate. This peak is centered on a binding energy of 169.1 eV. This binding energy is characteristic of sulfur in metal-sulfate species. Through further preparation steps neither the location nor intensity of this peak changes, even after the calcination of the treated commercial zirconia. Therefore after treatment with ammonium sulfate, stable sulfate species are present on the catalyst surface. Repeated calcinations at 500°C and the addition of metal to the surface do not affect them. Examination of the zirconium $3d_{5/2}$ peak reveals a shift from 181.5 eV to 182.2 eV after treatment of the zirconia support with ammonium sulfate. This shift has been previously observed in the literature, and is the result of decreased electron density around the Zr atoms due to the increased surface acidity imparted by the sulfate species. There is no further shift in the Zr $3d_{5/2}$ peak location with the additional preparation steps. Again it appears that the catalyst surface environment does not change through these steps, and supports the observation that the added sulfate species are stable.

Figure 30 shows the oxygen 1s binding energy region for the five 0.5%Pd/SZ preparation steps. The peak maximum undergoes a binding energy shift from an initial 529.4 eV that is characteristic of metal oxides, to a value of 531.1 eV after addition of ammonium sulfate. This shift could be due, as was observed in the Zr 3d signal, to a change in electron density around ZrO_2 lattice oxygen. After treatment with ammonium sulfate the formation of a shoulder peak in the O 1s region is also observed. This shoulder is centered on 532.0 eV and is characteristic of oxygen present in sulfate species. Through additional preparation steps there is no further shift in binding energy, and the intensity of the 532.0 eV shoulder does not change.

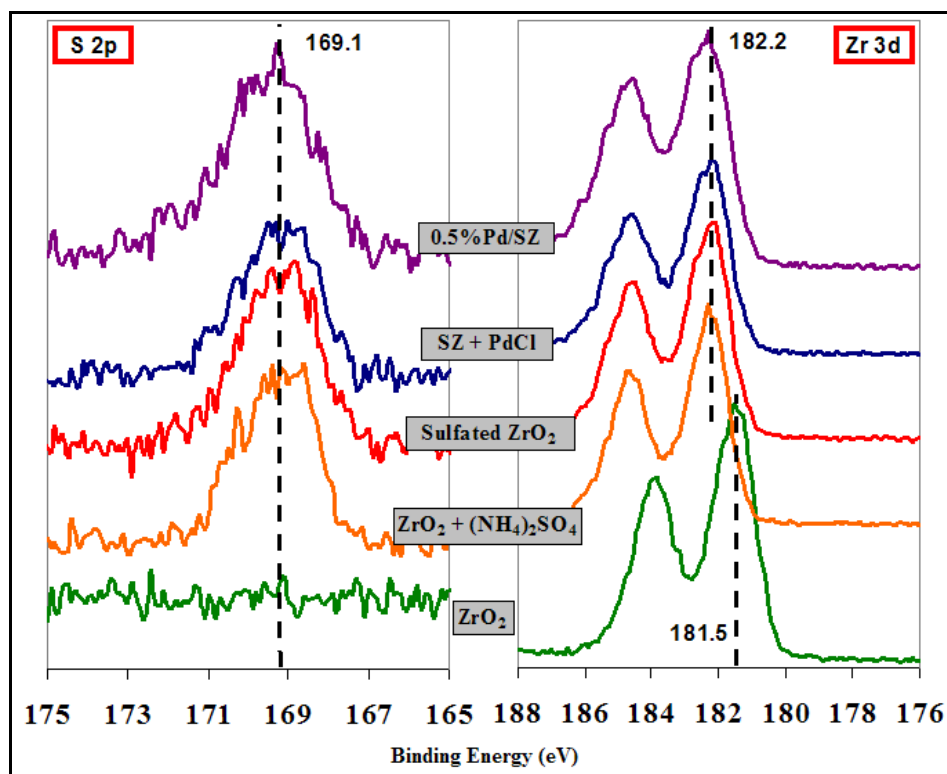


Figure 29: XPS spectra of the S 2p and Zr 5d regions after each step in the synthesis of 0.5%Pd/5%SZ.

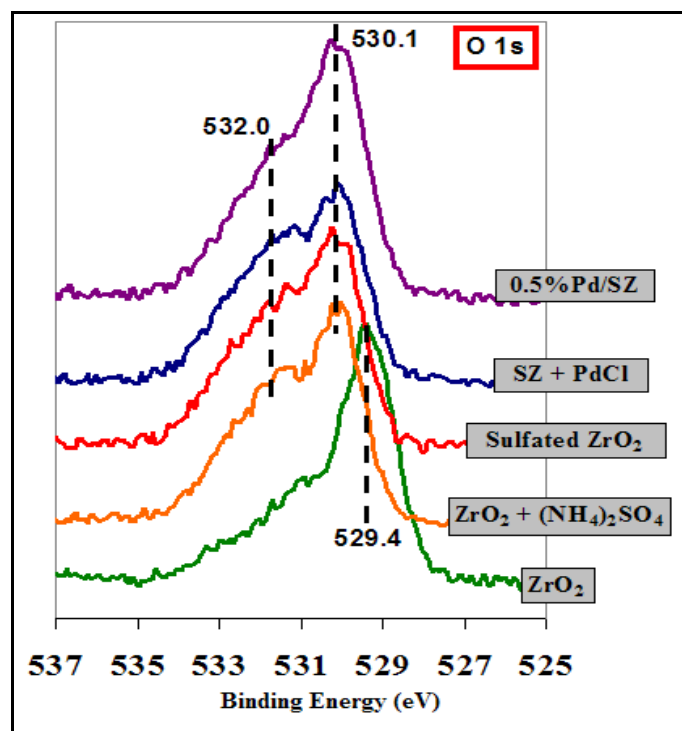


Figure 30: XPS spectra of the O 1s region after each step in the synthesis of 0.5%Pd/5%SZ.

As Pd is a relatively expensive precious metal, reduction of Pd loading in a catalyst formulation translates to a significant cost savings in the commercialization of the system. The results of the $\text{NO}_2 + \text{CH}_4$ reduction reaction performed over Pd/SZ catalysts with different Pd loadings are presented in Figure 31. The three formulations presented

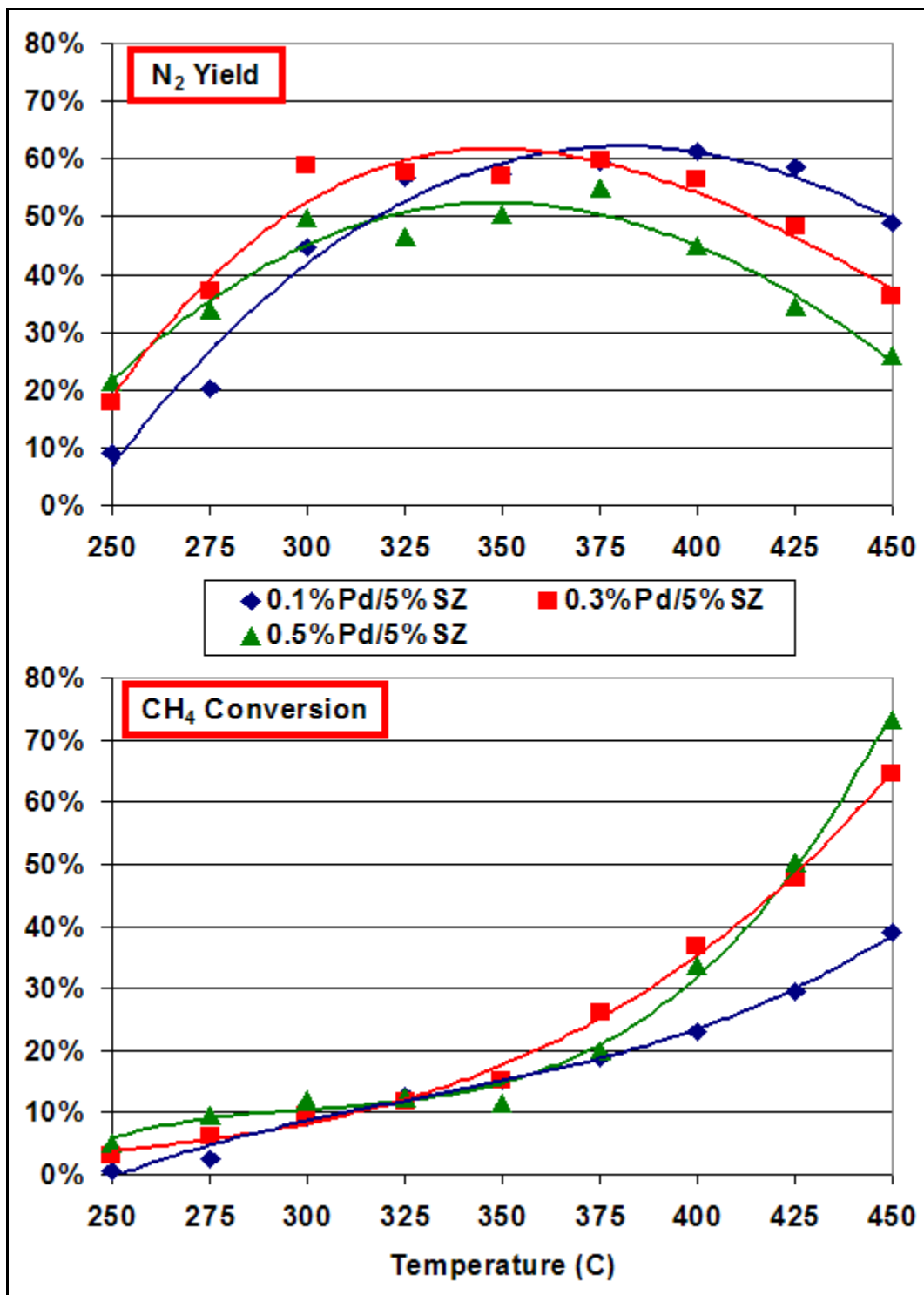


Figure 31: Effect metal loading on activity of Pd/SZ catalysts for the $\text{NO}_2 + \text{CH}_4$ reduction reaction.

are 0.5%Pd/5%SZ, 0.3%Pd/5%SZ, and 0.1%Pd/5%SZ. The results demonstrate that N₂ yield tends to increase with a decrease in Pd loading across this range. The 0.3%Pd/5%SZ catalyst reaches a maximum N₂ yield of 60% at 375°C, and the 0.1%Pd/5%SZ reaches a maximum N₂ yield of 62% at 400°C. It is also important to note that the maximum in N₂ yield is a very broad one, indicating that the working temperature range for the catalyst does not have to be very narrow. In the same figure, CH₄ conversion is shown to decrease by reducing Pd loading across this range. The 0.3%Pd/5%SZ catalyst reaches a CH₄ conversion of 64% at 450°C, while the 0.1%Pd/5%SZ reaches only 39% at the same temperature. These observations support the conclusion that reduced Pd content slows the CH₄ combustion reaction, allowing higher selectivities for the NO₂ reduction. Reducing the loading too far may result in the increase in maximum activity temperature seen between the 0.3% and 0.1% samples. It is likely therefore that an optimal loading exists in this range.

Mechanistic studies focused on understanding the differences in the CH₄ reduction of NO and NO₂ were performed by *in-situ* diffuse reflectance infrared Fourier transform spectroscopy. Three types of experiments were carried out. The first was IR spectra of a mixture of KBr and the 0.5%Pd/5%SZ catalyst. This experiment was designed to allow the observation of catalyst sulfate species and their interaction with adsorbing NO and NO₂. The second set of experiments were performed by TPD-DRIFTS to observe the thermal transformation of adsorbed NO and NO₂. The third set of experiments repeated the TPD-DRIFTS of NO or NO₂, but did so under a flow of either CH₄ or CH₄+O₂. These allowed for the monitoring of the transformations of adsorbed NO_x species in the presence of the other reactant gases in an effort to identify reaction intermediates. In all experiments NO_x species were adsorbed for 30 minutes at a concentration of 1000ppm. The TPD runs under reactant gases the concentrations were 2000ppm CH₄ and 5000ppm O₂.

Figure 32 shows spectra taken of 15wt% mixture of 0.5%Pd/5%SZ in KBr. Examination of the sample with no adsorbed gases showed one major band at 1398 cm⁻¹. This band is due to the S=O stretching of adsorbed sulfate species.^{14,15} After NO adsorption a decrease in the 1398 cm⁻¹ band is observed due to interaction of NO with the sulfate species. An additional band is seen at 1615 cm⁻¹ and is assigned to bridging nitrate species.^{16,17} This same band also appears upon NO₂ adsorption. Upon adsorption of NO₂, there is also a broad feature in the 1200–1100 cm⁻¹ region, which can be associated with bidentate nitrates.

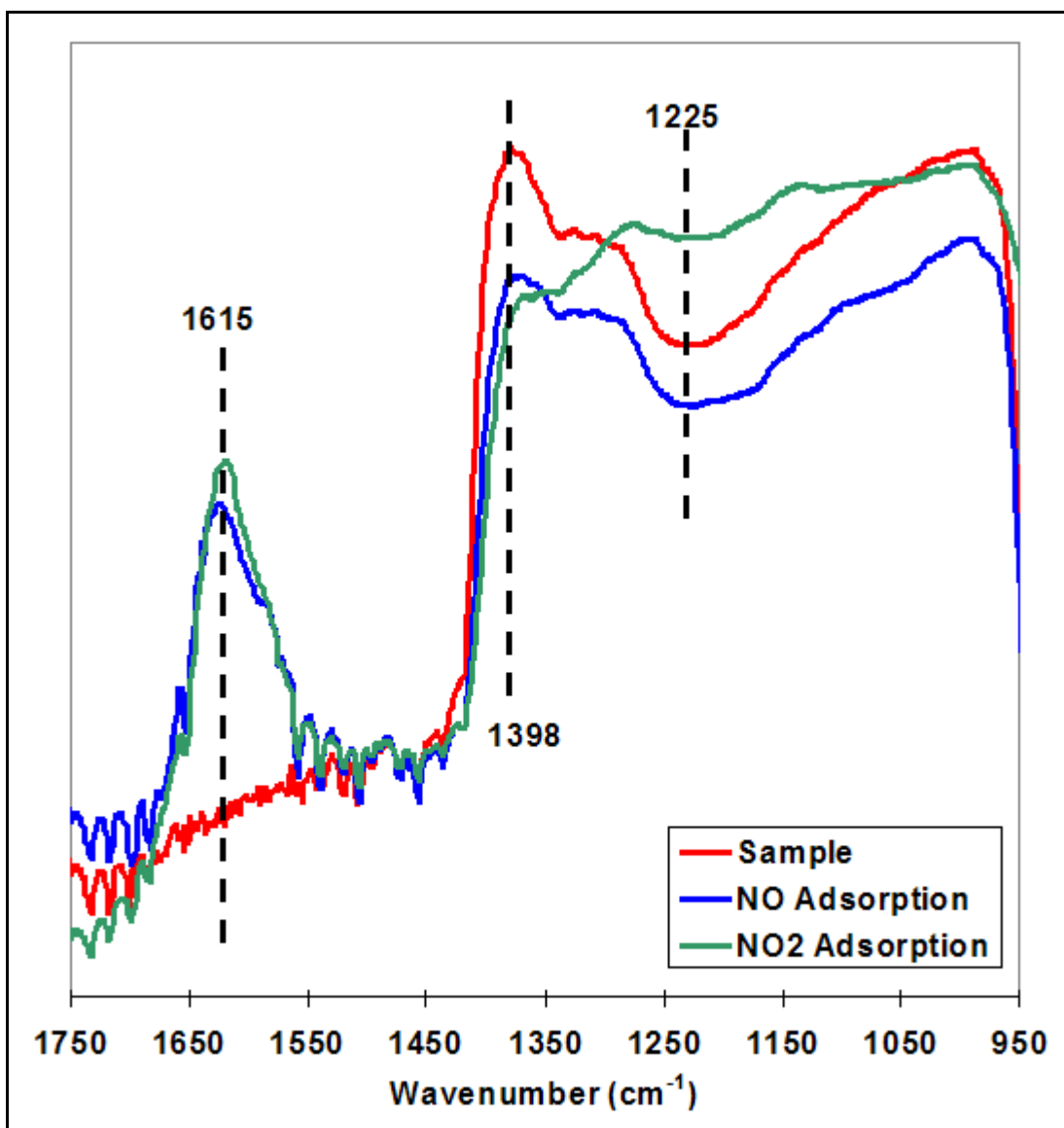


Figure 32: Adsorption of NO and NO₂ on a 0.5%Pd/5%SZ and KBr mixture.

NO TPD-DRIFTS results are presented in figures 33 and 34. Upon NO adsorption, bands at 1688, 1628, 1579, and a negative band at 1398 cm⁻¹ are observed. The negative band at 1398 cm⁻¹ is due to interaction of NO with sulfate species and decreases with increasing temperature, indicating the desorption of NO. The feature at 1688 cm⁻¹ appears as a shoulder that decreases with temperature, disappearing by 300°C. The appearance of this band is due to a linearly adsorbed NO species.¹⁸ The 1628/1579 cm⁻¹ pair appears together and grow with increasing temperature, but disappear at 350°C. These two bands are assigned to bridging and bidentate nitrates, respectively. They are commonly observed with NO₂ adsorption, and indicates that NO is transformed to adsorbed NO₂ species on the surface.^{19,20} At 300°C bands at 1385 and 1287 cm⁻¹ appear and grow with temperature. These bands may be associated with sulfate species and may also be due to free or bridged nitrates.^{16,21} At 350°C a band at 1617 cm⁻¹ appears which changes intensity with temperature, reaching a maximum at 400°C. This band is also in

the bridged nitrate region. The pair of room temperature peaks centered on 1850 cm^{-1} is due to gas phase NO remaining from the adsorption step.

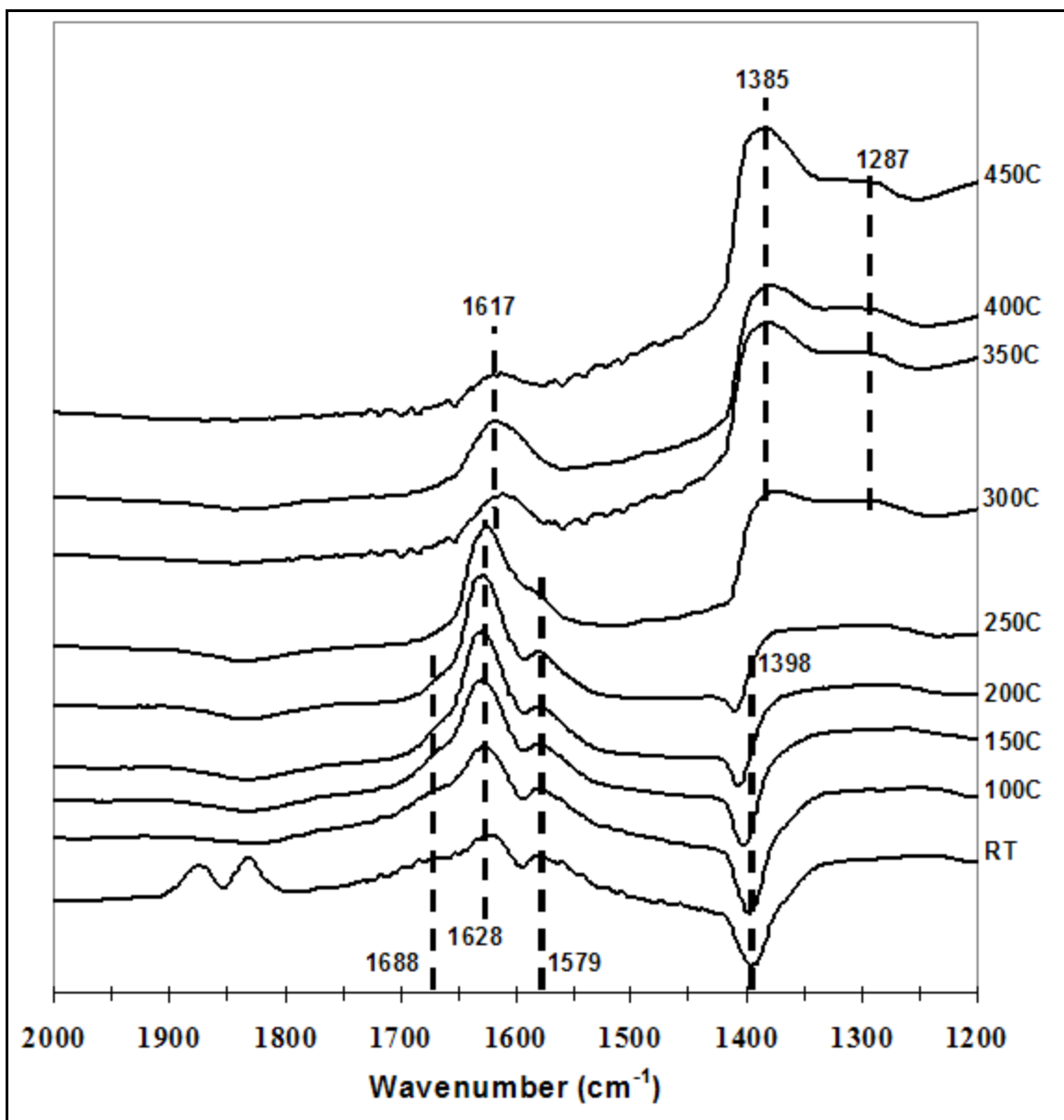


Figure 33: NO temperature programmed desorption by DRIFTS.

In the high wavenumber region (Figure 34) the evolution of several bands in the hydroxyl region around 3600 cm^{-1} is observed. Clear band assignment in this region is difficult because of the wide range of hydroxyl interactions that can occur with reactant adsorption. There is some evidence in the literature however that the bands at 3680 and 3550 cm^{-1} are associated with sulfate interactions with surface hydroxyls. Specifically they are associated with sulfite-like species on basic sites.^{22,23}

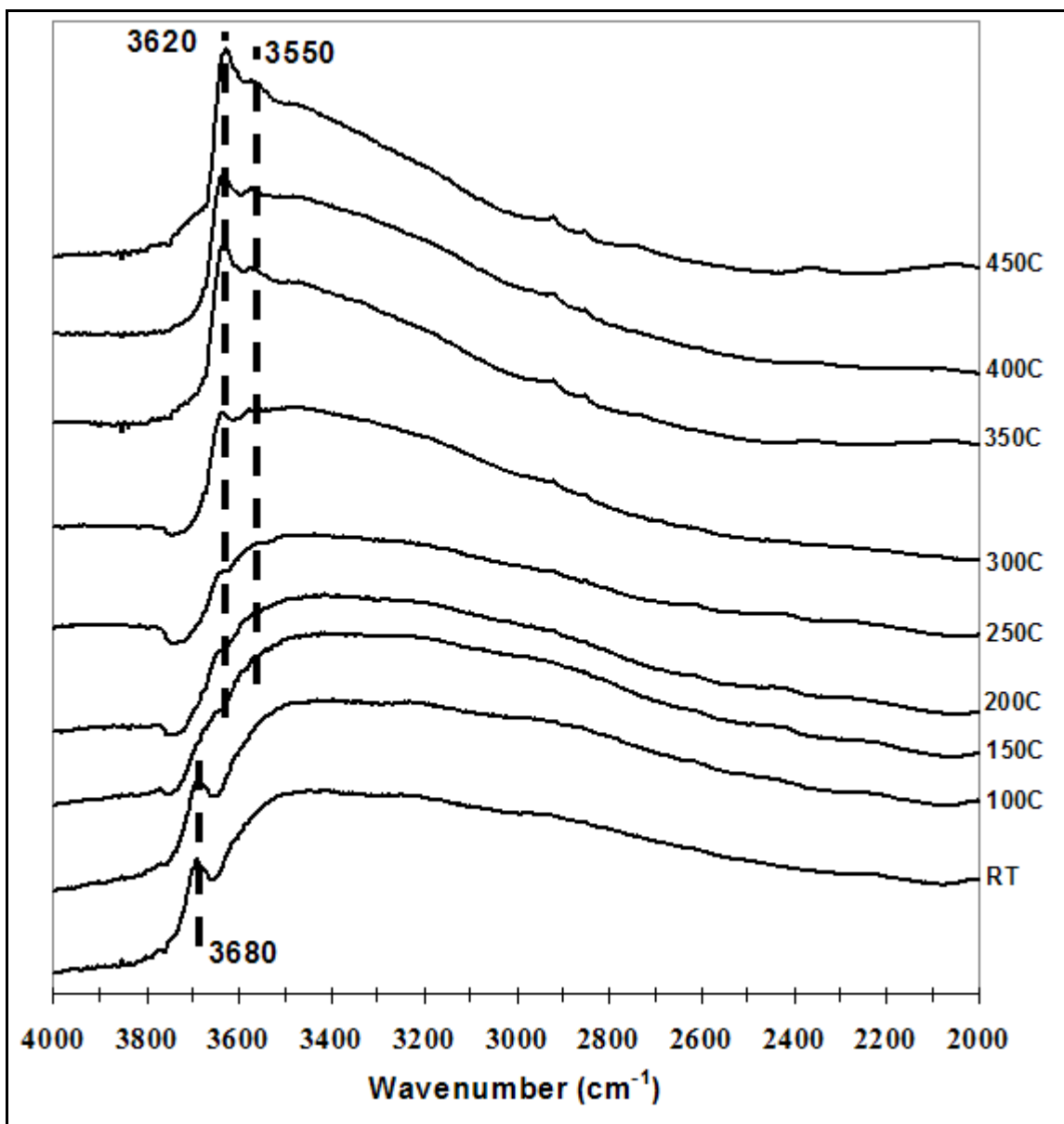


Figure 34: NO temperature programmed desorption by DRIFTS. High wavenumber region.

Figures 35 and 36 contain spectra from the NO_2 TPD-DRIFTS experiment. Three bands appear on adsorption of NO_2 , and are the only bands observed over the temperature range. The large negative band at 1398 cm^{-1} is again associated with NO_2 interaction with the sulfate species. This band is of greater intensity than for NO adsorption, and persists up to the maximum temperature of 450°C . These observations indicate that NO_2 interacts with the surface sulfates more strongly than does NO . A pair at 1628 and 1579 cm^{-1} is present as previously observed due to bridged and bidentate nitrates. Compared with the NO adsorption observations these bands are larger in intensity, persist to a higher temperature (350°C), and do not evolve to the bridged nitrate at 1617 cm^{-1} .

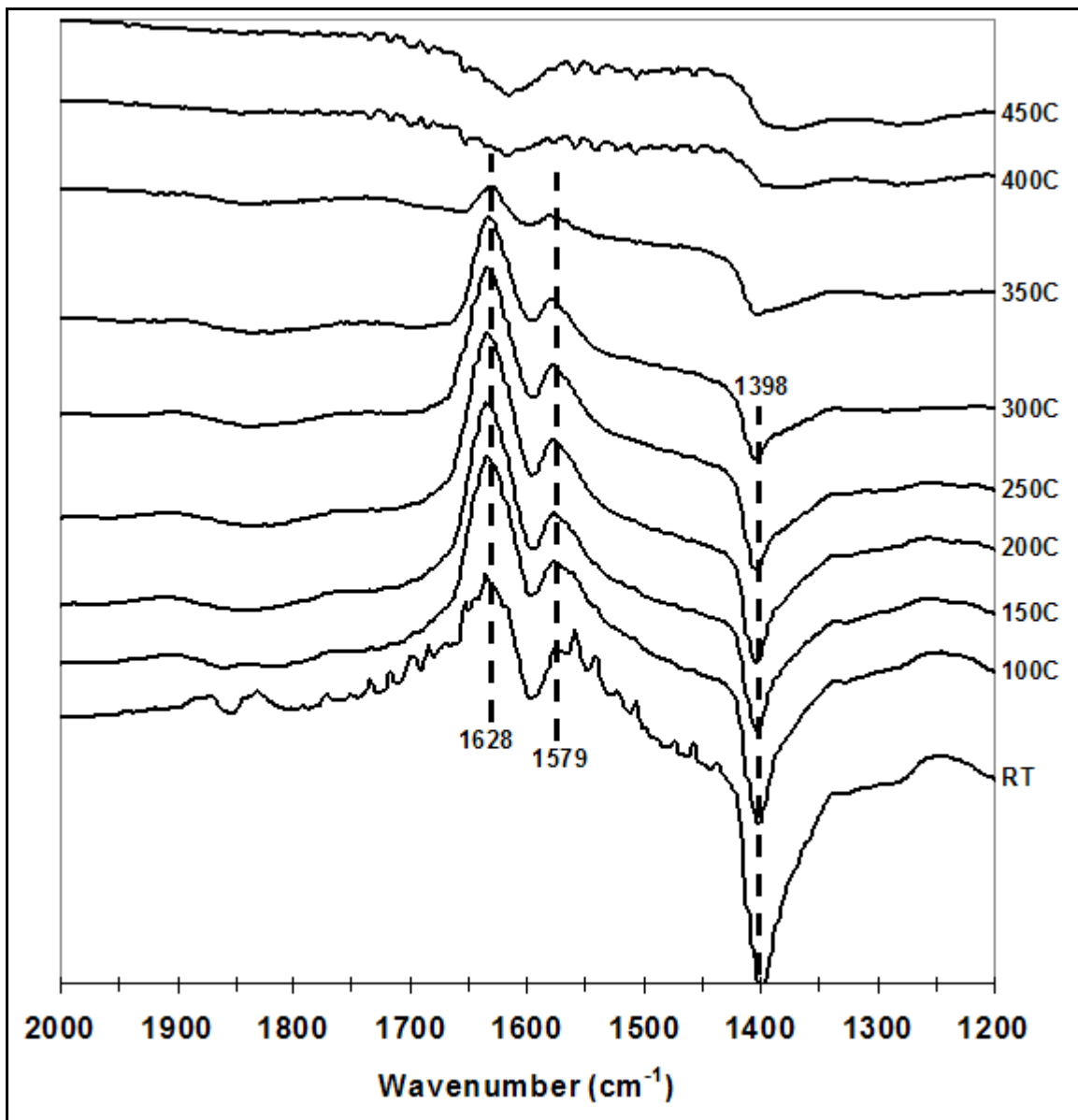


Figure 35: NO_2 temperature programmed desorption by DRIFTS.

Figure 36 contains the high wavenumber region of the NO₂ TPD experiment. The band at 3680 cm⁻¹ may indicate interaction with similar hydroxyls as after NO adsorption, but differences in the other bands, such as the lack of the 3550 cm⁻¹ species, are observed. The band near 2235 cm⁻¹ that is present for only the low temperature spectra is in the region assigned to NO²⁺ or NO⁺ acidic hydroxyls.^{24,25,26} Formation of this species was not observed under NO adsorption.

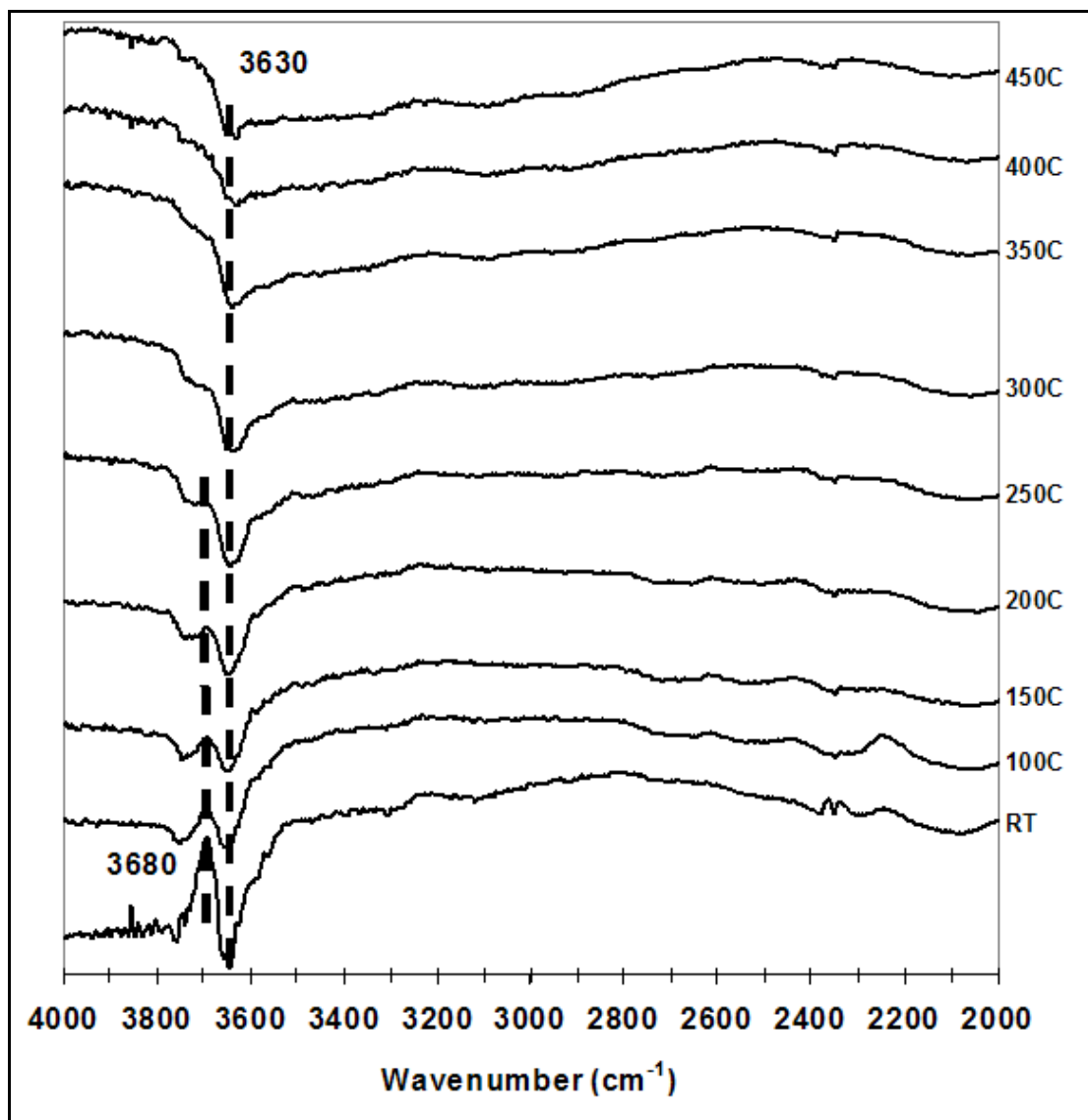


Figure 36: NO₂ temperature programmed desorption by DRIFTS. High wavenumber region.

Spectra taken of the NO TPD-DRIFTS performed under CH_4 are presented in figures 37 and 38. After NO adsorption bands at 1688, 1628, 1579 and the negative at 1398 cm^{-1} are again present. After the introduction of CH_4 the linear NO species at 1688 cm^{-1} does not persist above room temperature. The 1628/1579 cm^{-1} nitrate pair intensity initially increases with temperature but then appears to diminish above 200°C. This loss of intensity was not observed in the NO TPD experiment. As in the NO TPD run however, the pair evolves into the 1617 cm^{-1} bridging nitrate species at 350°C. The negative 1398 cm^{-1} band from sulfate interactions remains until after 350°C, a full 100°C higher than in the NO only case. Its disappearance is again accompanied by the observation of the 1385 and 1287 cm^{-1} species. The most significant difference observed is the appearance of a strong band at 300°C located at 1836 cm^{-1} . This species remains until 400°C.

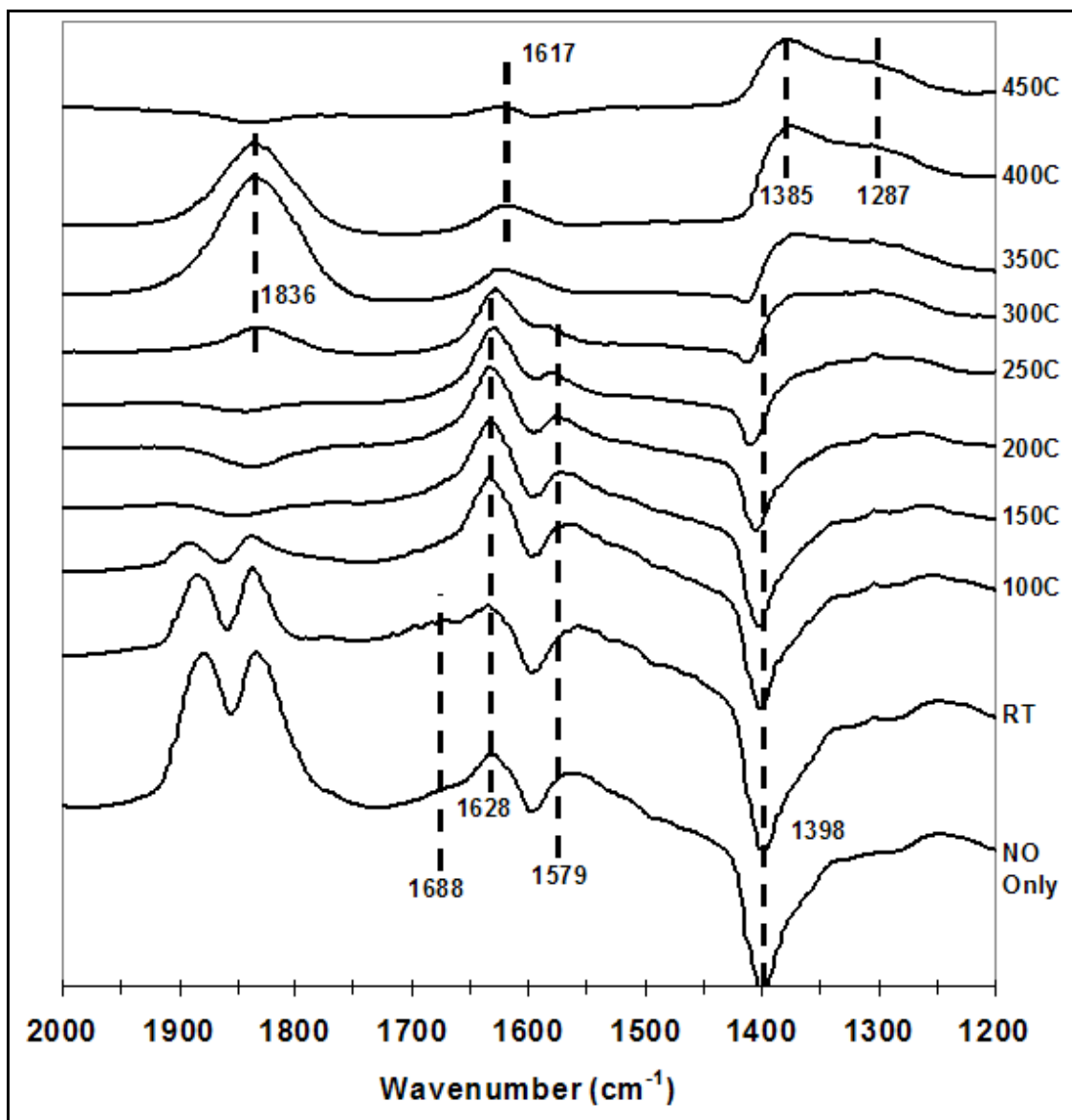


Figure 37: NO temperature programmed desorption by DRIFTS. TPD performed under CH_4 flow.

In the high wavenumber region the hydroxyl bands appear similar to those previously observed, but under CH₄ flow the band at 3550 cm⁻¹ does not form at high temperatures. After the introduction of CH₄ flow a band at 3012 cm⁻¹ appears. This band is due to gas phase CH₄. At 350°C, and growing with temperature, a pair appears centered on 2335 cm⁻¹. These bands are due to CO₂, and indicate that the reaction of CH₄ is occurring.

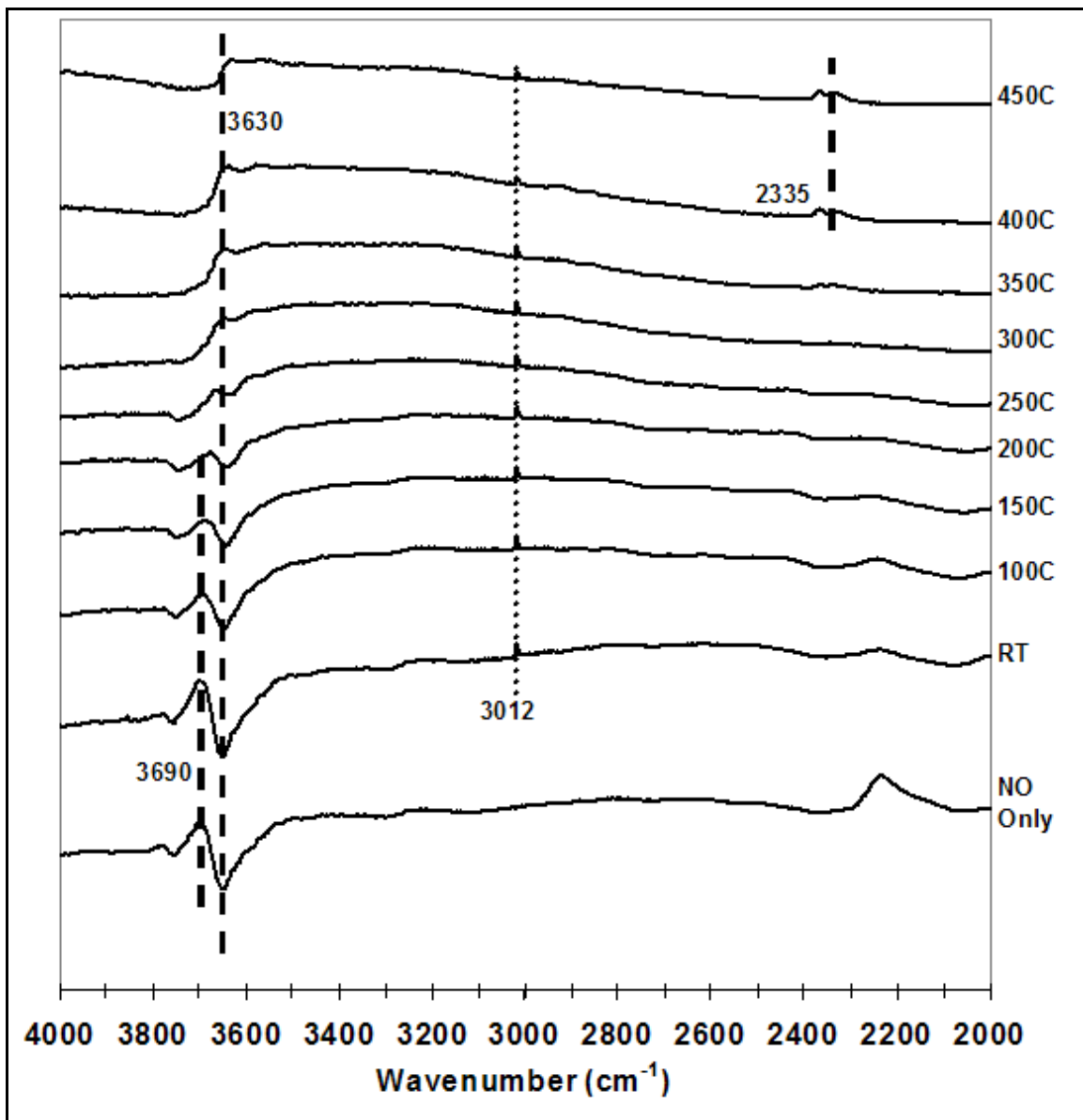


Figure 38: NO temperature programmed desorption by DRIFTS. TPD performed under CH₄ flow. High wavenumber region.

Figures 39 and 40 show the results of the NO₂ TPD-DRIFTS performed under CH₄ flow. Upon NO₂ adsorption the bands 1628, 1579, and the negative 1398 cm⁻¹ appear. Under CH₄ flow the sulfate interaction band at 1398 cm⁻¹ disappears by 350°C, while during NO₂ TPD it was never completely removed. Additionally its disappearance is accompanied by the formation of species at 1385 and 1287 cm⁻¹ as in the previous NO adsorption experiments. The bridged/bidentate nitrate species at 1628 and 1579 cm⁻¹ grow until 200°C, then decrease and evolve into the 1617 cm⁻¹ bridged nitrate by 300°C. The band at 1836 cm⁻¹ appears at 300°C as in the NO under CH₄ case, but is stronger than observed in that experiment. The 1836 cm⁻¹ species is gone at 400°C, disappearing at a lower temperature than in the NO under CH₄ case. Resasco has assigned a band here to NO adsorbed on Pd²⁺ ions over various catalysts.²⁷ In those experiments however a second band at 1883 cm⁻¹ that maintained its relative intensity to 1836 cm⁻¹ was always observed. This second band was not observed in these experiments. Additionally the band is not observed after only NO_x adsorption, but after exposure to CH₄ at elevated temperatures. It may be that this band is associated with a NO_x reduction intermediate. If so it may explain some of the observations made in the above TPD-DRIFTS experiments. From steady-state reaction experiments it is known that NO₂ is significantly more reactive in the reduction with methane, which may correlate to the earlier disappearance of the 1836 cm⁻¹ band in the NO₂ experiment. Also it was observed in reactions that some NO₂ is reduced to NO with methane. The formation of NO during the NO₂ reduction may serve to explain the formation of the higher temperature features at 1617, 1385, and 1287 cm⁻¹, which in NO_x adsorption TPD-DRIFTS were only observed for NO. It is also possible that the band at 1836 cm⁻¹ corresponds to a carbonyl group adsorbed on Pd sites. It is not possible, however, to have a definitive assignment without further studies using isotopic labeling techniques.

Bands observed above 2000 cm⁻¹ are similar to those seen in the NO TPD under CH₄. With the introduction of CH₄ the 3012 cm⁻¹ band characteristic of the gas phase appears. The CO₂ peaks centered on 2335 cm⁻¹ appear in the high temperature range. As in the NO₂ TPD, a band near 2235 cm⁻¹ is observed.

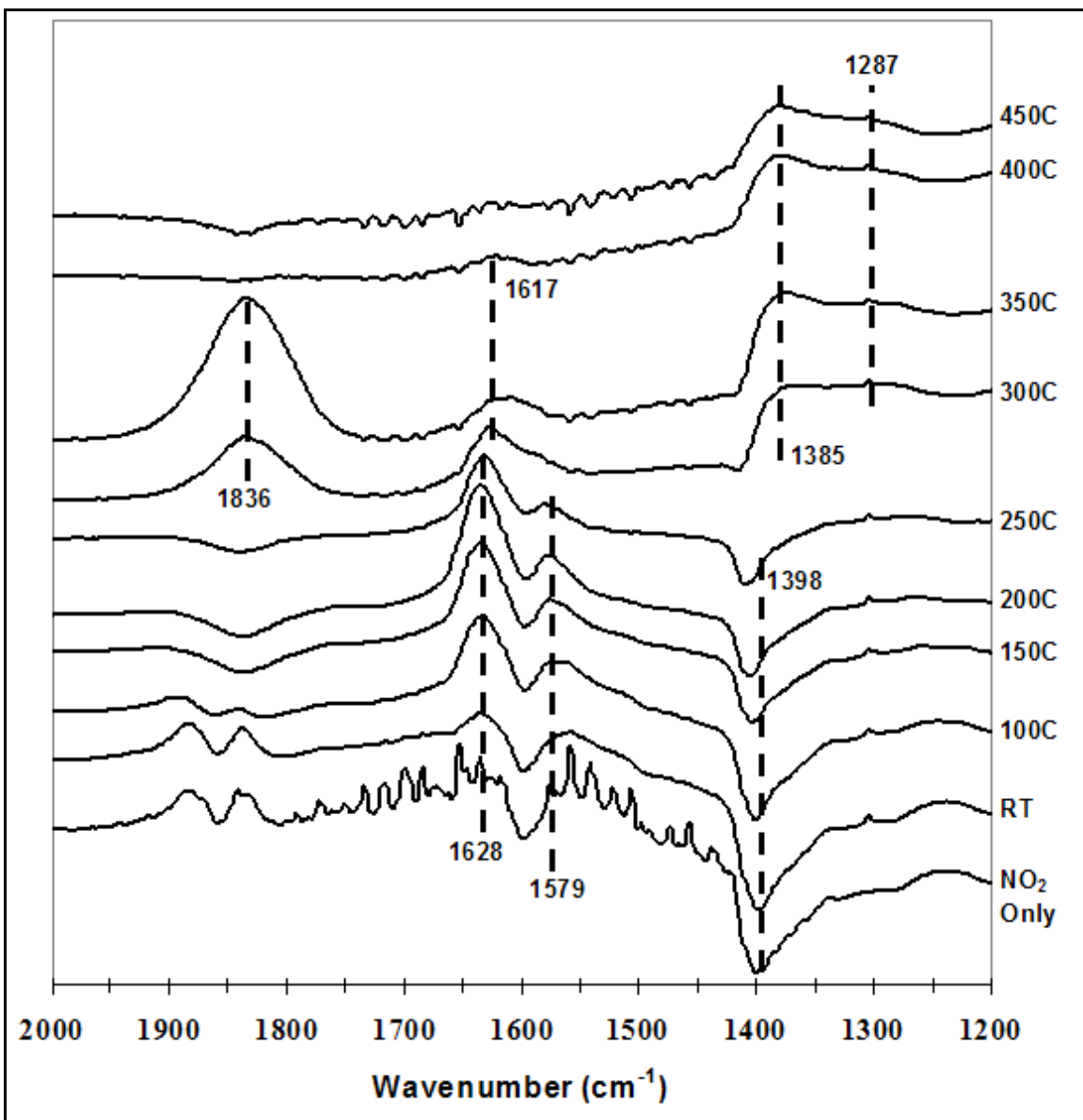


Figure 39: NO₂ temperature programmed desorption by DRIFTS. TPD performed under CH₄ flow.

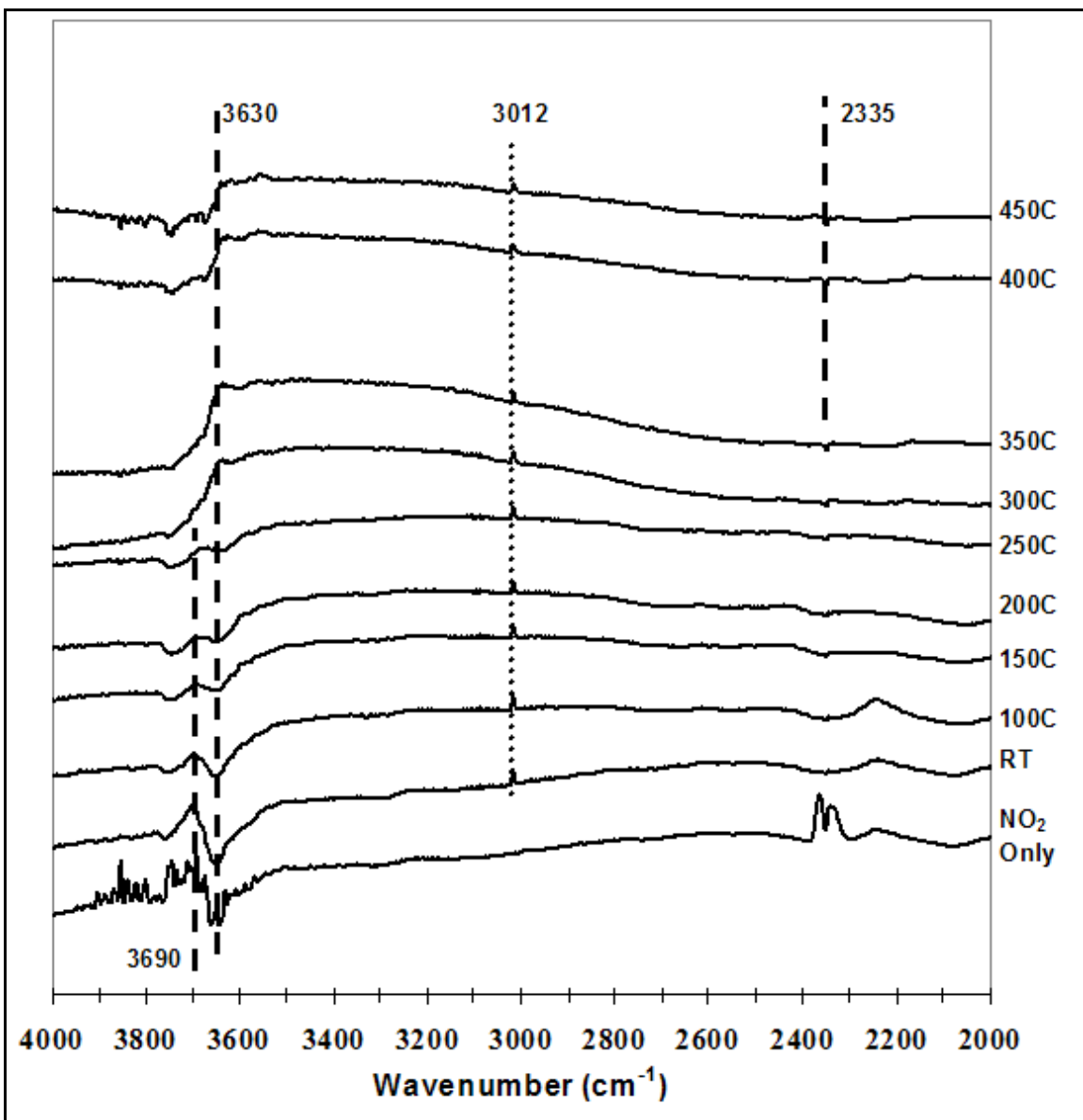


Figure 40: NO₂ temperature programmed desorption by DRIFTS. TPD performed under CH₄ flow. High wavenumber region.

TPD-DRIFTS experiments were also performed for both NO and NO₂ under a flow of CH₄+O₂. The results of the NO TPD-DRIFTS under CH₄+O₂ are presented in Figures 41 and 42. The sulfate interaction indicated by the negative band at 1398 cm⁻¹ persists across the entire investigated temperature range. Unlike in the NO under CH₄ case it does not disappear, and the 1385/1287 cm⁻¹ pair to not form. The 1628 and 1579 cm⁻¹ species again grow with temperature until 200°C, then decrease and evolve into the 1617 cm⁻¹ bridged nitrate at 350°C as in the CH₄ only experiment. Under CH₄+O₂ the 1836 cm⁻¹ band does not appear until 350°C, and remains present until 450°C. This represents a 50°C shift to higher temperature for the formation and presence of this species.

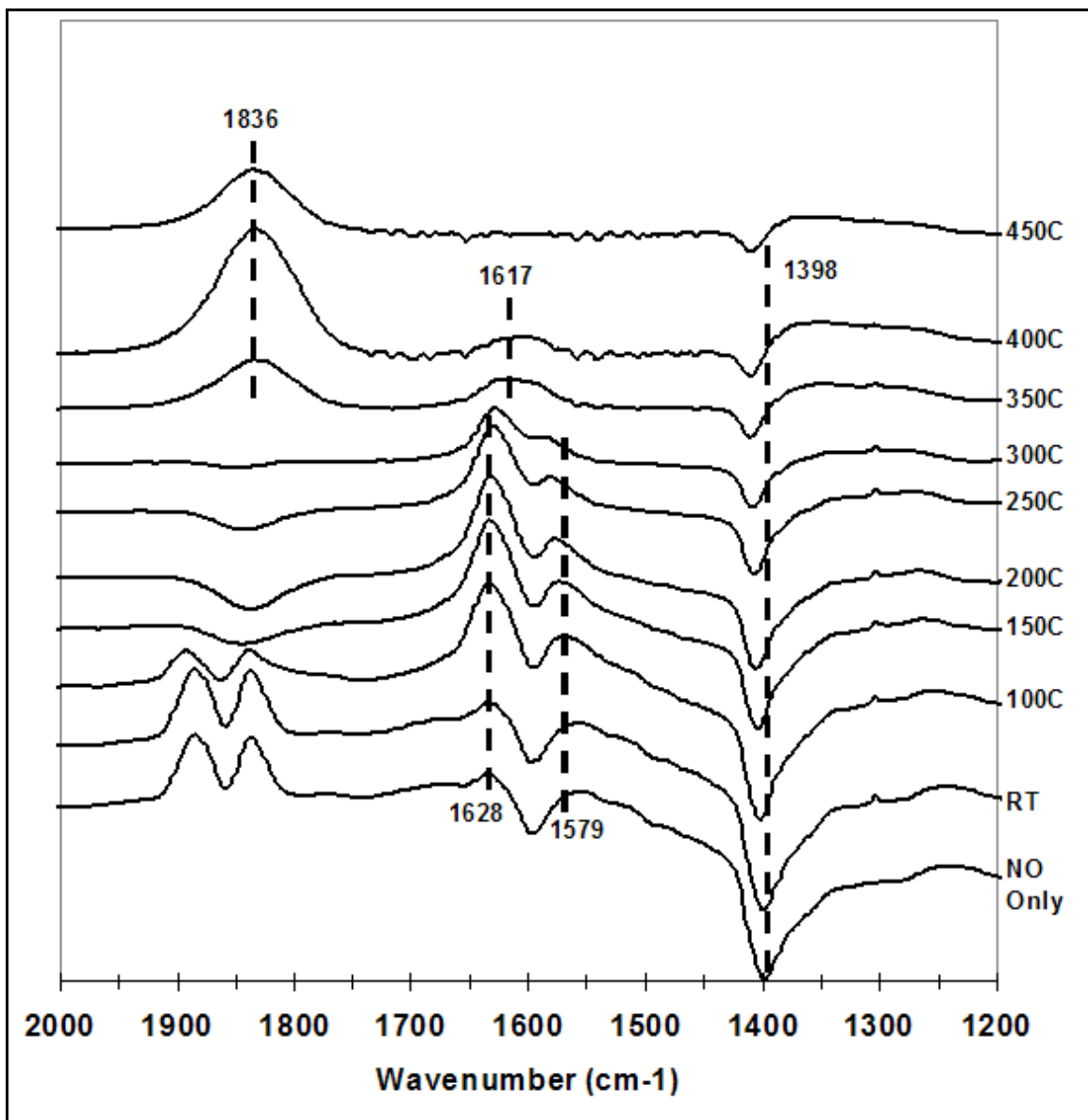


Figure 41: NO temperature programmed desorption by DRIFTS. TPD performed under CH₄ and O₂ flow.

In the high wavenumber range the formation of CO₂ bands at 350°C are larger than in the CH₄ only TPD. In the presence of O₂ the combustion of CH₄ is expected to occur.

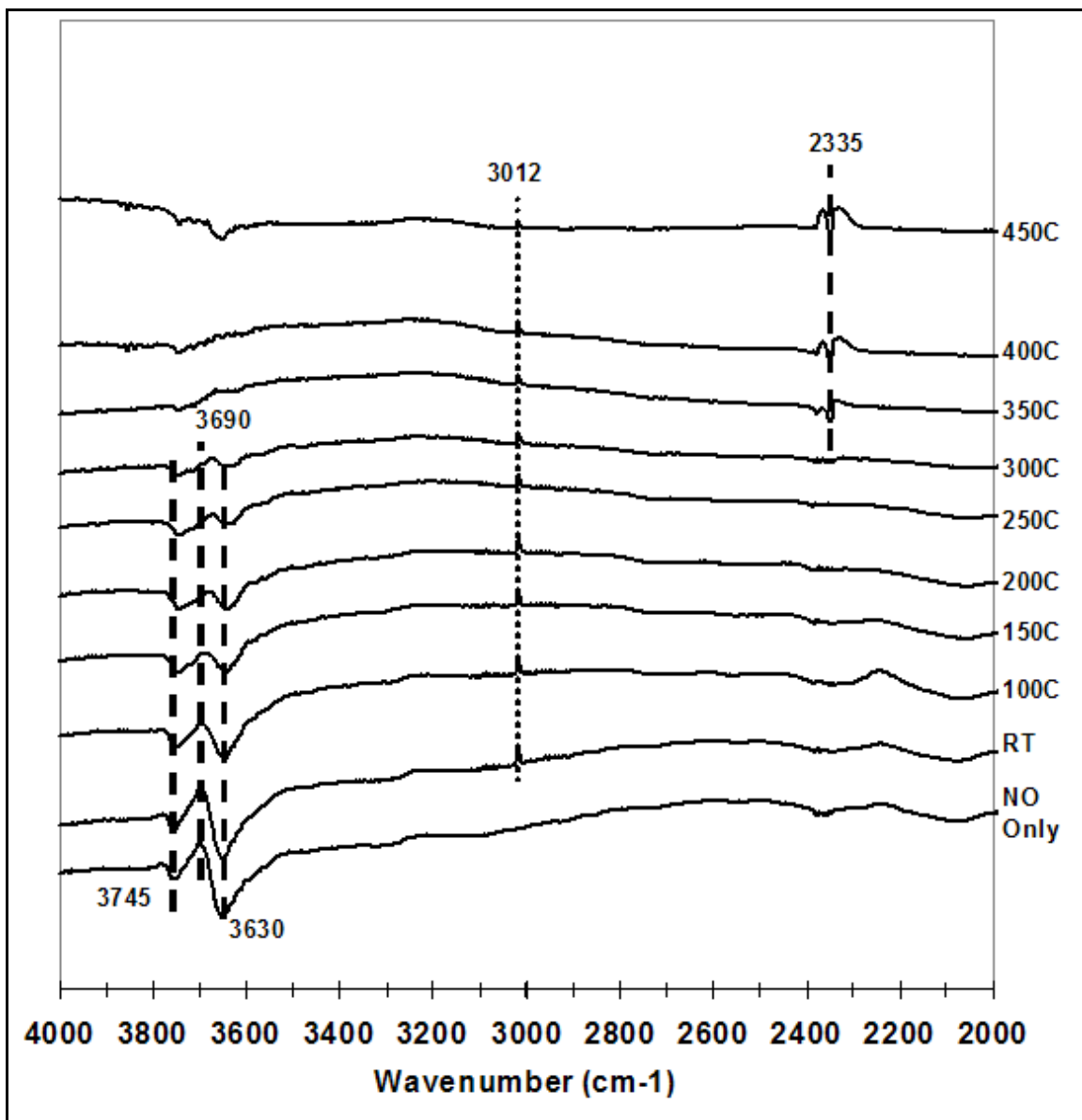


Figure 42: NO temperature programmed desorption by DRIFTS. TPD performed under CH₄ and O₂ flow. High wavenumber region.

Results for NO₂ TPD-DRIFTS under CH₄+O₂ flow, presented in Figure 43 and 44 are similar to those observed in the NO experiment. The conversion of the 1628/1579 cm⁻¹ bridged/bidentate nitrate pair to the 1617 cm⁻¹ bridged nitrate occurs at 350°C, which is 50°C higher than in the CH₄ only run. The negative 1398 cm⁻¹ band remains up to 450°C. As in the NO experiment the formation of the 1836 cm⁻¹ species occurs at 350°C and remains until 450°C. In this temperature range however the 1836 cm⁻¹ band is more intense with NO₂ adsorption.

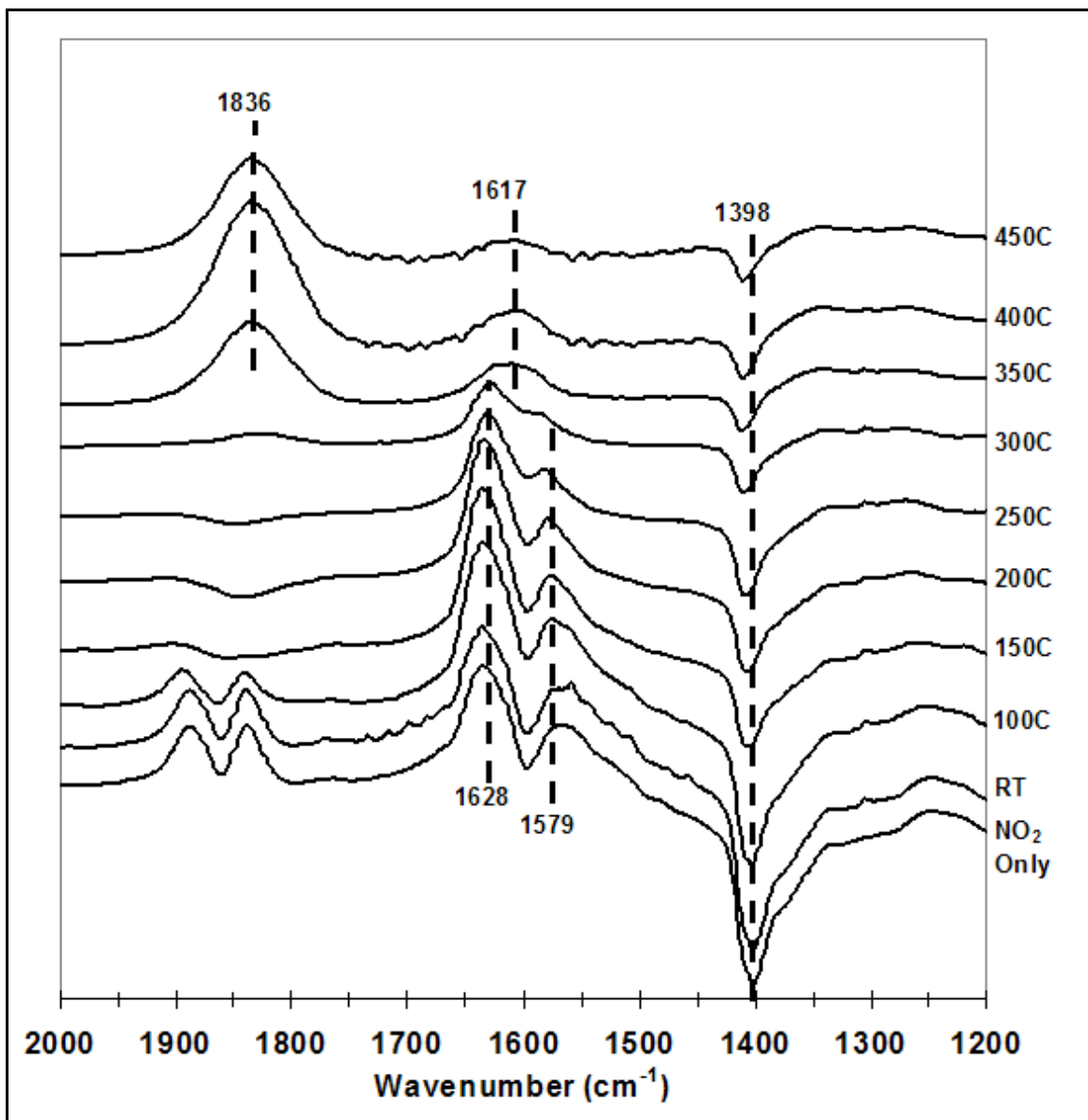


Figure 43: NO₂ temperature programmed desorption by DRIFTS. TPD performed under CH₄ and O₂.

Above 2000 cm^{-1} the greater formation of CO_2 is again observed as compared to the TPD under only CH_4 . The CO_2 bands are present at 300°C , possible further evidence of the improved reducibility of NO_2 . The hydroxyl region appears similar to the NO experiment, with the formation of a negative at 3750 cm^{-1} again observed. For both experiments performed under $\text{CH}_4 + \text{O}_2$ flow, an increase in sulfate interaction and in the temperature window for the 1898 cm^{-1} species is observed. This may indicate that the presence of O_2 in the feed stream stabilizes surface nitrate species.

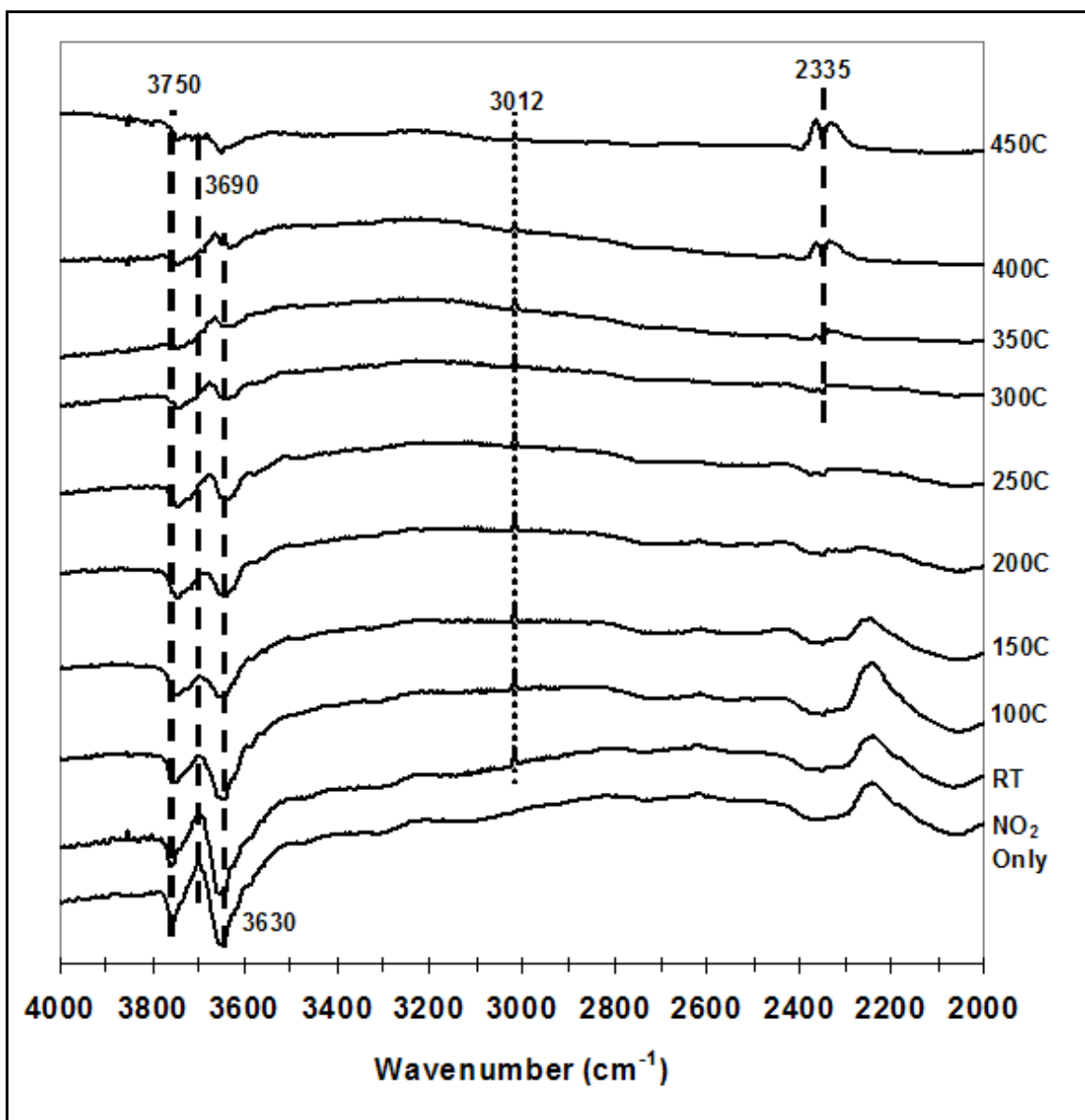


Figure 44: NO_2 temperature programmed desorption by DRIFTS. TPD performed under CH_4 and O_2 . High wavenumber region.

Several important differences are observed through *in-situ* DRIFTS studies of NO and NO₂ reduction with CH₄ over 0.5%Pd/5%SZ. It is clear that upon adsorption of the NO_x different surface are present. Furthermore, monitoring of the sulfate band at 1398 cm⁻¹ indicates that the NO₂ interacts more strongly with these surface acid sites. In the presence of CH₄ or CH₄+O₂ the production of CO₂ begins earlier with NO₂. Additionally a band at 1836 cm⁻¹, which may be a reaction intermediate, both forms and disappears at lower temperature with adsorbed NO₂ than with adsorbed NO. Further mechanistic studies are needed to fully understand the mechanistic differences in the NO and NO₂ reduction, as well as to identify important reaction intermediates and catalytic active sites.

NO Reduction with CH₄ Over Mixed Oxidation and Reduction Catalyst Beds

To test the overall performance of the two-stage system, activity tests of the reduction of NO with CH₄ were performed over a combined system. Oxidation and reduction catalysts were physically mixed into a single packed bed reactor. Such an arrangement allows for the production of NO₂ on the oxidation catalyst in close proximity to the reduction catalyst. Additionally reduction of NO₂ to N₂ will help to overcome the thermodynamic limitations of the oxidation catalyst. As NO₂ is consumed, the oxidation equilibrium will be driven towards producing more NO₂.

The initial tested mixture consisted of 0.05g of 10%Co/TiO₂ IWI400 and 0.20g of 0.5%Pd/5%SZ. The steady-state reaction tests were performed in the standard feed of 1000ppm NO, 3000ppm CH₄ and 10% O₂ at GHSVs of 50,000 hr⁻¹ and 35,000hr⁻¹. Figures 45 and 46 compare the results of the NO reduction over the catalyst mixture to the NO₂ and NO reduction results over just 0.5%Pd/5%SZ. These experiments were performed at the same space velocity. Below 350°C N₂ yield over the mixture remains lower than seen over the reduction catalyst with NO₂, although it is better than yields observed for the NO reaction over only the reduction catalyst. At 350°C and above, the N₂ yields are similar for NO₂ reduction and NO reduction over the catalysts mixture. Since a smaller amount of oxidation catalyst was present in the mixed bed when compared to the oxidation test reactions, it would be expected that equilibrium conversions are not reached at as low a temperature, explaining the activity difference below 350°C. It was very promising however that in the maximum activity range for the reduction reaction, N₂ yields over the mixture are nearly the same as those for direct NO₂ reduction. Comparing CH₄ conversions from these reaction runs in figure 46 shows that above 350°C higher conversions are reached over the catalyst mixture than over the 0.5%Pd/5%SZ. This indicates that the oxidation catalyst has some activity at higher temperatures for the CH₄ combustion reaction, although below 400°C the methane conversion observed over the mixed catalyst bed is not significantly higher than that seen over the reduction catalyst.

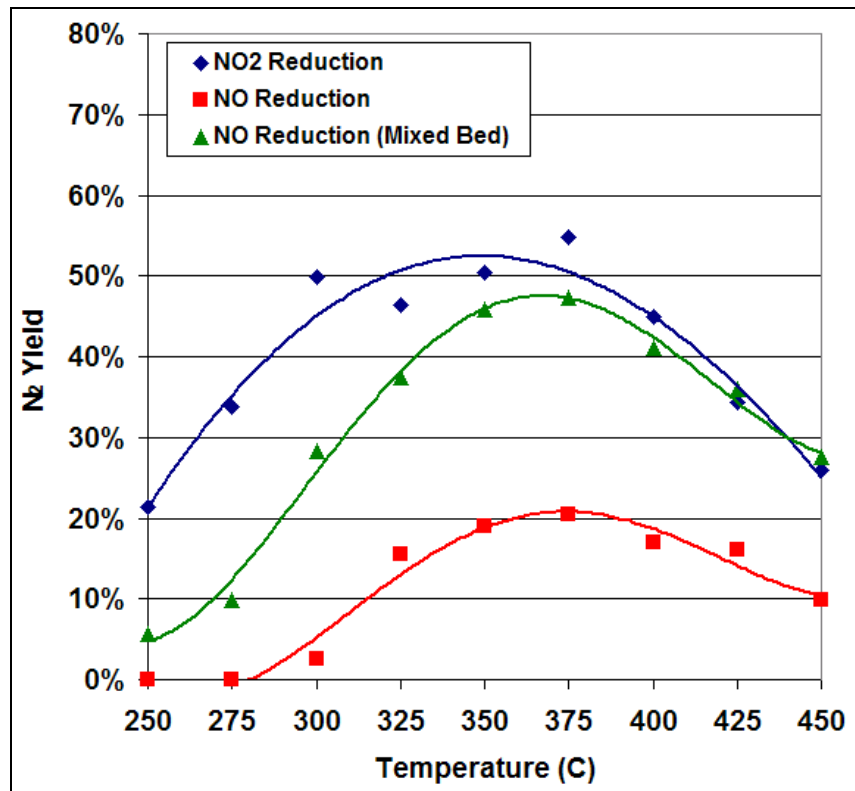


Figure 45: N₂ yield from the NO reduction over mixed bed of 0.5%Pd/5%SZ and 10%Co/TiO₂.

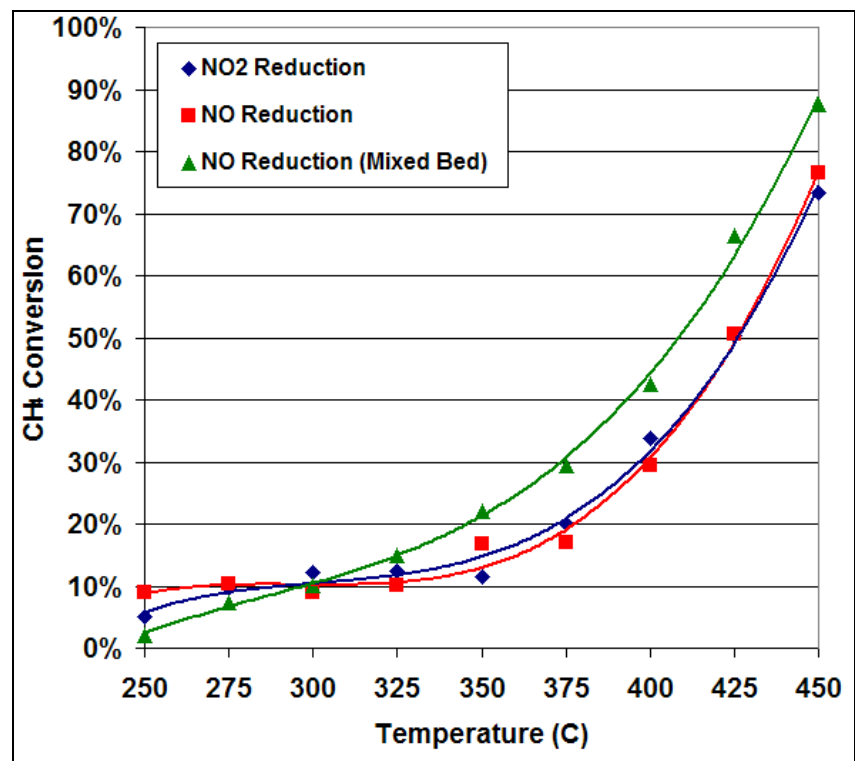


Figure 46: CH₄ conversion from the NO reduction over mixed bed of 0.5%Pd/5%SZ and 10%Co/TiO₂.

The steady-state reaction results of an initial residence time study over the physical mixture of oxidation and reduction catalysts are presented in figure 47. Gas flow rate was reduced over the catalysts bed to produce a GHSV of 35,000 hr⁻¹. The N₂ yield at the lower space velocity is shifted toward lower temperatures. Below 375°C N₂ yields are 5-10% higher than at 50,000 hr⁻¹. At 400°C and above the yields in the lower space velocity run fall below those observed at high space velocity. Examination of CH₄ conversion results shows that higher conversions are reached for a given temperature at the lower space velocity. Higher conversions are expected based on the N₂ yield data, and explain the N₂ yield decrease occurring at lower temperatures in the 35,000 hr⁻¹ GHSV run.

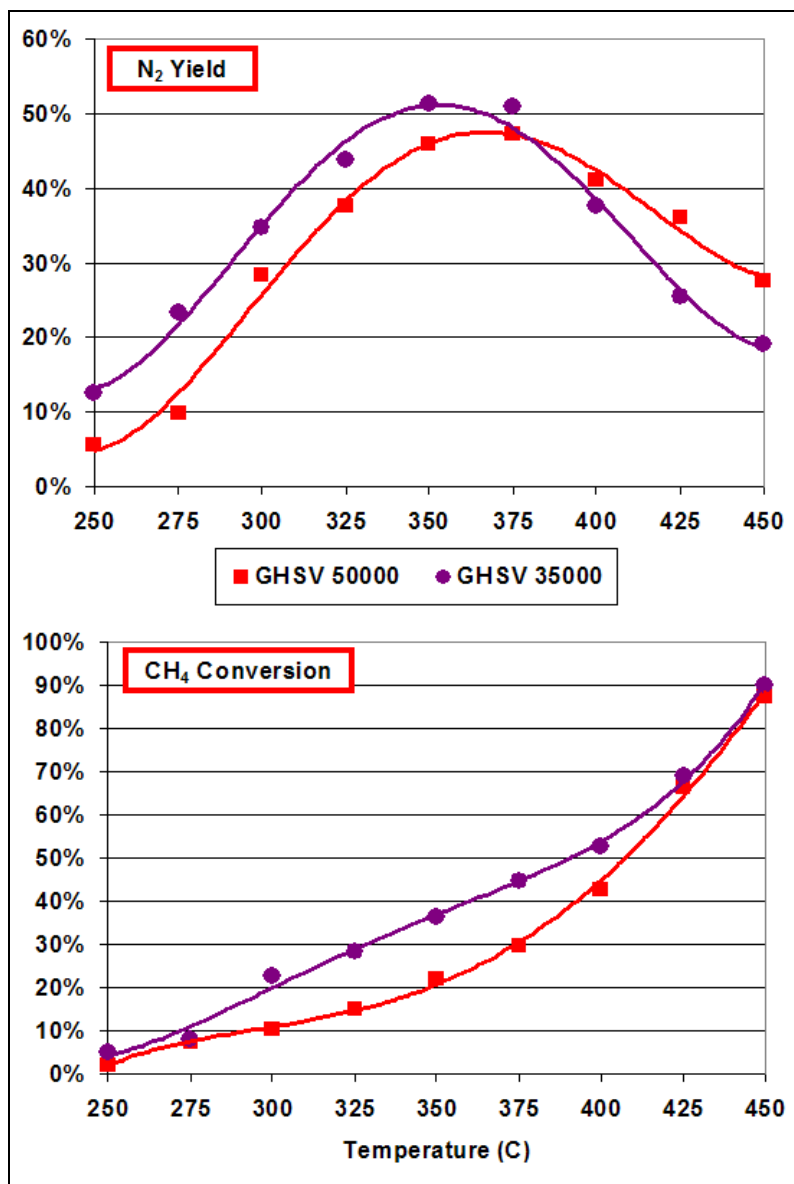


Figure 47: Effect of residence time on NO reduction over a mixture of 10%Co/TiO₂ IWI400 and 0.5%Pd/5%SZ.

As discussed in previous sections catalyst development led to the synthesis of more active oxidation and reduction catalysts. Mixed bed testing using better performing catalysts in each stage resulted in significantly improved performance for the reduction of NO with CH₄. 0.3%Pd/5%SZ was seen to give higher N₂ yields in the reduction of NO₂ with CH₄. Work from the oxidation catalyst project showed 10%Co/ZrO₂ to be the best performing oxidation catalyst. A mixed bed of these two catalysts in the same ratio as the previous test was tested for the reduction of NO with CH₄. An identical feed stream of 1000 ppm NO, 3000 ppm CH₄, and 10% O₂ in balance He was used. Space velocity was also kept constant at 20,000 hr⁻¹. Figure 48 contains N₂ yield results, showing a maximum of 80%. Yields were higher across the entire temperature range. This mixed bed composition achieved higher N₂ yields than even the direct reduction of NO₂ over the reduction catalyst.

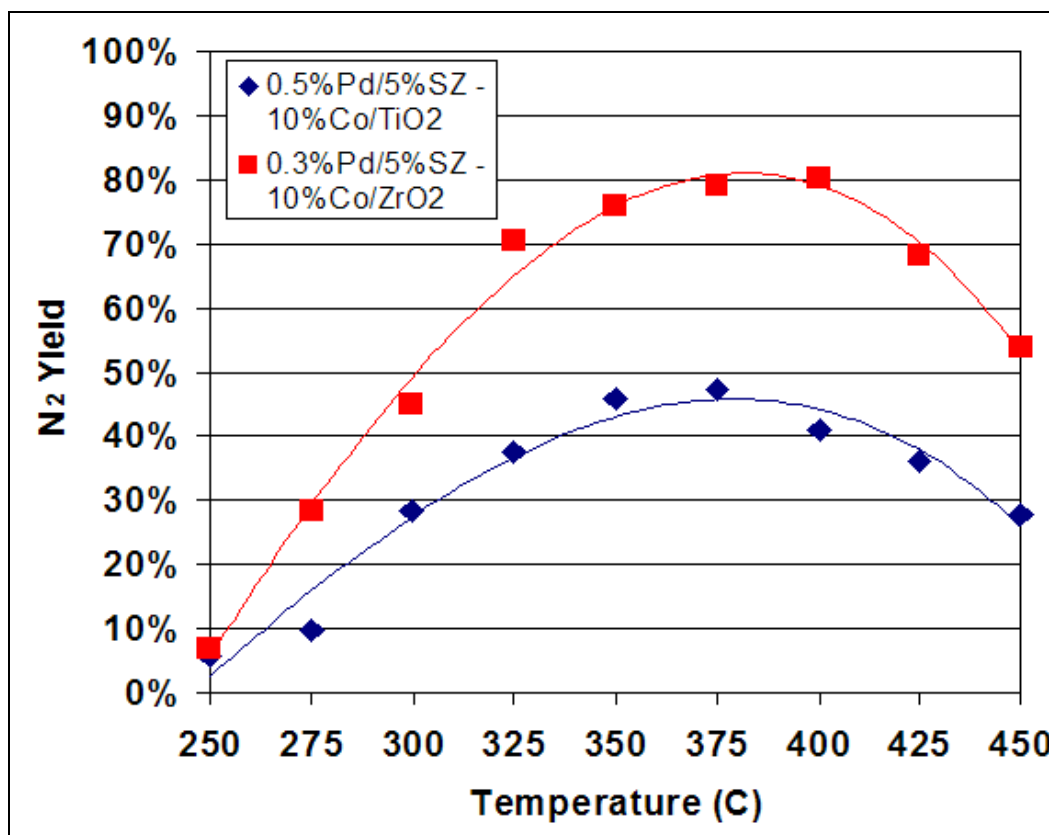


Figure 48: N₂ yield from the NO reduction over mixed bed of 0.3%Pd/5%SZ and 10%Co/ZrO₂.

CH₄ conversion as a function of temperature is shown in Figure 49. The bed containing the better performing components that reached higher N₂ yields, also reached higher CH₄ conversions at each reaction temperature. At the high and low temperatures investigated conversions were within 5%. However in the range of maximum N₂ yield the difference is large, 30-40%. Overall, the mixed bed reduction of NO reached high yields with lower levels of CH₄ present at a given reaction temperature.

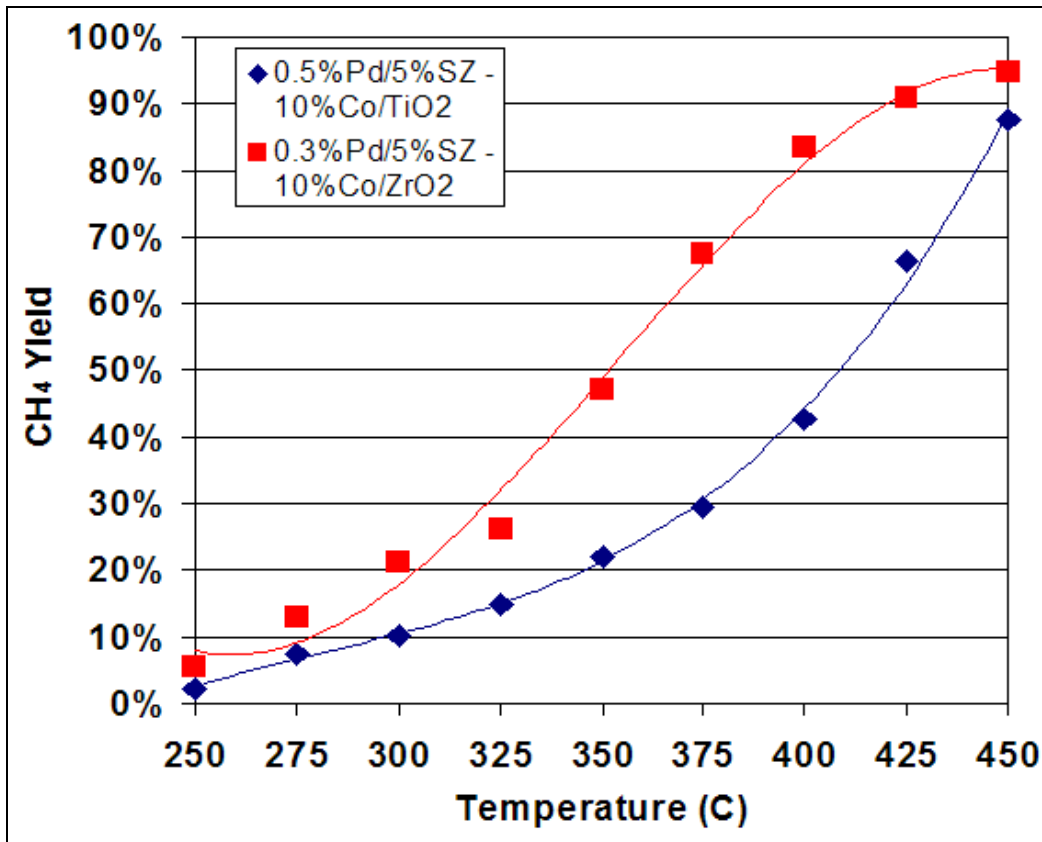


Figure 49: CH₄ conversion from the NO reduction over mixed bed of 0.3%Pd/5%SZ and 10%Co/ZrO₂.

Testing of the combined two-stage system has been demonstrated to give very high N₂ yields in the reduction of NO with CH₄. N₂ yields near 80% are attained across a broad temperature range of 350-400°C under model gas feeds. Additionally, the system is effective at removing excess CH₄ from the feed stream. As unburned hydrocarbons are potentially an additional pollution concern from natural gas engines, this result represents an added benefit.

Two-Stage Reduction of NO Under Simulated Lean Exhaust

Actual lean-burn natural gas engines exhaust contains a significantly different gas composition than in the model conditions used to evaluate the individual catalysts and the combined system. Real exhaust also contains higher unburned hydrocarbons such as C_2H_6 and C_3H_8 , CO, CO_2 , and H_2O . These species are both additional pollutants, and could potentially react over the NO reduction catalyst system. Testing of these species in the system was thus performed.

The effect of CO was tested first, and it was shown that CO had no activity as a reducing agent over the Pd/SZ reduction catalyst. However preliminary tests over the 10%Co/ZrO₂ IW oxidation catalyst demonstrated that the catalyst is highly active for the oxidation of CO to CO₂. In a feed containing 600 ppm CO and 10% O₂ in balance He, the catalyst was able to completely oxidize the CO at to CO₂ 20°C. Further testing of the catalyst examined the activity in much more concentrated CO streams. Slightly elevated temperatures were necessary to reach complete CO conversion in a feed of 1.5% CO and 10% O₂ in balance He. Figure 50 contains the results from this reaction test. Complete conversion of the concentrated CO stream was achieved at 135°C. Activity of the catalyst was also very stable, with the total test lasting 182 hours.

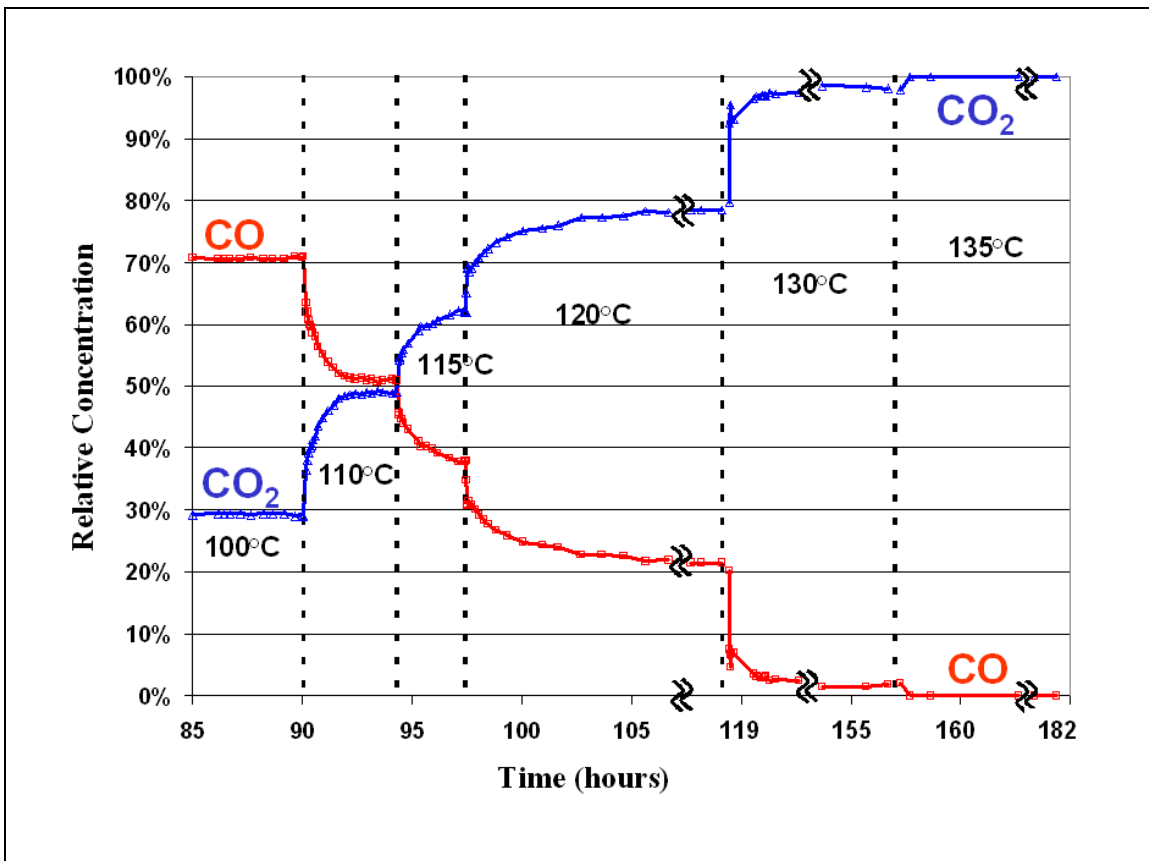


Figure 50: Steady-state CO oxidation on 10%Co/ZrO₂. CO and CO₂ concentrations are presented as % of inlet concentration at various temperatures.

Mixed beds containing 0.3%Pd/5%SZ and 10%Co/ZrO₂ were tested for the reduction of NO with a simulated natural gas feed. Gas compositions were 400ppm NO, 1700ppm CH₄, 200ppm C₂H₆, 100ppm C₃H₈, 600 ppm CO and 10% O₂ in balance He. Total gas flow was 45cm³/min. In these tests the ratio of catalysts in the mixed bed was changed by adjusting the amount of oxidation catalyst. Figure 51 show the N₂ yields from the reduction of NO with a simulated natural gas. N₂ yield was observed to have a higher maximum when the amount of oxidation catalyst in the bed was reduced. The 1:0.25 mixture reached a maximum of 79% at 375°C. Changing the catalyst ratio to 1:1 significantly reduced the maximum N₂ yield as only 61% was reached.

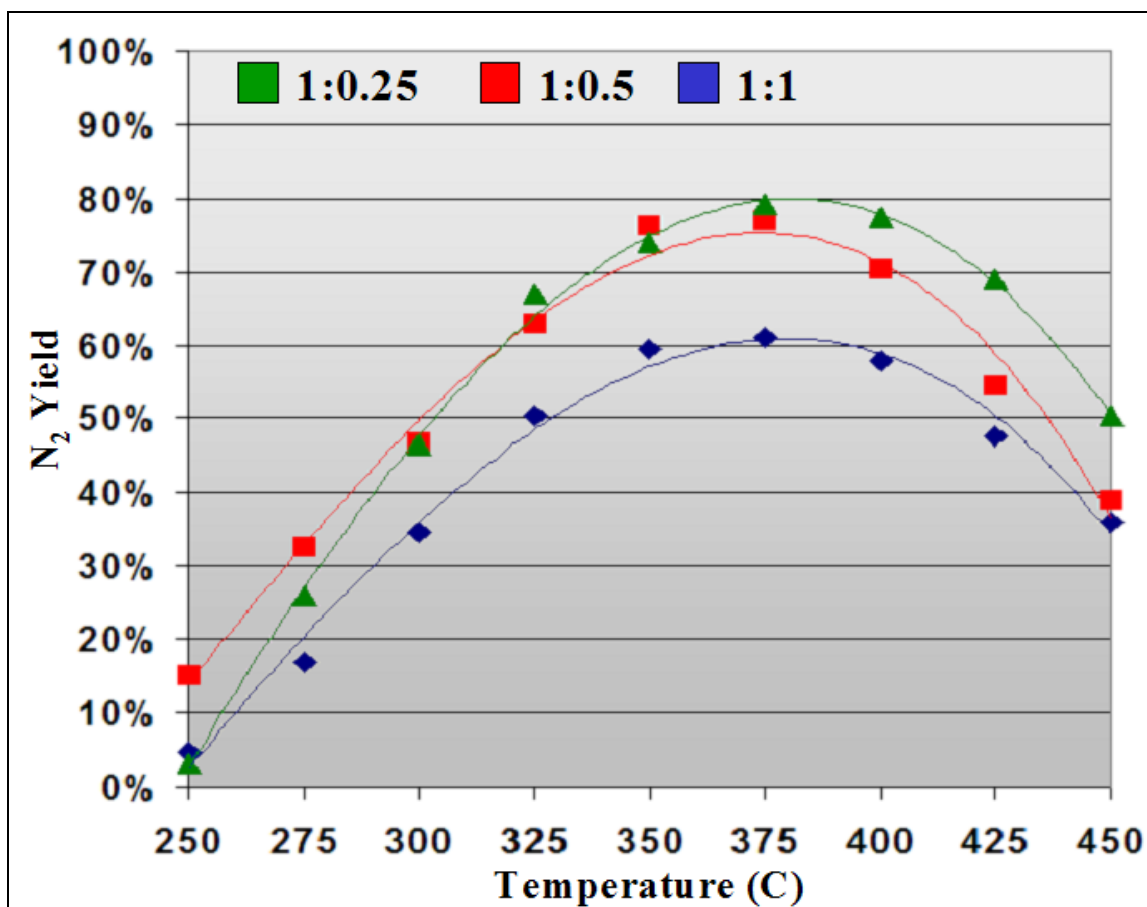


Figure 51: N₂ yield from the NO reduction over mixed beds containing 0.3%Pd/5%SZ and 10%Co/ZrO₂.

Examination of the hydrocarbon conversion (Figure 52) during these NO reduction reactions showed that conversions were highest over the 1:1 ratio, and lowest over the 1:0.5 ratio. In all three experiments conversion of C₂H₆ and C₃H₈ was complete by 300°C. CH₄ conversion increased with temperature over all three beds, and was complete at 450°C. Differences in hydrocarbon conversion again showed that the oxidation catalyst plays a role in these reactions. N₂ yield in the mixed bed using a simulated natural gas was much higher than over only the reduction catalyst. It appears from the reduction catalyst test that the higher hydrocarbons are selective for the

reduction of NO_2 to NO . In the mixed bed any NO formed in this way is quickly reoxidized to NO_2 . Such a cycle maintains NO_2 over the reduction catalyst for reaction to N_2 , but also may result in the very high hydrocarbon conversions observed at low temperatures. CO in the simulated exhaust was completely oxidized to CO_2 across the entire temperature range.

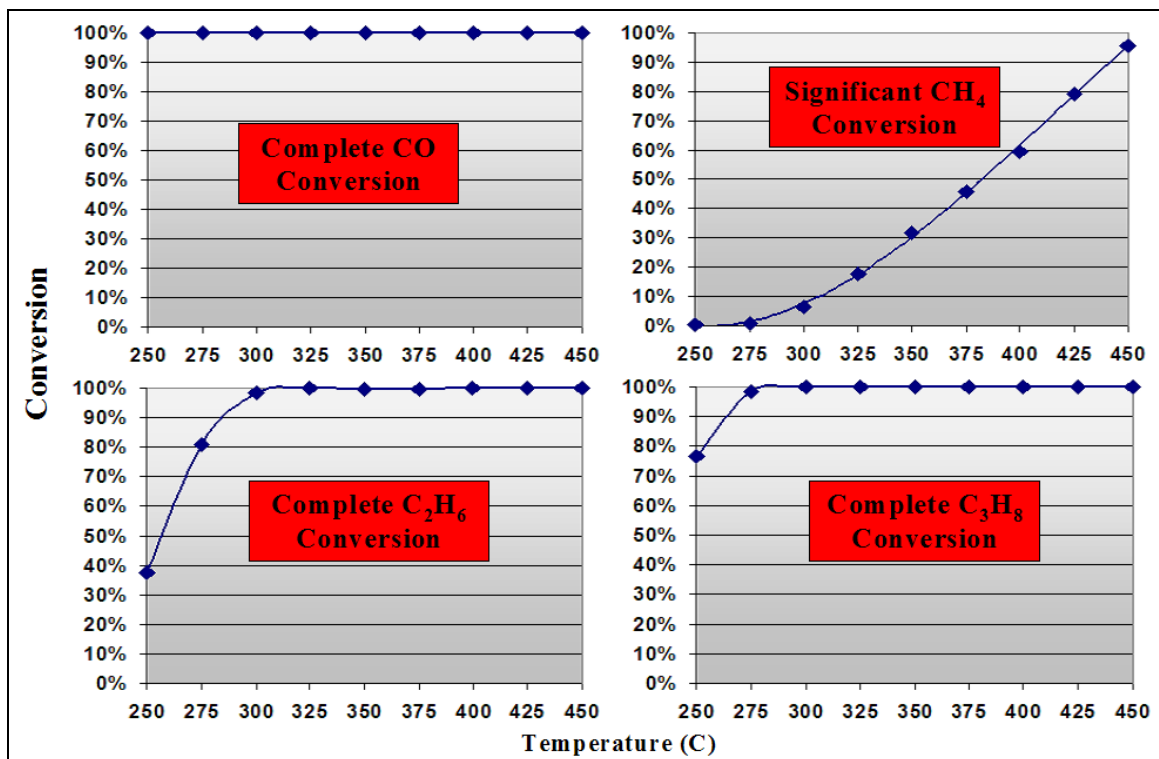


Figure 52: Hydrocarbon conversions from the NO reduction over mixed beds containing 0.3%Pd/5%SZ and 10%Co/ZrO₂.

Testing the combined two-stage system under simulated exhaust yielded promising results. Firstly the addition of exhaust components did not result in a loss of activity for the reduction of NO to N_2 . N_2 yields of near 80% across a broad temperature range were reached. The system is also very effective at the removal of CO and unburned hydrocarbons; species that are additional exhaust pollutants. In the temperature range of maximum N_2 yield oxidation of CO , C_2H_6 , and C_3H_8 are complete and CH_4 conversion is in the range of 60-80%.

Effect of Water Vapor

Water vapor represents a significant fraction of engine exhaust streams. Several reaction experiments were performed to assess the affect of water on the catalyst system performance. To further examine the ability of 10%Co/ZrO₂ IWI 300 to oxidize CO to CO₂, temperature-programmed reaction (TPrxn) experiments were conducted with reactants and products monitored via mass spectrometry. The reaction conditions were as follows: 5000ppm CO, 1% O₂, and 0 or 2% H₂O in balance He.

Figure 53 shows the TPrxn results for CO oxidation of a dry and wet gas stream. By monitoring the CO and CO₂ profiles it can be clearly observed that CO₂ formation occurs when CO is consumed, which would be consistent with the steady-state reaction experiments showing that CO₂ was the only product formed during this experiment. For the dry experiment, the results obtained agreed with the steady-state reaction experiment. By 135°C, complete conversion of CO was achieved. At 110°C in both experiments, 50% conversion of CO was reached.

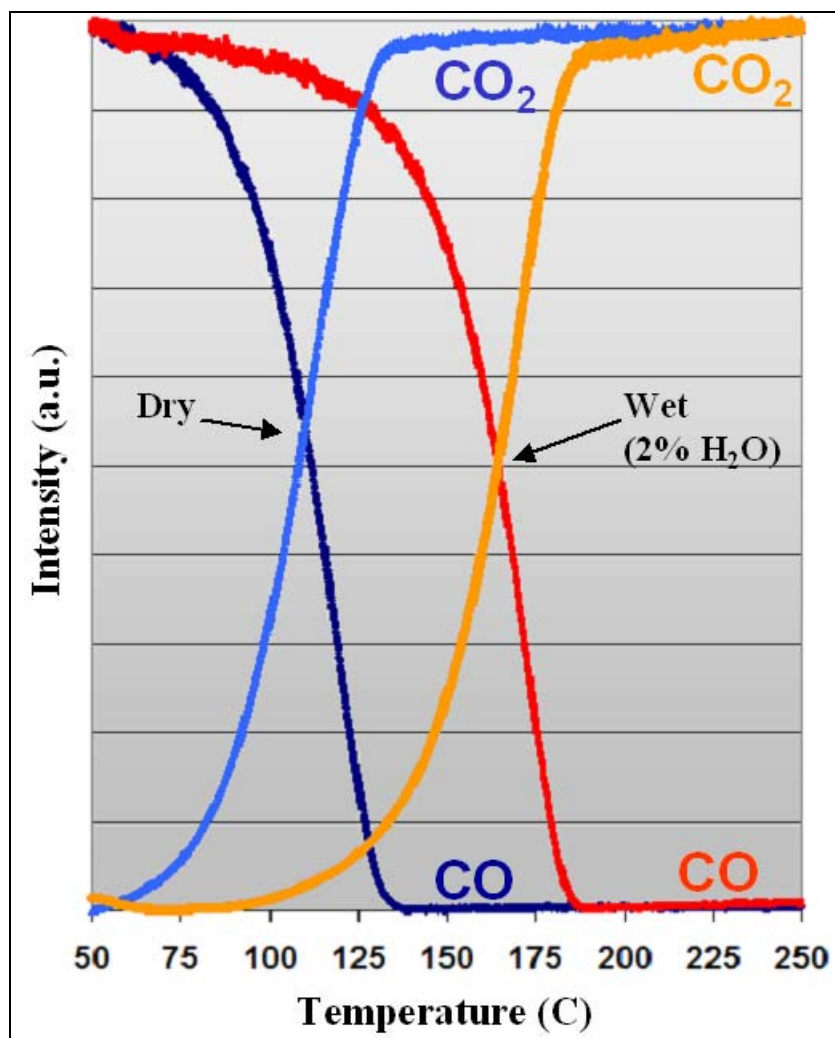


Figure 53: TPrxn for CO oxidation on 10%Co/ZrO₂.

50% conversion of CO was reached. When 2% H₂O was introduced to the reactant stream, there was an observed shift to higher temperatures by about 50°C when compared to the dry experiment for the same level of CO conversion. Even in the presence of 2% H₂O, however, 100% conversion of CO to CO₂ was achieved by 185°C, well below reaction temperature of the NO reduction system.

The activity of the two-stage system for NO reduction with CH₄ in water vapor was also tested. Results were compared to the dry run using the same mixed bed composition, 0.3%Pd/5%SZ and 10%Co/ZrO₂ (2:1). Reaction conditions were 1000ppm NO, 3000ppm CH₄, and 10% O₂ in balance He. 3% H₂O was added by sending the O₂ and He streams through a heated bubbler. N₂ yields are presented in Figure 54.

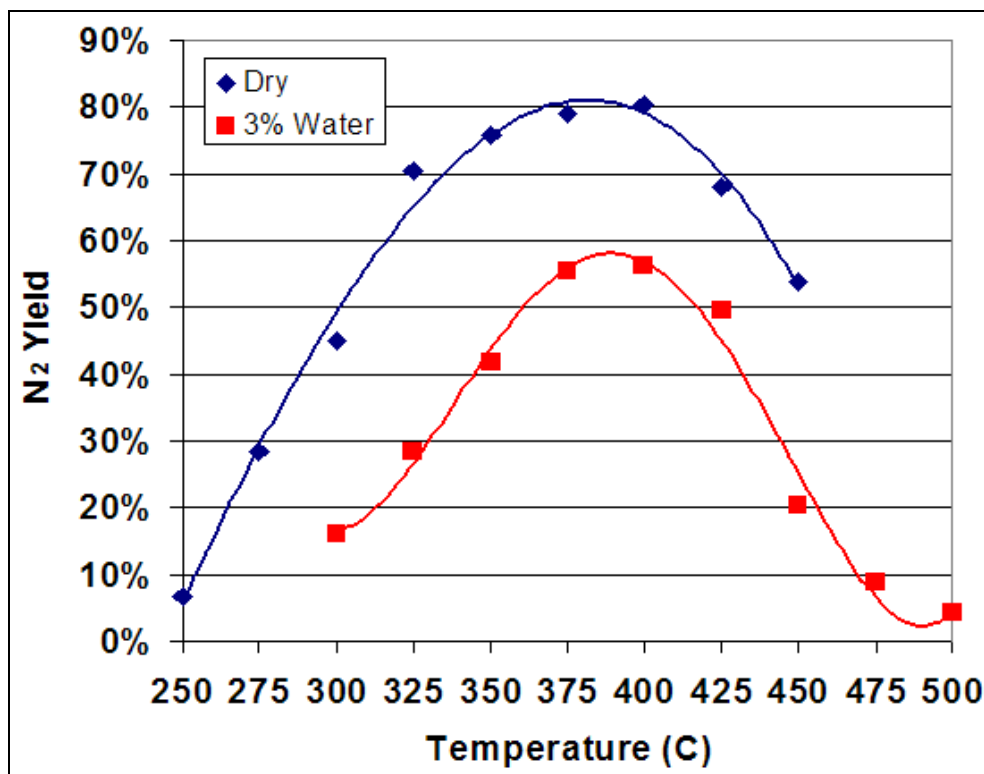


Figure 54: N₂ yields from NO reduction under dry and 3% H₂O streams, over mixed beds containing 0.3%Pd/5%SZ and 10%Co/ZrO₂.

With the addition of 3% water to the feed stream N₂ yields are reduced over the mixed bed. A maximum N₂ yield of 56% was observed around 375-400°C. Across the temperature range N₂ yield was reduced by more than 20% in comparison to the dry NO reduction reaction. Figure 55 contains CH₄ conversion results from the dry and 3% H₂O runs. The light off of CH₄ conversion was delayed by approximately 50°C by the addition of H₂O. The decreased activation of CH₄ over the catalyst may be a partial cause in the decreased reduction activity. Steady-state reaction tests of the same mixed bed composition performed under increasing H₂O concentration showed a loss of activity with the introduction of more H₂O. These results are presented in Figure 56.

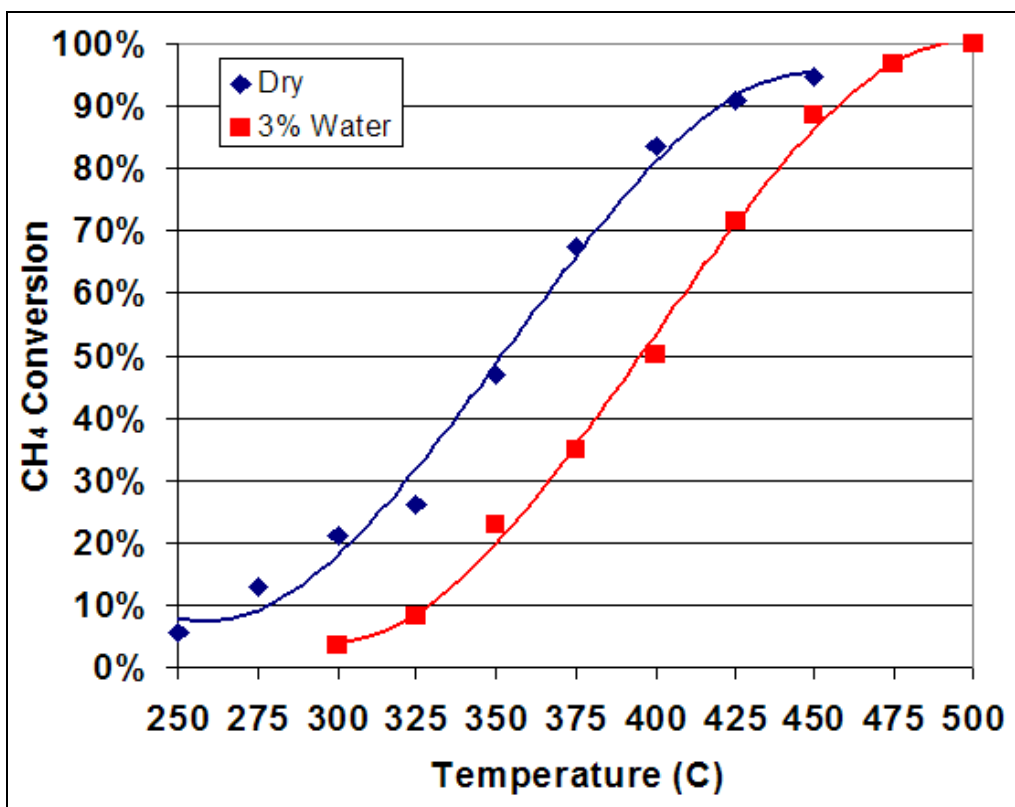


Figure 55: CH₄ conversion from NO reduction under dry and 3% H₂O streams, over mixed beds containing 0.3%Pd/5%SZ and 10%Co/ZrO₂.

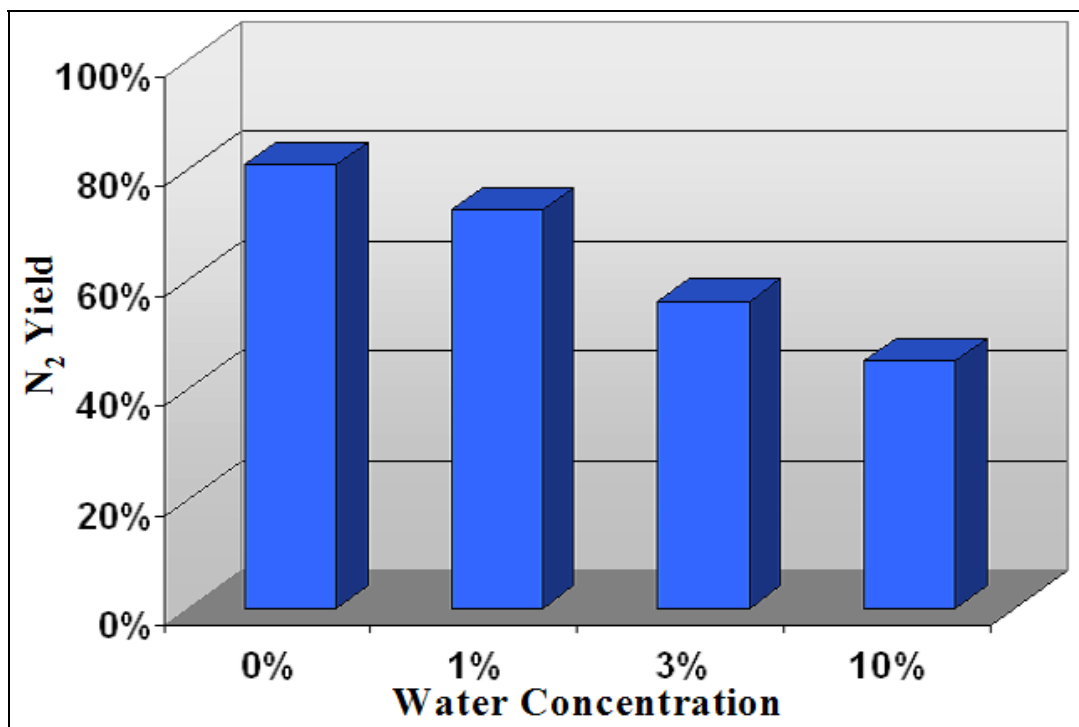


Figure 56: Maximum N₂ yield in NO reduction with CH₄ over the mixed bed as a function of H₂O concentration.

Testing of the individual catalysts in the two-stage system demonstrated that the oxidation catalyst was not affected by the presence of up to 10% H₂O in the feed stream. Results of the NO oxidation reaction performed under 1000 ppm NO, 10% O₂, and 10% H₂O in balance He on 10%Co/TiO₂ IW are shown in Figure 57. Deactivation therefore appears to occur over the Pd/SZ reduction catalyst.

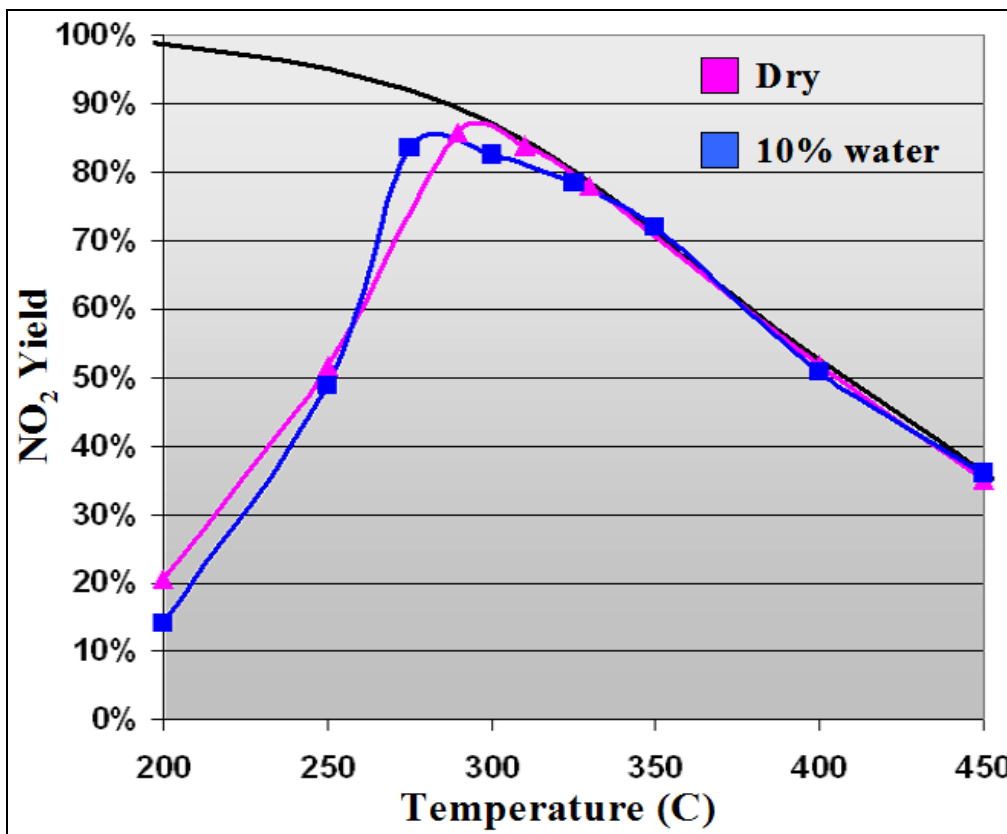


Figure 57: NO oxidation under dry and 10% H₂O streams over 10%Co/TiO₂ IW.

Investigation of the mechanism of deactivation was performed using temperature programmed reaction and *in-situ* DRIFTS techniques. Sulfate groups were shown to be necessary for activity in the reduction of NO₂ with CH₄. These species are known to be unstable at high reaction temperatures, or under reducing atmospheres. Temperature programmed reaction was used to determine whether the addition of water to the reaction feed resulted in the loss of surface sulfate groups. The NO reduction with CH₄ was performed over a mixed bed containing 0.3%Pd/5%SZ and 10%Co/ZrO₂ (2:1). Reaction conditions were 1000ppm NO, 3000ppm CH₄, and 5% O₂ in balance He. For the water-containing run 1% H₂O was introduced by sending the O₂ and He streams through a room temperature bubbler. The sample was calcined in 20% O₂/He for 30 minutes, then cooled under He. The temperature program was run at 10°C/min. Gas species were monitored by mass spectrometry.

Figure 58 shows the CO₂ (m/z = 44) and SO₂ (m/z = 64) signals from the temperature programmed reaction run under dry and 3% H₂O containing feeds. CO₂ production occurs from both the NO reduction with CH₄, and the CH₄ combustion reaction. As in the steady-state reaction experiments the presence of H₂O in the feed stream suppressed these reactions. Below 600°C no desorption of SO₂ was observed under either the dry or H₂O containing conditions.

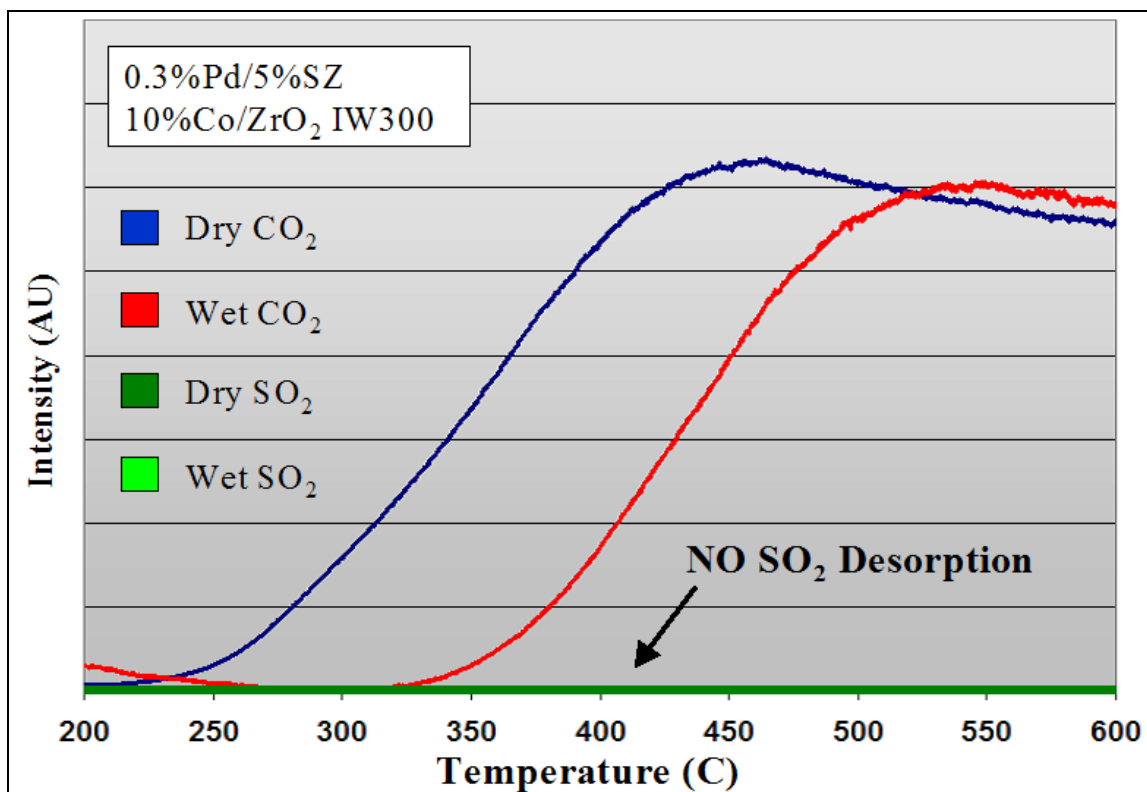


Figure 58: CO₂ and SO₂ mass spectra during the temperature programmed reaction of NO+CH₄, with and without 1% H₂O in the feed.

The addition of water vapor to the reaction feed does not result in the removal of surface sulfate species, and the deactivation is therefore not obviously irreversible. The interaction of adsorbed water with the surface of 0.3%Pd/5%SZ was examined using DRIFT spectroscopy. Sample was loaded into a controlled atmosphere spectroscopy cell and calcined in 20%O₂/He at 400°C for 30 minutes. The gas was then changed to He and the sample temperature raised to 450°C. Background spectra were taken at 50°C increments as the sample temperature was lowered to ambient. At room temperature 1% H₂O vapor was introduced to the sample by sending the He flow through a bubbler.

Water was adsorbed for 30 minutes. Subtracted background spectra were then taken to observe adsorbed water species. The first spectrum was taken during H₂O adsorption, and the rest taken at 50°C increments as the sample temperature was raised. Each temperature was held for 15 minutes before spectra were taken.

Figure 59 shows the low wavenumber region of the DRIFTS TPD of H₂O from 0.3%Pd/5%SZ. The observed positive peaks at 1650, 1225 and 1075 cm⁻¹ are all characteristic of adsorbed H₂O. The large negative band that appears between 1380 and 1400 cm⁻¹ is due to the interaction of adsorbed H₂O with surface S=O groups. All of these bands consistently decreased in intensity with increasing sample temperature. By 450°C essentially all H₂O was gone from the catalyst surface. Additionally the S=O band fully recovered. This indicated that the adsorption and desorption of H₂O did not permanently affect the surface acid sites.

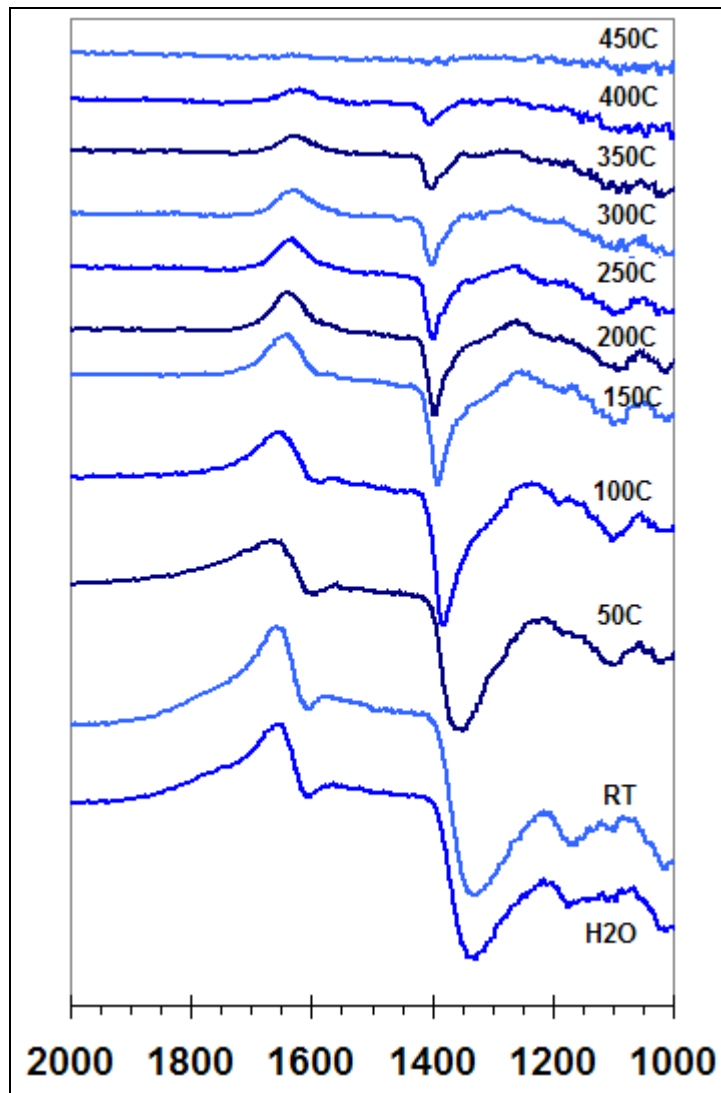


Figure 59: DRIFTS spectra of H₂O TPD from 0.3%Pd/5%SZ. Low wavenumber region.

Figure 60 contains the high wavenumber region of the H₂O TPD DRIFTS spectra. The very broad band between 3000-3600 cm⁻¹ is due to H₂ bonding in adsorbed H₂O. This band disappears with increasing temperature.

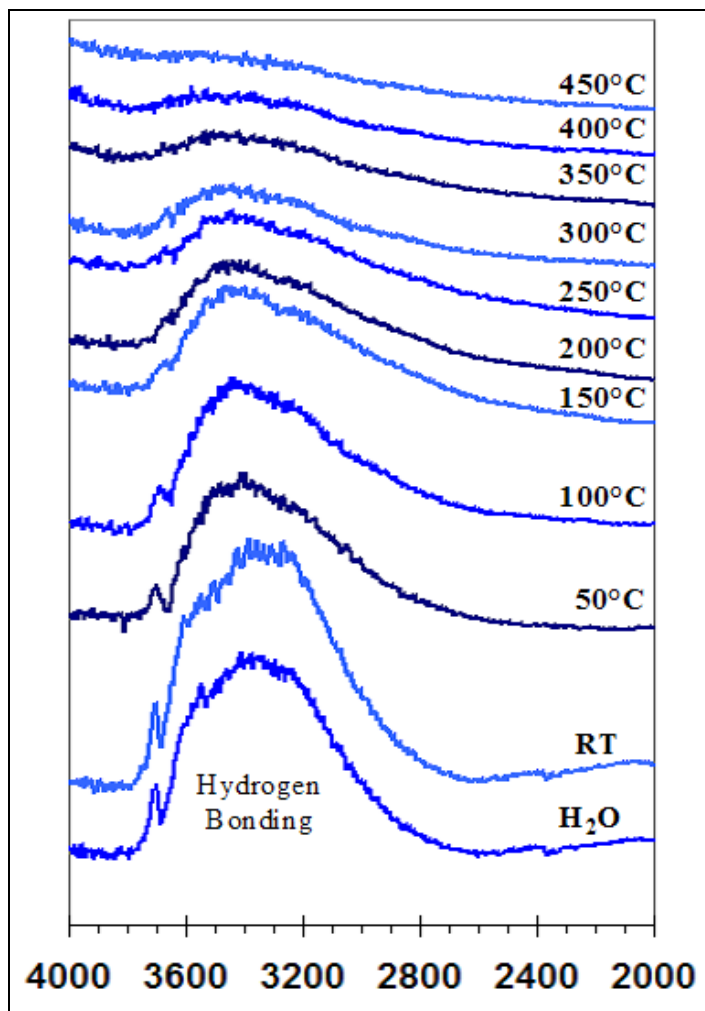


Figure 60: DRIFTS spectra of H₂O TPD from 0.3%Pd/5%SZ. High wavenumber region.

The combined information from temperature programmed reaction and TPD-DRIFTS studies indicated that deactivation by water vapor was due to competitive adsorption of H₂O. Increasing the surface acidity of the catalyst was explored as a method of improving activity in H₂O containing streams. 0.3%Pd/15%SZ was prepared and tested as a component of a mixed bed for the reduction of NO with CH₄ in the presence of H₂O.

Activity was measured under steady-state reaction conditions after approximately 1 hour on-stream. The sample was held at 400°C. Reactant concentrations were 1000ppm NO, 3000ppm CH₄, and 10% O₂ in balance He. Varying amounts of H₂O were introduced by sending the O₂ and He streams through a heated bubbler. Figure 61 shows the N₂ yields obtained under increasing H₂O concentrations. For comparison the steady-state

maximum yields of a bed containing 0.3%Pd/5%SZ are included. At each H₂O concentration N₂ yield is improved with the use of the 15%SZ support. Loss of activity is observed with increasing H₂O concentration, but is less severe than with the 5%SZ support. Under dry conditions N₂ yield was 91%, which decreased to 73% in the presence of 10% H₂O.

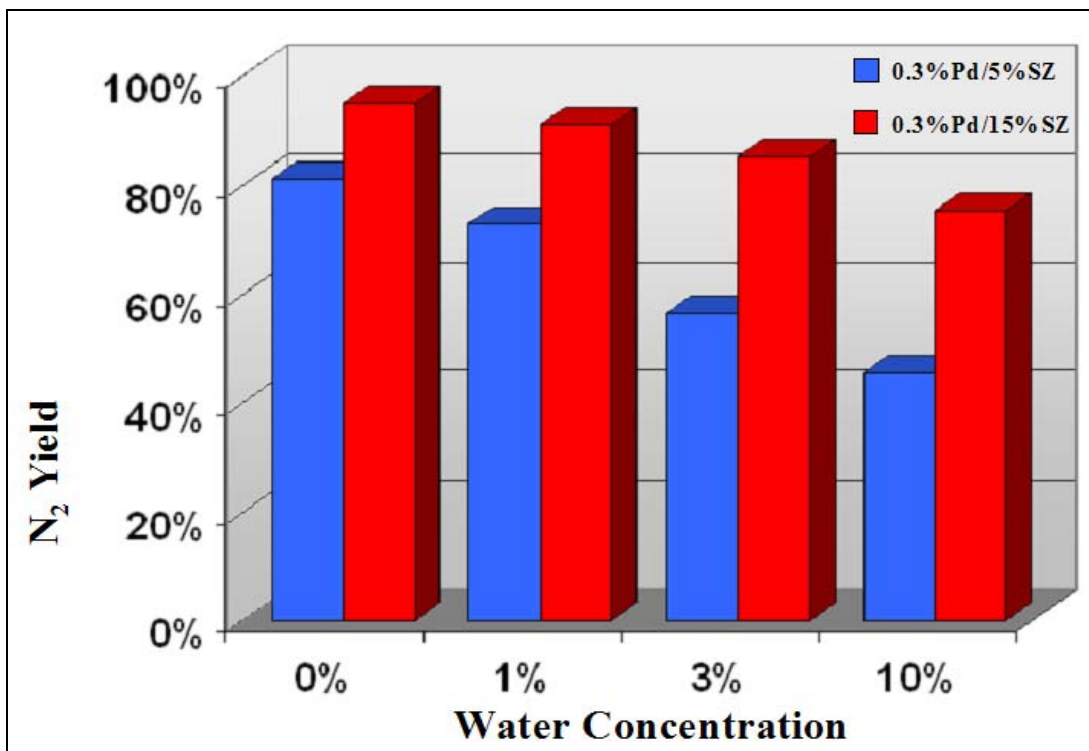


Figure 61: Effect of water vapor on N₂ yield over mixed beds containing 0.3%Pd/5%SZ and 0.3%Pd/15%SZ.

Outreach and Information Dissemination

Provisional Patent Applications Filed

Holmgreen, Erik M.; Yung, Matthew M.; Ozkan, Umit S., “Two-stage catalytic system for nitrogen oxide reduction with methane under lean conditions.”

Holmgreen, Erik M.; Yung, Matthew M.; Ozkan, Umit S., “Dual-catalyst system for lean exhaust aftertreatment.”

Holmgreen, Erik M.; Yung, Matthew M.; Ozkan, Umit S., “Low temperature oxidation of CO on Co/ZrO₂ catalysts.”

Publications

Holmgreen, E., Yung, M. and Ozkan, U.S., “Two-Stage Catalytic NO_x Reduction with Hydrocarbons for Lean Burn Gas Fired Reciprocating Engines” Proceedings of ICEF04 ASME Internal Combustion Engine Division 2004 Fall Technical Conference **893**, 1-7 (2004).

Yung, M., Holmgreen, E., and Ozkan, U.S., “Oxidation of NO to NO₂ over cobalt-based metal-oxide supported catalysts” to be submitted to *Journal of Catalysis*.

Holmgreen, E., Yung, M. and Ozkan, U.S., “NO and NO₂ reduction of Pd-based sulfated-zirconia catalysts” to be submitted to *Journal of Molecular Catalysis*.

Yung, M., Holmgreen, E., and Ozkan, U.S., “Low-temperature CO oxidation of Co/ZrO₂ catalysts” to be submitted to *Journal of Catalysis*.

Holmgreen, E., Yung, M. and Ozkan, U.S., “Two-stage catalytic reduction of NO with methane” to be submitted to *Applied Catalysis*.

Papers and Presentations

Holmgreen, Erik M.; Yung, Matthew M.; Ozkan, Umit S.; “Dual-catalyst system for lean exhaust aftertreatment from reciprocating engines.” Distributed Energy Peer Review, Crystal City VA, December 2005.; Poster Presentation.

Holmgreen, Erik M.; Yung, Matthew M.; Ozkan, Umit S.; “Oxidation of NO and CO over cobalt based metal oxide supported catalysts.” American Institute of Chemical Engineers Annual Meeting, Cincinnati OH, October 2005.

Holmgreen, Erik M.; Yung, Matthew M.; Ozkan, Umit S.; “Dual-catalyst system for lean exhaust aftertreatment.” American Institute of Chemical Engineers Annual Meeting, Cincinnati OH, October 2005.

Holmgreen, Erik M.; Yung, Matthew M.; Ozkan, Umit S.; "Two-Stage Catalytic Reduction of NO_x Methane Under Lean Conditions." North American Catalysis Society Annual Meeting, Philadelphia PA, May 2005.

Yung, Matthew M.; Holmgreen, Erik M.; Ozkan, Umit S.; "Two-Stage Catalytic Reduction of NO_x with Hydrocarbons in Lean Conditions." Ohio State Hayes Graduate Research Forum, Columbus OH, April 2005. (**1st Place Award**)

Holmgreen, Erik M.; Yung, Matthew M.; Ozkan, Umit S.; "Two-Stage Catalytic Reduction of NO_x Under Lean Conditions." 2nd Annual Advanced Stationary Reciprocating Engines Conference, Moving Forward in Low-Emissions and High-Efficiency Technologies, U.S. DOE, California Energy Commission, Diamond Bar, CA, March 2005.

Yung, Matthew M.; Holmgreen, Erik M.; Ozkan, Umit S.; "Two-Stage Catalytic Reduction of NO_x Under Lean Exhaust Conditions." Ohio Air Quality Research Symposium, Athens OH, December 2004; Poster Presentation. (**3rd Place Award**)

Yung, Matthew M.; Holmgreen, Erik M.; Ozkan, Umit S.; "Two-Stage Catalytic Reduction of NO_x with Hydrocarbons." American Society of Mechanical Engineers, Internal Combustion Engine Division Meeting, Long Beach CA, October 2004.

Holmgreen, Erik M.; Yung, Matthew M.; Ozkan, Umit S.; "Two-Stage Catalytic Reduction of NO_x with Hydrocarbons for Lean-Burn Gas Fired Reciprocating Engines." American Society of Mechanical Engineers, Internal Combustion Engine Division Meeting, Long Beach CA, October 2004.

Holmgreen, Erik M.; Yung, Matthew M.; Ozkan, Umit S.; "Nitrogen Oxide Emission Control for Lean-Burn Engines by Two-Stage Catalytic Reduction with Hydrocarbons." Great Lakes Pollution Prevention Roundtable, Columbus OH, September 2004; Poster Presentation.

Holmgreen, Erik M.; Yung, Matthew M.; Ozkan, Umit S.; "Two-Stage Catalytic Reduction of NO_x with Hydrocarbons." ARES University Peer Review, Chicago IL, May 2004.

Holmgreen, Erik M.; Yung, Matthew M.; Ozkan, Umit S.; "Two-Stage Catalytic Reduction of NO with Hydrocarbons in Lean Conditions." Distributed Energy Resources Peer Review Meeting, Washington DC, December 2003; Poster Presentation.

Mitome-Watson, Junko; Oktar, Nuray; Holmgreen, Erik M.; Yung, Matthew M.; Ozkan, Umit S.; "Sulfur Dioxide Poisoning of Palladium-Based Catalysts in NO_x Reduction." American Institute of Chemical Engineers Annual Meeting, San Francisco CA, November 2003.

Mitome-Watson, Junko; Oktar, Nuray; Holmgreen, Erik M.; Ozkan, Umit S.; "SO₂ Deactivation of Pd-Based NO_x Reduction Catalysts." Ohio Air Quality Research Symposium, Toledo OH, October 2003.

Watson, Junko M.; Munteanu, Raluca; Oktar, Nury; Holmgreen, Erik M.; Ozkan, Umit S.; "SO₂ Deactivation and Regeneration of Palladium-Based Catalysts for the Reduction of Nitric Oxides with CH₄." Tri-State Catalysis Society Meeting, Lexington KY, January 2002; Poster Presentation.

Conclusions

The project has been very successful in developing a catalytic system that can work for exhaust treatment of lean-burn natural gas reciprocating engines. The catalytic system has dual functionality such that it not only reduces NO_x, but also converts all the carbon monoxide and unburned hydrocarbons in the exhaust. The reducing agent is already present in the exhaust in the form of unburned methane. So, there is no fuel penalty. The system is quite straightforward and would be easy to implement in existing engines. Table 4 presents a summary of project highlights.

Dual-Catalyst Lean Exhaust Aftertreatment System	
<i>Simulated lean exhaust. 375-425 °C, 50,000 hr⁻¹ GHSV.</i>	
Pollutant	Conversion
NO	80%
CO	100%
C ₃ H ₈	100%
C ₂ H ₆	100%
CH ₄	60-80%
Zero Fuel Penalty: Operates solely on engine exhaust. No fuel addition required.	
Replaces oxidation catalyst: CO and hydrocarbons are oxidized over this catalyst system.	
Ease of installation, retrofitting: It can work with existing engines without modification or additional control systems.	
RESULTS ARE VERY PROMISING, BUT MORE WORK IS NEEDED TO REALIZE THE BENEFITS OF THE RESULTS OBTAINED SO FAR.	

Table 4: Summary of project highlights.

If funding continues, future work will be important to bringing the system closer to commercial application. Additional fundamental work is necessary for "fine-tuning" the catalyst for long-term hydrothermal stability. Mechanistic studies of the complex interaction of the various exhaust components will provide a better understanding of catalyst behavior and help in the formulation of better catalysts. With regard to eventual application more rigorous reaction studies need to be performed, including analysis of extended time-on-stream activity and testing in real engine exhaust.

References

- [1] Bogdanchikova, N.; Meunier, F.C.; Avalos-Borja, M.; Breen, J.P.; Pestryakov, A.; *Appl. Catal. B: Environmental*, **36**, (2002), 287
- [2] Christoforou, S. C., Iliopoulou, E. F., Efthimiadis, E. A., Nikolopoulos, A. A., Vasalos, I.A., *Global Nest: The Int. J.*, **2**, 159 (2000)
- [3] Lu, W.; Zhao, X.; Wang, H.; Xiao, W.; *Cuihua Xuebao*, **21**, (2000), 423
- [4] Luo, L.; Li, S.; *Huanjing Gongcheng*, **15**, (1997), 30
- [5] Meunier, F.C.; Breen, J.P.; Zuzaniuk, V.; Olsson, M.; Ross, J.R.H.; *J. Catal.*, **187**, (1999), 493
- [6] Shimizu, Ken-ichi; Shibata, Junji; Yoshida, Hisao; Satsuma, Atsushi; Hattori, Tadashi; *Appl. Catal. B: Environmental*, **30**, (2001)
- [7] Bethke, K.A.; Kung, H.H.; *J. Catal.*, **172**, (1997)
- [8] Meunier, F.C.; Ross, J.R.H.; *Appl. Catal. B: Environmental*, **24**, (2000)
- [9] Nishizaka, Y.; Misono, M.; *Chem. Lett.*, 2237 (1994)
- [10] Misono, M.; Hirao, Y.; and Yokoyama, C.; *Catal. Today*, **38**, (1997)
- [11] Lobree, L.J.; Aylor, A.W.; Reimer, J.A.; Bell, A.T.; *J. Catal.*, **181**, (1999)
- [12] White, R.L.; Sikabwe, E.C.; Coelho, M.A.; Resasco, D.E.; *J. Catal.*, **157**, (1995)
- [13] Ohtsuka, H.; *Appl. Catal. B: Environmental*, **33**, (2001)
- [14] Guo, C.; Yao, S.; Cao, J.; Qian, Z.; *Appl. Catal. A: General*, **107**, (1994)
- [15] Babou, F., Coudurier, G.; Vedrine, J.C.; *J. Catal.*, **152**, (1995)
- [16] Muslehiddinoglu, J.; Vannice, M.A.; *J. Catal.*, **217**, (2003), 442
- [17] Sadykov, V.A.; Lunin, V.V.; Matyshak, V.A.; Paukshtis, E.A.; Rozovskii, A.Ya.; Bulgakov, N.N.; Ross, J.R.H.; *Kinetics and Catalysis*, **44**, No. 3, (2003), 379
- [18] Orlik, S.N.; Struzhko, V.L.; Mironyuk, T.V.; Tel'biz, G.M.; *Kinetics and Catalysis*, **44**, (2003)
- [19] Ogura, Masaru; Hayashi, Masayoshi; Kikuchi, Eiichi; *Cat. Today*, **42**, (1998)
- [20] Hadjiivanov, K.; Dimitrov, L.; *Microporous and Mesoporous Materials*, **27**, (1999)
- [21] Mihaylov, M.; Hadjiivanov, K.; Panayotov, D.; *Appl. Catal. B: Environmental*, **51**, (2004)
- [22] Datta, A.; Cavell, R.G.; *J. Phys. Chem.*, **89**, (1985)
- [23] Watson, J.M.; Ozkan, U.S.; *J. Catal.*, **210**, (2002)
- [24] Descorme, C.; Gelin, P.; Primet, M.; Lecuyer, C.; *Catal. Lett.*, **41**, (1996)
- [25] Hoost, T.; Laframboise, K.; Otto, K.; *Catal. Lett.*, **33**, (1995)
- [26] L.J. Lobree, A.W. Aylor, J.A. Reimer, A.T. Bell, 1998. AIChE Proceed. 2nd World Congress on Environmental Catal. J.N.Armor (Ed.) p. 70 (1998).
- [27] Chin, Y.-H.; Pisanu, A.; Serventi, L.; Alvarez, W.E.; Resasco, D.E.; *Cat. Today*, **54**, (1999)

List of Acronyms and Abbreviations

Al ₂ O ₃	-	Alumina
DRIFTS	-	Diffuse Reflectance Infrared Fourier Transform Spectroscopy
GC	-	Gas Chromatograph
GHSV	-	Gas Hourly Space Velocity
IWI	-	Incipient Wetness Impregnation
MS	-	Mass Spectrometer
NO	-	Nitric Oxide
NO ₂	-	Nitrogen Dioxide
NO _x	-	Nitrogen Oxides (NO, NO ₂ , N ₂ O)
SCR	-	Selective Catalytic Reduction
SG	-	Sol-gel
SZ	-	Sulfated Zirconia
TCD	-	Thermal Conductivity Detector
TiO ₂	-	Titania
TGA	-	Thermogravimetric Analysis
TPD	-	Temperature Programmed Desorption
TPR	-	Temperature Programmed Reduction
TPR _{xn}	-	Temperature Programmed Reaction
XPS	-	X-ray Photoelectron Spectroscopy
XRD	-	X-ray Diffraction
ZrO ₂	-	Zirconia